# Charakterisierung des Prozessierungsmechanismus des 20 S Proteasomkomplexes

**Dissertation**
**zur Erlangung des Doktorgrades**
**der Naturwissenschaften**

vorgelegt beim Fachbereich
Chemische und Pharmazeutische Wissenschaften (FB 14)
der Johann Wolfgang Goethe-Universität
in Frankfurt am Main

von
Silke Hutschenreiter
aus Kassel

Frankfurt am Main 2004

Vom Fachbereich Chemische und Pharmazeutische Wissenschaften (FB 14)
der Johann Wolfgang Goethe-Universität als Dissertation angenommen.

Dekan: Prof. Dr. H. Schwalbe
Gutachter: Prof. Dr. R. Tampé
Prof. Dr. V. Dötsch
Datum der Disputation:

Parts of the work are published in:

Hutschenreiter, S., Tinazli, A., Model, K. & Tampé, R. (2004). Two-substrate association with the 20 S proteasome at single-molecule level. EMBO J., in press.

Hutschenreiter, S., Neumann, L. Rädler, U., Schmitt, L. & Tampé, R. (2003). Metal-chelating amino acids as building blocks for synthetic receptors sensing metal ions and histidine-tagged proteins. ChemBiochem., 4, 1340-1344.

Thess, A., Hutschenreiter, S., Hofmann, M., Tampé, R., Baumeister, W. & Guckenberger, R. (2002). Specific orientation and two-dimensional crystallization of the proteasome at metal-chelating lipid interfaces. J. Biol. Chem., 277, 36321-36328.

Kyritsis, C., Gorbulev, S., Hutschenreiter, S., Pawlitschko, K., Abele, R. & Tampé, R. (2001). Molecular mechanism and structural aspects of transporter associated with antigen processing inhibition by the cytomegalovirus protein US6. J. Biol. Chem., 276, 48031-48039.

# Danksagung

Bei Prof. Dr. R. Tampé möchte ich mich ganz herzlich für sein Entgegenkommen, Engagement und Vertrauen während der Betreuung meiner Doktorarbeit bedanken.

Prof. Dr. V. Dötsch danke ich für die Korrektur meiner Dissertation.

Dr. Lutz Schmitt, Dr. Rupert Abele, Dr. Jakob Piehler und Priv.-Doz. Dr. Jochen Reinstein bin ich sehr dankbar für die zahlreichen Diskussionen und Dr. Hans Bäumert für die Hilfe bei Korrekturen.

Bei Dr. Karin Busch und Dr. Christian May bedanke ich mich für die Betreuung meiner Doktorarbeit.

Dr. Klaus Weisshart bin ich unendlich dankbar für die Einführung in die Kreuzkorrelation und die Beantwortung offener Fragen.

Der Arbeitsgruppe von Prof. Dr. W Kühlbrandt, insbesondere Dr. Kirstin Model und Åsa Böker, danke ich für die Unterstützung in der Elektronenmikroskopie.

Bei der Arbeitsgruppe von Prof. Dr. M. Karas möchte ich mich für die stete Offenheit für Diskussionen über massenspektrometrische Probleme bedanken.

Der Arbeitsgruppe um Prof. Dr. W. Baumeister, insbesondere Dr. R. Guckenberger, Dr. Matthias Hofmann, Dr. E. Seemüller, Dr. A. Thess und Dr. P. Zwickl, bin ich für Hilfe auf dem Proteasomprojekt sehr dankbar.

Dirk Schaible danke ich für sein Engagement auf dem Proteasomprojekt und Christoph Kyritsis danke ich für gute Zusammenarbeit und Treue auf dem US6-Projekt.

Bei Katrin Schulze, Dr. Jilin Tang und Ali Tinazli möchte ich mich für die Übernahme meines Projektes bzw. für die gute biophysikalische Kooperation bedanken.

Labor 120 (Eva Jaks, Peter Lamken, Dirk Schaible und Jennifer Strunk) bin ich sehr dankbar für die grosse Hilfsbereitschaft.

Den alten Marburger Kollegen (Dr. Stefan Ammer, Stanislav Gorbulev, Dr. Eva Janas, Dr. Lars Neumann, Kurt Pawlitschko und Dr. Ulf Rädler) bin ich besonders für die Einarbeitung in meine Doktorarbeit verbunden.

Martynas Gavutis, Nils Hanekop und Matthias Hofacker bin ich sehr dankbar für die Unterstützung bei Computerproblemen.

Bei Matthias Hofacker, Carsten Horn, Suman Lata und Srdjan Picuric möchte ich mich für die Herstellung von Proteinen, Peptiden und Lipiden bedanken.

Bei Ute Beck, Karlheinz Burk, Renate Guntrum, Gudrun Illig, Eckhard Linker und Gerhard Spatz-Kümbel möchte ich mich für die Assistenz meiner Forschung und die vielen aufmunternden Worte bedanken.

Stefan Kiontke und Martina Seitz bin ich sehr dankbar für die Hilfe auf meinen Projekten.

Meinen Eltern und Geschwistern sowie meinem „Lausbub“ möchte ich ganz herzlich für die seelisch-moralische Unterstützung während meiner Doktorarbeit danken, ohne die ein Abschluss der Arbeiten gar nicht möglich geworden wäre.

Allen, die mir bewusst oder unbewusst während meiner Doktorarbeit beiseite gestanden haben, gilt mein besonderer Dank.

# Contents

# Abbreviations

For amino acids the one- or three-letter code was used. Chemicals were named according to the IUPAC nomenclature.

| | |
|---|---|
| Ac | Acetyl |
| ADP | Adenosin-5'-diphosphate |
| AMC | 7-Amino-4-methylcoumarin |
| APS | Ammonium peroxodisulfate |
| ATP | Adenosin-5'-triphosphate |
| *Bam* HI | Restriction endonuclease from Bacillus amyloliquefaciens |
| BCA | Bicinchonic acid |
| bp | base pair(s) |
| BSA | Bovine serum albumin |
| Bz | Benzyl |
| C | Coulomb |
| ChT-L | Chymotrypsin-like |
| Csp-L | Caspase-like |
| CV | Column volume |
| D | Diffusion constant |
| Da | Dalton |
| dd NTP | 2',3'-dideoxynucleotide-5'-triphosphate |
| DMF | Dimethylformamide |
| DMSO | Dimethylsulfoxide |
| DNA | Deoxyribonucleic acid |
| d NTP | 2'-deoxynucleotide-5'-triphosphate |
| DTNB | 5,5-dithio-bis(2-nitrobenzoic acid) |
| DTT | Dithiothreitol |
| E | Electrical field strength |
| *E. coli* | *Escherichia coli* |
| EDTA | Ethylenediamintetraacetic acid |
| $E_{kin}$ | Kinetic energy |
| ELISA | Enzyme-linked immuno sorbent assay |

| | |
|---|---|
| em | emission |
| ER | Endoplasmic reticulum |
| ET | Energy transfer efficiency |
| ex | excitation |
| F | Farad |
| FC | Flow cell |
| FCS | Fluorescence correlation spectroscopy |
| Fmoc | 9-fluorenylmethoxycarbonyl |
| FPLC | Fast protein liquid chromatography |
| FRAP | Fluorescence recovery after photobleaching |
| FRET | Fluorescence resonance energy transfer |
| g | gram or gravity constant |
| G2 | premitotic phase of the cell cycle |
| h | hour |
| HBS | HEPES-buffered saline |
| HEPES | N-2-hydroxyethylpiperazine-N'-ethanesulfonic acid |
| *Hind* III | Restriction endonuclease from *Haemophilus influencae* |
| 5xHis-tagged peptide | $His_5$-tagged peptide |
| HPLC | High performance liquid chromatography |
| IDA | Iminodiacetic acid |
| IMAC | Immobilized metal-chelate affinity chromatography |
| IPTG | Isopropyl-β-D-thiogalactopyranoside |
| kb | kilo base |
| $k_{cat}$ | catalytic constant |
| $K_D$ | dissociation constant |
| $K_M$ | Michaelis-Menten constant |
| $k_{off}$ | off-rate constant |
| $k_{on}$ | on-rate constant |
| l | liter |
| LB | Luria-Bertani |
| LMP | low molecular mass polypeptide |
| LR | Labeling ratio |

| | |
|---|---|
| m | meter |
| M | mol/l |
| MALDI | Matrix-assisted laser desorption / ionization |
| MECL1 | Multicatalytic endopeptidase complex-like 1 |
| MHC | Major histocompatibility complex |
| min | minute |
| MS | mass spectrometry |
| M/z | Mass / charge ratio |
| NHS | N-hydroxysuccinimidyl |
| NTA | Nitrilotriacetic acid |
| NTA-DODA | $N^{\alpha}$, $N^{\alpha}$ -Bis[carboxymethyl]-$N^{\varepsilon}$-[(dioctadecylamino)-succinyl]-L-lysine |
| Ntn | N-terminal nucleophile |
| OD | optical density |
| PAGE | Polyacrylamide gelelectrophoresis |
| PAN | Proteasome-activating nucleotidase |
| PBS | Phosphate buffered saline |
| pI | isoelectric point |
| $P_i$ | inorganic phosphate |
| POMP | Proteasome maturation protein |
| pH | potentia hydrogenii |
| RNA | Ribonucleic acid |
| RU | Resonance unit(s) |
| s | second |
| S | Svedberg or axial structural parameter |
| SAM | Self-assembled monolayer |
| SEC | size exclusion chromatography |
| SDS | Sodium dodecyl sulphate |
| SOPC | 1-Stearoyl-2-oleoyl-3-sn-glycero-3-phosphatidylcholine |
| SPR | Surface plasmon resonance |
| Suc-LLVY-AMC | Succinyl-leucyl-leucyl-valinyl-tyrosinyl-7-amino-4-methylcoumarin |

| | |
|---|---|
| *T. acidophilum* | *Thermoplasma acidophilum* |
| TAP | Transporter associated with antigen processing |
| TBST | Tris-buffered saline with Triton X |
| TCA | Trichloroacetic acid |
| TCEP | Tris(2-carboxyethylphosphine) |
| TEMED | N,N,N'N'-Tetramethylethylenediamine |
| TFA | Trifluoroacetic acid |
| T-L | Trypsin-like |
| TOF | Time of flight |
| Tris | Tris-(hydroxymethyl)-aminomethane |
| Tween 20 | Polyoxyethylene-sorbitanmonolaurate |
| U | voltage |
| UV | ultraviolet |
| v | reaction velocity |
| V | Volt |
| Vis | visible |
| $v_{max}$ | maximum reaction velocity |
| W | Watt |
| Z-$L_3$VS | Carboxybenzyl-leucyl-leucyl-leucyl-vinylsulfone |

# 1. Introduction

## 1.1 Quality control

Different functions can be assigned to self-compartmentalizing machineries in the quality control within the cell (Baumeister et al., 1998; Goldberg, 2003; Wickner et al., 1999). GroEL/GroES, Hsp60/10 and TRiC are chaperonines facilitating protein refolding, whereas ClpAP, ClpXP, HslVU and the proteasome belong to the proteases degrading abnormal or misfolded proteins, in case of the proteasome after ubiquitination (Bochtler et al., 2000; Horwich et al., 1999; Rohrwild et al., 1996). Common to their architecture is the assembly of multisubunit rings to a barrel-shaped complex generating interconnected and functionalized nanocompartments in their interior. The outer rings of most proteases contain ATPase subunits energizing substrate unfolding and translocation into the central chamber, whereas the inner rings catalyze substrate degradation (Hoskins et al., 1998; Hoskins et al., 2000; Singh et al., 2000; Wang et al., 1997).

## 1.2 Importance of the proteasome

- Proteasomes eliminate misfolded and malfunctioning proteins, e.g. defective ribosomal products, by degradation.
- They regulate the cell-cycle, transcription and apoptosis by degradation of cyclins, transcription factors and pro-/anti-apoptotic molecules, respectively. As proteasomes degrade oncogenic products and tumor suppressors, they are involved in cancerogenesis.
- Proteasomes process major histocompatibility complex (MHC) class I-restricted antigens, which are subsequently transported in the endoplasmic reticulum by the transporter associated with antigen processing (TAP) and presented to cytotoxic T cells. Hence the proteasome participates in the immunological response.
- A nucleoside diphosphate kinase-like activity has been described (Yano et al., 1999).
- Tripeptidylpeptidase II can compensate for compromised proteasome activity (Geier et al., 1999; Wang et al., 2000). Thus cells can adapt to proteasomal inactivation (Glas et al., 1998).

Proteasomes are transferred cell-cycle-dependent between cytoplasm and nucleus, as several subunits of the proteasome harbor a putative nuclear localization sequence. 70 % of

the cellular proteasomes are located in the cytoplasmic matrix, 16 % in the nucleus and 14 % can be found in association with the ER-membrane. The distribution of proteasomes between nucleus and cytosol indicates that proteolysis in eukaryotic cells is in addition to the temporal restriction controlled spatially.

## 1.3 Proteasomal structures and their related functions

### 1.3.1 Archaeal and eukaryotic proteasomes

The proteasome is nearly ubiquitously distributed among eukarya, archaebacteria and some other prokarya, differing only slightly in subunit sequence (Voges et al., 1999). The simplest architecture can be ascribed to the 20 S proteasome from archaebacteria like *Thermoplasma acidophilum* (Figure 1) (Löwe et al., 1995; Zwickl et al., 1992; Zwickl et al., 1991). The evolutionary precursor of all prokaryotic and eukaryotic proteasomes is constructed from only two different subunits, which exhibit high homology due to divergent evolution. The structures of the α- and β-subunits are also similar, as they consist of a core of two antiparallel β-sheets flanked by α-helices on both sides. Seven α-subunits each are assembled in the outer rings channeling substrates via a central passageway into the degradation chamber, which is encircled by two stacked rings of seven β-subunits each. The 14 β-subunits harbor the 14 catalytic centers. Juxtaposed to the central cavity, the entrance channels dilate each into an 'antechamber'. The function of these two antechambers has not been investigated yet. They could play a role in accommodating substrates before their degradation in the central cavity. On their way into the central chamber, substrates have to pass two narrow constrictions. The α-ring outer aperture with a diameter of ~1.3 nm regulates the passage into the antechamber. The inner aperture located between the α- and β-rings has a diameter of ~1.8 nm and separates the anterior from the central chamber. In consequence, only unfolded substrates without disulfide bonds can enter the proteasome from *T. acidophilum*. The barrel-shaped complex (673 kDa) has dimensions of 15 nm in length and 11 nm in diameter. With respect to its $\alpha_7\beta_7\beta_7\alpha_7$-stoichiometry the complex is highly symmetrical ($D_7$-symmetry).

The eukaryotic 26 S proteasome consists of a 20 S core particle and a 19 S regulatory particle (Groll et al., 1997). The core complex resembles the 20 S proteasome from *T. acidophilum* with respect to the organization in α- and β-subunits and the nanocompartmentalization. But there are seven different types each of α- and β-subunits,

which are copied once in the structure and thus give rise to a complex with reduced symmetry ($C_2$-symmetry). The narrow entrance channel for substrates into the interior of the eukaryotic proteasome is constricted by protruding amino termini of the α–subunits. Based on mutagenesis, the N-terminus of the α3-subunit positions the N-termini of the other α-subunits, thereby impeding substrate entry into the yeast proteasome (Groll et al., 2000). Thus access is restricted to unfolded substrates. To circumvent this 'gate' unfolded substrates and products may pass narrow side windows (~1.0 nm in diameter) at the interface between the α- and β-rings.

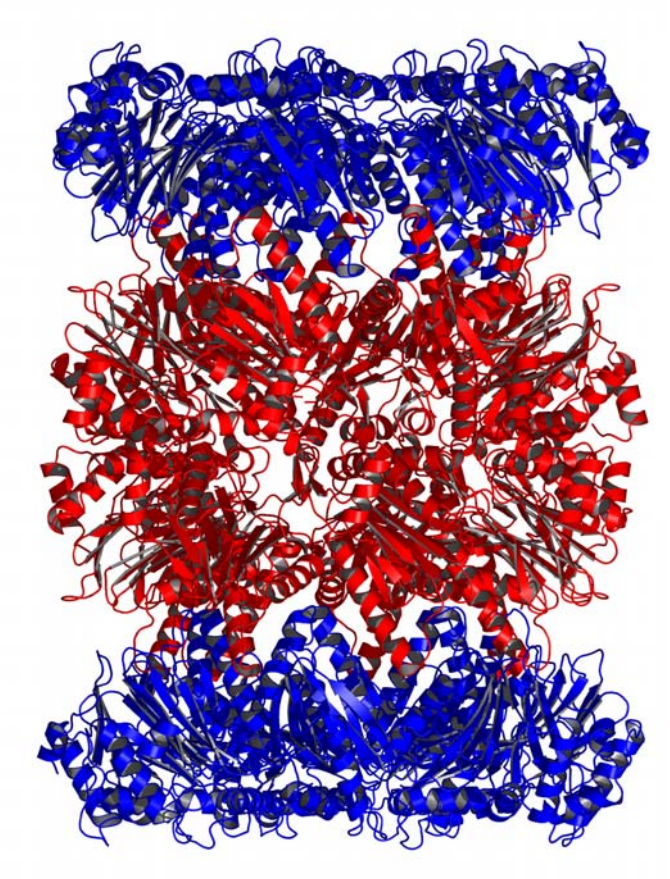

**Figure 1: Structure of the 20 S proteasome from *T. acidophilum*.** Left: Side view. The seven outer α-subunits at each terminus are highlighted in blue. The seven β-**subunits, which are localized in the two inner rings, are colored in red. Top: Top view. The narrow pore aperture is clearly visible (edited by PyMOL 0.95).**

### 1.3.2 Proteasome regulator PA700

The regulator PA700 is an ATP-dependent activator of the proteolytic activity of the eukaryotic proteasome (DeMartino et al., 1994; DeMartino et al., 1996). It binds to the core complex at the two cylindric termini with positive cooperativity (Adams et al., 1997) and stimulates the intrinsic peptidase activity in a cooperative manner (Adams et al., 1998). PA700 is composed of a base comprising eight subunits and a lid comprising nine

subunits. By chemical crosslinking it could be determined that subunits of the base form contacts with some α-subunits (Hartmann-Petersen et al., 2001). 26 S proteasomes function as stable entities, without releasing any subunits during substrate degradation (Hendil et al., 2002).

The lid subunits show significant sequence similarity to the signalosome subunits (Glickman et al., 1998; Kapelari et al., 2000). They are essential for recognition and binding or ubiquitinated substrates (Zwickl and Baumeister, 1999). Ubiquitination of RNA polymerase II leads to recruitment of PA700 and confers a non-proteolytic entering signal for the elongation phase of transcription (Ferdous et al., 2001). One lid subunit bears a deubiquitinase, which removes ubiquitin residues from the substrates, necessary for further translocation and processing (Verma et al., 2002; Yao and Cohen, 2002)

Six distinct AAA-type ATPases (ATPases associated with a variety of cellular activities) energize the base to actively unfold (reverse or anti-chaperone activity) and translocate substrates (Zwickl and Baumeister, 1999). Consequently, 26 S proteasomes are able to degrade folded substrates. The base is also competent in binding misfolded or partially denatured nonubiquitinated proteins and preventing their aggregation (Braun et al., 1999; Strickland et al., 2000). Thus substrates are maintained in a soluble state until refolding (chaperone-like activity) or degradation is complete.

### 1.3.3 Proteasome-activating nucleotidase

The archaeal homologue to the base is named proteasome-activating nucleotidase (PAN). PAN seems to be the evolutionary precursor of the eukaryotic 19 S regulatory complex, before coupling of proteasomal function to ubiquitination. The complex of ~12 subunits from *Methanococcus jannaschii* shares 41- 45 % sequence similarity with the six ATPases from the human and yeast 19 S regulatory complex (Zwickl et al., 1999). The N-terminal coiled-coil region of PAN is not required for assembly or function of the complex, but its C-terminal region contains a P-loop domain including Walker A and B motifs (Wilson et al., 2000). By binding and hydrolyzing nucleotides, expecially ATP, PAN can enhance proteasomal hydrolysis of unfolded proteins 8-25-fold, but does not promote degradation of peptides (Zwickl et al., 1999). Like the base of the regulator PA700, PAN can also promote refolding and prevent protein aggregation in an ATP-dependent fashion

(Benaroudj and Goldberg, 2000). Translocation and degradation of globular substrates are preceded by a threading (unfolding) through the ATPase (Navon and Goldberg, 2001).

### 1.3.4 Proteasome regulator PA28

The mammalian 20 S core complex can bind the barrel-shaped 11 S regulator PA28 from the cytosol at one or both ends. The 11 S regulator is composed of two subunits, α and β, which are arranged in a homohexameric or homoheptameric complex (Ahn et al., 1996; Song et al., 1996). Its central pore is proposed to align with the channel of 20 S proteasomes and cannot be penetrated by folded substrates (Knowlton et al., 1997). Both subunits are expressed after induction by γ-interferon. The regulator PA28 stimulates the degradation of small peptides in an ATP-independent manner (Dubiel et al., 1992; Ma et al., 1992). PA28 can enhance the generation of antigenic peptides by prompting the proteasome to cleave substrates by a coordinated double-cleavage mechanism (Dick et al., 1996b).

### 1.3.5 'Gating' of the eukaryotic proteasome

The existence of the 'gate' in the α-subunit rings renders substrate translocation in the proteasome interior rate-limiting. But the constraints can be bypassed, i. e. the 'gate' can be opened by

1) binding of PA700 to the core particle (Groll et al., 2000). One of the ATPase domains seems to change its conformation in dependence on the nucleotide bound.
2) docking of PA28-like PA26 from *Trypanosoma brucei* to the core particle and inducing conformational changes in the α-subunits. Thus 11 S regulators can open the product exit gate opposite to the substrate entrance, which is gated by the 19 S regulator (Whitby et al., 2000). Due to premature release of the fragments the product size is increased. Since the proteasome generates antigenic peptides from precursor molecules, the fragment size is optimized for loading of MHC-class I molecules (Uebel and Tampé, 1999).
3) binding of PAN to the core particle (Benaroudj et al., 2003). Gate opening in the 20 S proteasome and protein translocation require ATP hydrolysis (300-400 ATP molecules per globular or unfolded substrate).

4) substrates lacking accessible termini, because they can enter the latent (closed) proteasome and can be cleaved at internal peptide bonds (Liu et al., 2003).
5) standard proteasome substrates (peptides), which shift the equilibrium by allosteric transitions from the closed/barrel-like to the open/cylinder-like conformation (24 % and 74 % open conformer in the equilibrium, respectively). Conversely, proteasome inhibitors prevent the equilibrium shift induced by substrate association (Osmulski and Gaczynska, 2000; Osmulski and Gaczynska, 2002).
6) binding of hydrophobic peptides to several non-catalytic sites in the 20 S proteasome (Kisselev et al., 2002).
7) different chemical treatments, e.g. low concentrations of SDS (0.01 % - 0.02 %) (Kisselev et al., 2002), polylysine (Tanaka et al., 1986), cardiolipin (Ruiz et al., 1993), calcium and magnesium ions (25 mM – 500 mM) (Dahlmann et al., 1989; Dahlmann et al., 1992), heat (Mykles, 1989) or dialysis against water, i.e. removal of glycerol (McGuire et al., 1989). These substances are assumed to bind to the same non-catalytic sites as hydrophobic peptides (Kisselev et al., 2002). However, potassium ions suppress peptide hydrolysis, probably by maintaining the channel in a closed conformation (Kisselev et al., 2002).

### 1.4 Assembly of 26 S proteasomes

The assembly pathways of proteasomes differ for eukaryotes, eubacteria (Zühl et al., 1997) and archaebacteria (Seemüller et al., 1996; Zwickl et al., 1994), although the last two are not fully understood.

In *Saccharomyces cerevisiae* the α-subunits start to assemble spontaneously to homoheptameric rings. They form a scaffold for the ordered binding of N-terminally extended β-subunit precursors via assembly intermediates to 15 S halfproteasomes (Yang et al., 1995). Upon rapid and irreversible dimerization of the two $\alpha_7\beta_7$-rings, the proteasome maturation factor Ump1 is encased (Ramos et al., 1998). Ump1 affects the conformation of the propeptides, thus inducing autocatalytic processing of the β-subunits. Activation of the catalytic centers is followed by rapid degradation of Ump1. According to the sequence of events, premature activation of the proteasome is prevented (Chen and Hochstrasser, 1996). The human homologue of Ump1, designated POMP (proteasome maturation protein), is modulated by interferon γ (Burri et al., 2000; Witt et al., 2000).

The 20 S proteasome is capped end-on by the regulator PA700 after phosphorylation of one ATPase subunit (Rpt6) by a protein kinase. Vice versa, the 26 S proteasome can be disassembled into the constituent subcomplexes by dephosphorylation (Satoh et al., 2001; Yang et al., 1995).

## 1.5 Catalytic activity of the proteasome

### 1.5.1 Catalytic sites and catalytic properties

The catalytic activity of the proteasome resides in N-terminal threonine residues of the β-subunits, which are exposed during processing of their propeptides at the end of assembly (Chen and Hochstrasser, 1996; Ditzel et al., 1998; Seemüller et al., 1996). During substrate processing the threonine residue functions simultaneously as nucleophile and as base due to action of the hydroxyl group and amino group, respectively; thus the proteasome is member of the family of N-terminal nucleophile (Ntn) hydrolases (Löwe et al., 1995; Seemüller et al., 1995a). The family includes aspartylglucosaminidase, penicillin acylase and glutamine-phosphoribosylpyrophosphoryl-amidotransferase, which harbor catalytically active T1, S1 and C1 residues, respectively. Consequently, mutation of the aminoterminal threonines of the proteasomal β-subunits to alanines render the proteasome inactive, whereas βT1S proteasome mutants retain their activity (Seemüller et al., 1995a). However, βT1S mutants degrade peptides and proteins up to 10-fold slower than wild-type proteasomes (Kisselev et al., 2000). The catalytic threonine residues are protected by the propeptides against $N^{\alpha}$-acetylation and thereby inactivation (Arendt and Hochstrasser, 1999; Groll et al., 1999). In yeast, three different $N^{\alpha}$-acetyltransferases are able to modify co- or posttranslationally non-catalytic threonine residues of α- and β-subunits (Kimura et al., 2000) or catalytic threonine residues lacking propeptides (Jäger et al., 1999).

Several other β-subunit residues (E17, K33 and D166) are required for proteasomal activity. A K33R mutant is catalytically inactive, but viable. From a rearrangement of the N-terminal threonine residue in this mutant was concluded that K33 lowers the $pk_a$ of the T1-amino group by electrostatic interactions (Groll et al., 1999; Seemüller et al., 1995a).

The proteasome from *T. acidophilum* catalyzes peptide and protein degradation with a pH-optimum of pH 8-9, i.e. above the isoelectric point (pI 5.6) and a temperature optimum of 90 °C (Dahlmann et al., 1992). *T. acidophilum* proteasomes dissociate below pH 3.5 in the

single subunits leading to inactivation (Grziwa et al., 1994). However, reconstitution after low-pH treatment is possible in contrast to dissociation at high pH.

### 1.5.2 Cleavage specificity

#### 1.5.2.1 Cleavage specificity of 20 S proteasomes

Although the 20 S proteasome from *T. acidophilum* differs from any protease of the serine family with respect to the character of the catalytically active centers (Kisselev et al., 2000), it shares the cleavage specificity with chymotrypsin, i.e. cuts preferentially behind aromatic amino acids like tryptophane, tyrosine, phenylalanine or the hydrophobic leucine residue (Cardozo et al., 1999; Stein et al., 1996). The eukaryotic 20 S proteasome has only two copies of three catalytically active β-subunits, which resemble different proteases with respect to their cleavage specificities (Table 1) (Arendt and Hochstrasser, 1997; Dick et al., 1998; Heinemeyer et al., 1997).

| P1 residue | Cleavage specificity | Assignment of β-subunit | Specificity determinant |
|---|---|---|---|
| L,I,Y,F | Chymotrypsin-like (ChT-L) | β5 (Pre2) | M45 |
| R,K | Trypsin-like (T-L) | β2 (Pup1) | D53 |
| D,E | Peptidylglutamyl peptide-hydrolyzing, postacidic, Caspase-like (Csp-L) | β1 (Pre3) | R45 |
| I,L,V | Branched-chain amino acid prefering | β1 (Pre3) | |
| G,A | Small neutral amino acid prefering | | |

**Table 1: Catalytic properties of β–subunits of the eukaryotic proteasome.** P1 denotes the residue prior to the cleavage site. The specificity determinants are residues in the binding pocket, which regulate substrate specificity.

The cleavage specificities are determined by certain residues in the binding pocket. These are countercharged to the amino acid prior to the cleavage site or apolar in case of hydrophobic residues. Non-catalytic subunits β3 (Pup3), β4 (Pre1) and β6 (C5) lack the scissile GT-bond separating the propeptide by autolysis and subunit β7 (Pre4) has a K33R-replacement (Groll et al., 1999; Schmidtke et al., 1996). The hierarchy of the importance of

individual subunit activities for proteasomal function could be deduced from growth phenotypes of active site mutants without propeptides: β5 (Pre2) >> β2 (Pup1) ≥ β1 (Pre3) (Jäger et al., 1999).

### 1.5.2.2 Modulated cleavage specificity of immunoproteasomes

Mammalian cell lines related to the immune system express constitutively immunoproteasomes, in which the three catalytically active types of β-subunits are replaced by subunits with partially changed cleavage specificity (Table 2) (Driscoll et al., 1993; Foss et al., 1998; Gaczynska et al., 1993). In myocytes and erythrocytes immunoproteasomes are formed after induction by interferon γ, e.g. during viral infection. In the latter cells, the subunits MECL1 and LMP2 are recruited in an interdependent manner at the stage of proteasome precursor complexes to assemble the immunoproteasome (Groettrup et al., 1997). Preproteasomes containing LMP2 and MECL1 require LMP7 for efficient maturation (Griffin et al., 1998). According to this cooperative mechanism, the assembly of homogenous immunoproteasomes with all three inducible subunits is guaranteed.

| Substitution of β-subunit | | Changes in specificity determinant | |
|---|---|---|---|
| β5 (X) | β5i (LMP7) | M45 | M45 (conserved) |
| β2 (Z) | β2i (MECL1) | D53 | E53 |
| β1 (Y) | β1i (LMP2) | R45 | L45 |

**Table 2: Influence of γ-interferon on the cleavage specificity of the eukaryotic proteasome.** During viral infection β-subunits with modified cleavage specificity are induced (i) by γ-interferon. These are constitutively expressed in immunocompetent cells.

The activity of immunoproteasomes against substrates with an acidic residue in the P1 position is abolished due to changes in the specificity determinant. However, immunoproteasomes can be attributed an increased activity against substrates with a hydrophobic or branched chain amino acid in the P1 position. In consequence, the cleavage specificity of immunoproteasomes adapts to the binding properties of MHC-class I receptors.

### 1.5.3 Recognition of cleavage motifs

Human 20 S and 26 S proteasomes generate overlapping, but substantially different sets of fragments, although they make use of similar principles (Emmerich et al., 2000). Cleavages of 20 S and 26 S protesomes are directed by a span of 10 amino acid residues (positions P6-P4´) in the substrate (Table 3) (Kuttler et al., 2000; Nussbaum et al., 1998).

P6 P5 P4 P3 P2 P1 ✂ P1´ P2´ P3´ P4´ ✂ cleavage site

| Position | Cut-promoting residues | Cut-inhibiting residues |
|---|---|---|
| P1´ | β-turn-promoting, small | |
| P1 | L,R | G |
| P4 | P | |

**Table 3: Cleavage motifs of 20 S and 26 S proteasomes.** The residue positions are indicated schematically.

Especially the position P1 prior to the cleavage site and the immediate C-terminal flanking position P1´ are of importance (Altuvia and Margalit, 2000). As the N-termini of antigenic peptides are trimmed by γ-interferon-inducible leucine aminopeptidase downstream of the proteasome (Beninga et al., 1998; Harris et al., 1992), they send only weak cleavage signals (Altuvia and Margalit, 2000). Proline residues within epitopic sequences play an important role in the efficient production of MHC class I ligands by preventing random proteasomal cleavages (Shimbara et al., 1998). Wild-type proteasomes and active site mutants generate fragments of comparable lengths (Nussbaum et al., 1998). So the fragment size does not reflect the distance between the active sites according to the molecular ruler hypothesis (Groll et al., 1997; Wenzel et al., 1994).

Cleavage prediction of 26 S proteasomes is performed by three methods. PAProC (developed at Tübingen University) is based on in-vitro experimental verification of cleavage sites and non-cleavage sites. MAPPP (developed at the Max-Planck Institute, Berlin) combines proteasomal cleavage prediction with MHC-binding prediction. The neural network-based method of Net Chop (developed at the Center for Biological Sequence Analysis at the Technical University of Denmark) is trained on MHC class I ligands generated by human proteasomes. Up to 70 % of the produced C-termini can be

captured correctly (Saxova et al., 2003). But the stochastic nature of degradation and differences between the cleavage characteristics of immunoproteasomes and constitutive proteasomes impair the performance.

### 1.5.4 Processive degradation mechanism

The HPLC-pattern of cleavage products generated by 20 S or 26 S proteasomes is independent of the degradation time (Akopian et al., 1997; Kisselev et al., 1999b). However, the cleavage pattern obtained from degradation of the same substrates by trypsin or chymotrypsin changes time-dependently, because the products detach from the enzyme after each cut. Consequently, it was concluded that the proteasome displays processivity in contrast to conventional endopeptidases. Substrates are chopped down to small fragments prior to their release (Akopian et al., 1997; Kisselev et al., 1999b). The number of cleavages per minute decreases with increasing length of the substrate, probably due to retarded exposure to the active sites. Product sizes fit closely a normal distribution, when plotted against the logarithm of their molecular weights (Kisselev et al., 1998). According to the log-normal distribution, 95 % of the products comprise 3 to 22 residues with a mean size of ~8 residues. Since median fragment sizes were 5 residues for 26 S proteasomes and 6 residues for 20 S proteasomes, 19 S particles presumably slow down the release of peptidic products and lead to additional cleavages. However, only 10 % - 15 % of the peptidic products can be presented by MHC class I molecules due to size limitations (8-9 residues) and two-thirds are too short to function in antigen presentation (Kisselev et al., 1999b).

### 1.5.5 Allosteric interactions between catalytic sites in eukaryotic proteasomes

Binding of hydrophobic substrates of the chymotrypsin-like activity at certain non-catalytic sites is positive cooperative and activates allosterically the chymotrypsin-like, caspase-like activities (Kisselev et al., 1999a) and the trypsin-like activity (Kisselev et al., 2002). This general stimulatory effect may be due to gating of the channel in the 20 S proteasome (Kisselev et al., 2002).

Conversely, acidic peptides inhibit the chymotrypsin-like activity by binding to a non-catalytic site (Kisselev et al., 2003; Myung et al., 2001). Acidic peptides stimulate the trypsin-like activity by binding to a caspase-like site and a non-catalytic modifier site

(Kisselev et al., 2003; Schmidtke et al., 2000). As proteasomal protein breakdown is rate-limited by the chymotrypsin-like activity, acidic peptides inhibit proteolysis, whereas hydrophobic peptides have little effect (Kisselev et al., 2003).

### 1.5.6 Inhibition of catalytic activity

Proteasome inhibitors can be classified according to Table 4.

| Inhibitor class | Examples | Selectivity | Mechanism |
|---|---|---|---|
| α´,β´-epoxyketones (Elofsson et al., 1999) | Ac-hFLFL-epoxide, epoxomicin, eponemycin | ChT-L activity of the proteasome | Morpholino-adduct formation (covalent and irreversible modification) |
| Peptidyl boronic acids (Gardner et al., 2000) | Bz-Phe-boroleucine | ChT-L activity of the proteasome, serine proteases | Transition state analogues (covalent and reversible modification, competitive) |
| Peptide aldehydes (Savory and Rivett, 1993) | Leupeptin, Antipain | T-L activity of the proteasome, serine and cysteine proteases | Hemiacetal formation (covalent and reversible modification) |
| Peptide vinyl sulfones (Bogyo et al., 1997) | Carboxybenzyl-LLL-vinylsulfone ($Z\text{-}L_3VS$) | T-L, ChT-L and Csp-L activity of the proteasome, HslV, cysteine proteases | Michael-adduct formation (covalent modification) |
| (Dick et al., 1996a; Fenteany and Schreiber, 1998; Fenteany et al., 1995) | Lactacystin | ChT-L, T-L and Csp-L activity of the proteasome, cathepsin A and tripeptidylpeptidase II | Clasto-lactacystin β-lactone-adduct formation (covalent modification, irreversible (ChT-L and T-L activity), reversible (Csp-L activity)) |

| | | | |
|---|---|---|---|
| (Groll et al., 2001) | TMC-95A | ChT-L, T-L and Csp-L activity of the proteasome | Interaction with the active sites via hydrogen bonds (noncovalent, reversible, competitive) |
| Proline- and argini-ne-rich peptides (Gaczynska et al., 2003; McCutchen-Maloney et al., 2000) | PI31, PR39 | ChT-L, T-L and Csp-L activity of the proteasome, inhibition of binding to PA28 and PA700 | Interaction with α7-subunit (allosteric and reversible modification, noncompetitive) |

**Table 4: Overview of proteasome inhibitors.**

Proteasome inhibitors are useful as molecular probes or therapeutic agents. They are characterized by potency, selectivity, cell permeability and bioavailability.

### 1.6 Diagnostics and disease

By tagging green fluorescent protein with N-end rule or ubiquitin fusion degradation signals ubiquitin/proteasome-dependent proteolysis in living cells can be quantified (Dantuma et al., 2000). Accordingly, proteasome inhibitors can be screened by measuring accumulation of the fluorescent reporters in inhibitor-treated cells. A ubiquitin-sandwich technique was established to detect and measure cotranslational protein degradation in living cells (Turner and Varshavsky, 2000).

Defects of the ubiquitin-proteasome pathway leading to abnormal degradation of cell cycle regulators and pro-apoptotic proteins were shown to correlate with uncontrolled cell growth. Thus proteasome inhibitors may arrest or retard cancer progression (Adams et al., 1999; Teicher et al., 1999).

In neurodegenerative diseases (Table 5), the ubiquitin/proteasome system is impaired causing protein aggregation in aggresomes and inclusion bodies (Bence et al., 2001). Probably, the engagement of the proteasomes by ubiquitylated aggregates leads to cell cycle arrest in G2. The positive feedback of aggregates on the malfunction of the ubiquitin-proteasome system explains the precipitous loss of neuronal function.

| Disease | Involvement of the proteasome | Therapy with enzyme modulators |
|---|---|---|
| Alzheimer | *Aβ fragments* of the *β-amyloid precursor protein* inhibit the proteasome (Gregori et al., 1995)<br>γ-secretase competes with the proteasome for turnover of *C-terminal fragments* of the *β-amyloid precursor protein* (Skovronsky et al., 2000)<br>*Presenilins 1 and 2* and their cleavage products are substrates of the proteasome (da Costa et al., 1999; Kim et al., 1997; Marambaud et al., 1998) | Proteasome activators |
| Parkinson | *Parkin* ubiquitinylates itself as ubiquitin-protein isopeptide ligase (E3) and becomes substrate of the proteasome; after sequestration of *parkin* into inclusions its E3-function is inhibited, thus leading to accumulation of its toxic substrates (Junn et al., 2002)<br>*DJ-1 (L166P mutant)* promotes its own degradation by the proteasome, resulting in lower DJ-1 protein concentrations (Miller et al., 2003)<br>*α-Synuclein (A30P or A53T mutant)* inhibits the proteasome (Petrucelli et al., 2002), presumably by binding of aggregated forms to the 19 S base complex (Snyder et al., 2003) | Proteasome activators |
| Huntington | Polyglutamine expansions of *huntingtin* suppress up-regulation of proteasomal activity and Hsp activity in response to stress and inhibit the ubiquitin-proteasome system (Ding et al., 2002)<br>*Huntingtin* with polyglutamine expansions is degraded by aspartic endopeptidases and the proteasome to aggregation-prone *Cp-A* and *Cp-B* fragments (Lunkes et al., 2002) | Proteasome activators<br><br>Inhibitors of aspartic endopeptidases |

| | | |
|---|---|---|
| Prion | Cellular form (wild-type and mutant) of the *prion protein ($PrP^C$)* underlies retrograde transport from the ER (Ma and Lindquist, 2001; Yedidia et al., 2001), especially due to misfolding (sporadic and familial disease) (Ma and Lindquist, 1999; Ma et al., 2002). In the cytosol, $PrP^C$ accumulates and thus aggregates or is converted into the Scrapie-associated form $PrP^{Sc}$ (infectious disease) (Ma and Lindquist, 2002), if proteasomal activity is compromised.<br>High-risk $V_{136}R_{154}Q_{171}$-*PrP* is degraded slowly by the proteasome, consequently enhancing its neurotoxic effect (Tenzer et al., 2004). | Proteasome activators |

**Table 5: Overview of neurodegenerative diseases.**

## 1.7 Structurally related proteases

In prokaryotes like *E. coli* abnormal and incompletely synthesized proteins are degraded by at least five ATP-dependent proteases. Most of them belong to the Clp or Hsp100 family of $AAA^+$ proteins including ClpXP, ClpAP and ClpYQ (HslUV). ClpP, the peptidase component of ClpXP and ClpAP, is composed of two homoheptameric stacked rings, which enclose a chamber harboring 14 catalytic triades (Ser 97, His 122, Asp 171) (Maurizi et al., 1990; Wang et al., 1997). ClpP displays serine-peptidase activity against oligopeptides smaller than hexapeptides, preferentially cleaving after hydrophobic residues (Maurizi et al., 1994; Woo et al., 1989). Degradation of longer oligopeptides requires ATP-dependent binding of homohexameric mono-ring structure ClpX or double-ring structure ClpA to one or both ends of ClpP (Grimaud et al., 1998; Kessel et al., 1995). In contrast, protein degradation by ClpAP or ClpXP is accomplished in several ATP-consuming steps. Protein unfolding by the chaperones ClpX or ClpY requires ATP hydrolysis (Singh et al., 2000) and is the rate-determining step in degradation (Kim et al., 2000). Access to the proteolytic chamber is restricted by two axial pores with a diameter ~ 10 Å (Wang et al., 1997). Substrate translocation is a reptation-like process, which proceeds in several steps along an axial path (Ishikawa et al., 2001). It is fuelled by ATP hydrolysis (Hoskins et al., 1998). Protein substrates are subsequently degraded in a processive manner by ClpP and

produce 7- to 10-mers (Thompson et al., 1994). If proteolysis is blocked, denatured substrates are released from ClpP in a step, which requires ATP and additional substrate (Hoskins et al., 2000; Kim et al., 2000). Proteins are usually designed for proteolysis by a tagging mechanism reminiscent of ubiquitination. The ssrA gene is translated, if a nascent polypeptide chain becomes stalled at the ribosome due to premature transcriptional termination or nuclease cleavage (Keiler et al., 1996). The C-terminal ssrA-tag on a protein overrides its sequence (Kim et al., 2000) and mediates directional translocation of the substrate into ClpP protease with the C-terminus leading (Reid et al., 2001). ClpAP and ClpXP degrade also proteins with N-terminal and internal recognition motifs (Hoskins et al., 2002). Degradation proceeds always from the position of the tag (Lee et al., 2001). A zinc binding domain in each ClpX subunit stimulates as dimer substrate recognition and promotes degradation of some substrates by ClpP (Wojtyra et al., 2003).

The architecture of ClpYQ is similar to ClpXP (Bochtler et al., 2000), although the fold of the single subunits differs (Bochtler et al., 1997) and though ClpQ and ClpY assemble both in homohexameric rings (Kessel et al., 1996; Rohrwild et al., 1997). Like ClpP, HslV has a low oligopeptidase activity. Its proteolytic activity is enhanced more than one order of magnitude by HslU (Huang and Goldberg, 1997; Seol et al., 1997). HslUV is the 'prokaryotic proteasome' (Sousa et al., 2000), as the HslV sequence and fold is similar to the β-type proteasome subunits and as HslUV shares the threonine-dependent catalytic mechanism and the chymotryptic cleavage specificity with the proteasome (Rohrwild et al., 1996).

### 1.8 Chaperonins

Hsp60 chaperones, also termed 'chaperonins', can be divided into two groups. Group I chaperonins, such as GroEL, have a structure similar to the proteasome and require co-chaperones such as GroES. In eubacteria and in mitochondria and chloroplasts of eukaryotic cells, these chaperones assist in protein folding and minimize thereby aggregation. GroEL and GroES are both necessary for the viability of *E .coli*.

GroEL consists of two stacked homoheptameric rings giving rise to a barrel (Braig et al., 1994; Xu et al., 1997). In the interior, two separate cavities are formed in juxtaposition. The GroEL subunits can be dissected into three domains: 1) The equatorial domains mediating intersubunit contacts hydrolyze ATP. 2) The apical domains bind protein

substrates and the homoheptameric GroES resembling a lid. 3) Intermediate domains, which permit large structural rearrangements during the functional cycle, connect the equatorial and apical domains. GroEL can associate at the ends with one GroES in the ADP-bound state or two GroES in the ATP-bound state, thus creating 'bullets' or 'footballs', respectively.

As unfolded (non-native) proteins display hydrophobic patches, they are bound to their hydrophobic counterparts in the apical domains of the nucleotide-free *cis* ring (Wang et al., 1999b). Binding of GroES in the ATP-bound state induces a 90° outward rotation of the apical domains, thereby dilating the proximal cavity (Falke et al., 2001). The hydrophobic amino acids in the apical domains become buried and the now hydrophilic inner surface induces release of the bound polypeptide into the closed cavity. Folding commences inside the 'Anfinsen cage' and can be significantly faster than in solution, probably because of smoothing the energy landscape for folding (Brinker et al., 2001). Additionally, the 'Anfinsen cage' protects substrates from aggregation before reaching the correctly folded state (Ellis, 1996; Ellis, 2001). Subsequently, the seven molecules of ATP in the *cis* ring are hydrolyzed at a rate of 0.25-0.5 $min^{-1}$ (rate-determining step) (Jackson et al., 1993; Todd et al., 1994). Thus a conformational change is induced in GroEL, which triggers ATP binding to the *trans* ring after picking up polypeptide. Due to an allosteric signal GroES and "folded" substrate are released from the *cis* ring, whereas GroES binds to the *trans* ring (Rye et al., 1999). Only substrates < 60 kDa can be folded inside the cavity. Substrates, especially ≥ 60 kDa are folded via multiple rounds of binding on the outside and release. GroES binding to the *trans* ring is then required to release non-native substrate, which probably folds in solution (Chaudhuri et al., 2001; Farr et al., 2003). But this process is less efficient than *cis* encapsulation. In addition, substrate selectivity is determined by the encapsulation time (usually 15 s) corresponding to the rate of ATP hydrolysis and the hydrophilicity of the *cis* cavity (Erbse et al., 2003; Wang et al., 2002). GroEL/ES makes a compromise on these parameters in order to act as a folding machine for the majority of proteins.

### 1.9 Immobilization of His-tagged proteins

Formation of metal-chelate complexes was employed in the purification of proteins harboring an engineered His-tag, i. e. a stretch of five or six consecutive histidines (Hochuli, 1990; Hochuli et al., 1988; Porath et al., 1975). This strategy was transferred to the self-assembly of lipid or thiol layers doped with chelating lipids as 'chelator concept' (Schmitt et al., 1994). The tetradentate ligand nitrilotriacetic acid (NTA) binds divalent metal ions such as $Ni^{2+}$, $Co^{2+}$, $Cu^{2+}$ or $Zn^{2+}$ coordinatively to form a hexagonal complex, while the remaining two binding sites can be occupied e. g. by the histidine side chains of a His-tag. Other substituting electron donor groups are the side chains of cysteine and, to a lesser extent, glutamate, aspartate, arginine or lysine. As these side chains have to be orientated on the protein surface in positions to fit into the hexagonal coordination sphere, binding is very specific for His-tagged proteins (Dietrich et al., 1995; Schmitt et al., 2000). The binding constant for NiNTA-His-tag interactions is located in the micromolar range (Dorn et al., 1998). Complex formation can easily be reversed by addition of EDTA of imidazole or by acidification.

Chelator lipids based on the nitrilotriacetic acid (Schmitt et al., 1994) or iminodiacetic acid (IDA) (Shnek et al., 1994) proved as useful tools in the immobilization of His-tagged fusion proteins at surfaces. The chelator concept was adopted in the formation of lipid monolayers (Dietrich et al., 1996; Dietrich et al., 1995; Schmitt et al., 1996), liposomes (Dorn et al., 1998), thiol-based self-assembled monolayers (SAMs) on gold surfaces (Sigal et al., 1996) and in the two-dimensional crystallization at lipid interfaces (Kubalek et al., 1994; Thess et al., 2002; Venien-Bryan et al., 1997). In all approaches proteins were immobilized in an orientated fashion, while retaining their native conformation. Thus via judicious introduction of a His-tag in the protein of interest the site of interaction with the chelating support and the orientation with respect to the chelating support can be controlled (Thess et al., 2002), while the functionality of the protein is preserved.

As the proteasome from *T. acidophilum* is a highly symmetrical construct, His-tags were engineered either to the 14 α-subunits (N- or C-termini) or the 14 β-subunits (C-termini) (Figure 2). Thus proteasomes bearing His-tags at the N-termini of the α-subunits are destined to be immobilized end-on at chelating supports, whereas proteasomes harboring His-tags at the C-termini of the α- or β-subunits were designed for side-on orientation at chelating interfaces.

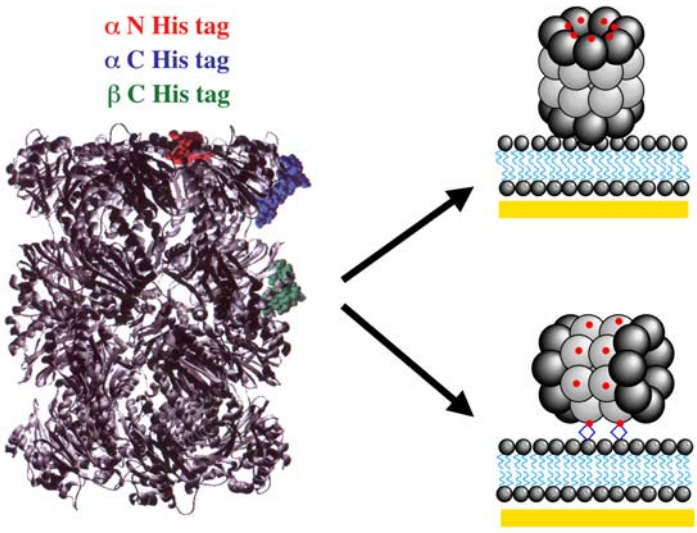


**Figure 2: Engineered His-tags control orientation of the proteasome upon immobilization.** His-tags at the N-termini of the α-subunits lead to end-on immobilization of the proteasome at chelating interfaces, whereas His-tags at the C-termini of the β-subunits control side-on orientation of the proteasome at chelating supports.

## 1.10 Aim of the work

Catalytic features of the 20 S proteasome have been the object of interest for many years. Cleavage specificities of the eukaryotic 20 S proteasome could be assigned to single subunits (Arendt and Hochstrasser, 1997; Chen and Hochstrasser, 1996; Heinemeyer et al., 1997) and the importance of immunosubunits in antigen presentation could be deciphered (Aki et al., 1994; Driscoll et al., 1993; Gaczynska et al., 1993). The cleavage potential of the 20 S and 26 S proteasome can be described by several models (Holzhütter et al., 1999; Kuttler et al., 2000), which have been refined over the past years. However, the degradation mode of the proteasome could be analyzed only indirectly from digestion patterns (Akopian et al., 1997; Kisselev et al., 1999b), but not online on the single-molecule level. Hence many mechanistic details remain obscure. The interplay between the different nanocompartments has not been investigated yet. One can envisage two basic modes of communication between the central chamber, the antechambers and the internal passageways: Either substrates enter the central cavity of the proteasome through one channel, while products exit through the second channel, or each passageway into the central chamber functions simultaneously as entrance and exit (Köhler et al., 2001). Presently, it is not known whether the 20 S proteasome works unidirectionally or whether the bipartite structure of the proteasome is correlated somehow with its function. Furthermore, it is unsettled how many substrates associate with the proteasome in one cycle and whether they are degraded simultaneously at the catalytic centers. The processive degradation mode might result from the proteasomal architecture or substrate handling.

To address these questions we had to disable the functionality of one aperture in order to dissect whether the other pore can compensate for the loss. We chose a novel approach by unique orientation of the proteasome at interfaces, as it is challenging to introduce mutations solely around one pore aperture of the highly symmetrical degradation machinery. For this purpose we compared two purified recombinant 20 S proteasomes, where hexahistidine tags were attached either around the entrances (end-on orientation) or at the sides (side-on orientation). The immobilization of the proteasomes was tested at metal-chelating lipid interfaces (lipid vesicles and lipid monolayers) and surfaces. The goals of my work could be summarized as following:

- Purification and identification of differently His-tagged proteasomes
- Determination of the influence of the His-tag on proteasomal activity
- Verification of uniform orientation of the proteasomes upon immobilization
- Comparison of the activities of soluble and immobilized proteasomes
- Determination of the substrate/proteasome stoichiometry for the different proteasomes
- Co-localization of two substrates in the proteasome

# 2. Theory

## 2.1 Surface plasmon resonance

Surface plasmon resonance spectroscopy allows to measure changes in refractive index at the interface of a conductor and a fluid. Adsorption of biomolecules to a functionalized conductor surface can be studied, as the refractive index of the analytes differs from the refractive index of the bulk solution. The interaction of the immobilized analyte with a soluble ligand can be monitored in real time, thus revealing kinetic and thermodynamic constants.

Surface plasmons are collective vibrations of the free electrons at a conductor surface. The charge fluctuations propagate along the surface of the metal and resemble light waves trapped on the surface (Figure 3). Thus the resonant interaction between the surface charge oscillation and the electromagmetic field of the light constitutes the surface plasmon. Perpendicularly to the surface an electrical field is induced, which decays exponentially with distance from the surface. The electrical field is assumed to be evanescent according to the bound, non-radiative nature of surface plasmons. In the dielectric medium above the conductor, the decay length of the evanescent field is of the order of half the wavelength of the exciting light, whereas the decay length in the metal is determined by the skin depth. The attenuation of the charge fluctuation (propagation length of the surface plasmon mode) depends on the absorption of the conductor material and on the wavelength of the exciting light.

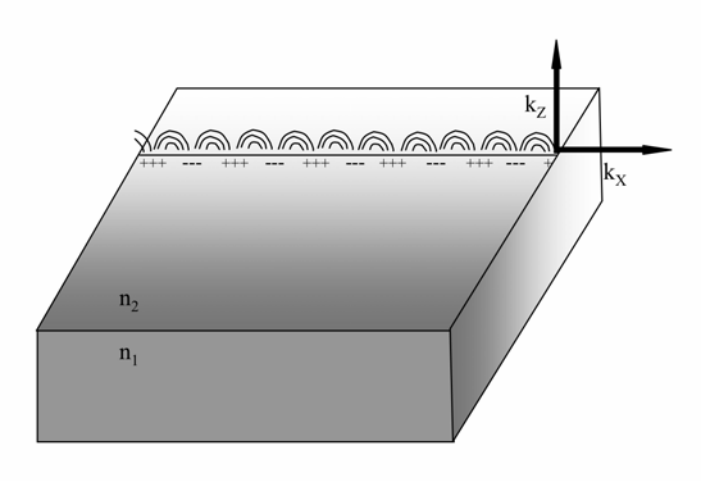


**Figure 3: Surface plasmon propagation along a conductor surface.** Charges fluctuate at the surface of a conductor with refractive index $n_1$ coupled to a medium with refractive index $n_2 > 1$. The surface plasmon propagates in x-direction (wavevector $k_X$), whereby the electrical field decays exponentially in z-direction (wavevector $k_Z$).

To excite a plasmon by light the momentum mismatch of surface plasmon mode and photon must be overcome, i. e. the dispersion curves of surface plasmon mode and light must intersect (Figure 4). The problem can be solved by coupling the conductor surface to a medium with a refractive index $n_2 > 1$. The light has to be polarized parallel to the plane of incidence (p-polarized).

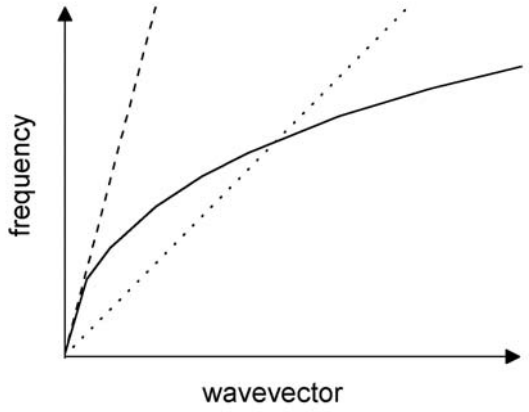


**Figure 4: Dispersion curves of surface plasmon, photon in free space and medium.** The dispersion curve for a surface plasmon (bold line), a free space photon (dashed line) and a photon in medium with refractive index $n_2 > 1$ (dotted line) are displayed, whereby the angular frequency of a photon in a medium is $\omega = k_X * c/n$ (c: velocity of light, n: refractive index of the medium).

The surface plasmon resonance instrument is constructed according to the Kretschmann-Raether configuration (Figure 5). In this set-up a laser beam passes through a triangular prism and is directed to the backside of a gold film deposited on a glass slide, i. e. the inserted chip. The inciding light is p-polarized by two polarizers. Two flow cells are mounted onto the chip to measure and compare the adsorption of biomolecules. A two-valve system allows the exchange of solutions without introducing air into the cells. A photodiode detects the reflected light.

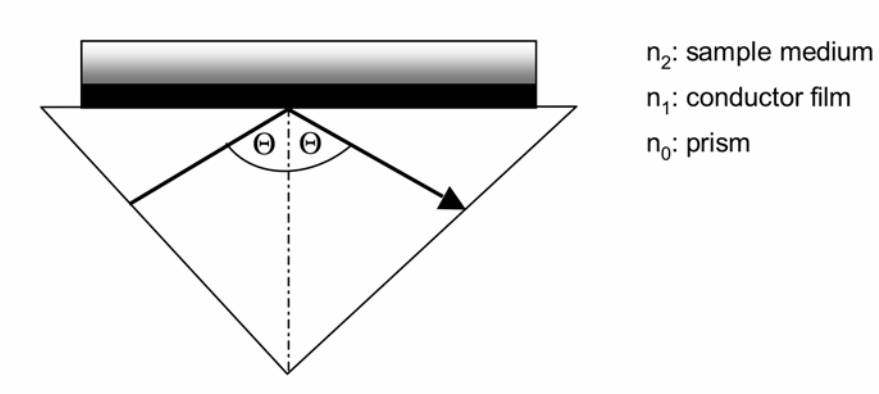


**Figure 5: Kretschmann-Raether configuration.** p-polarized light from a laser passes through a prism and is totally reflected at the interface of a thin conductor film surrounded by sample medium. Reflected light is recorded by a photodiode in dependence on the angle of the incident light.

The reflected intensity is recorded as a function of the angle of incidence θ. Due to energy absorption the minimum $\theta_{min}$ indicates the excitation of surface plasmons at the gold-solution interface (Figure 6).

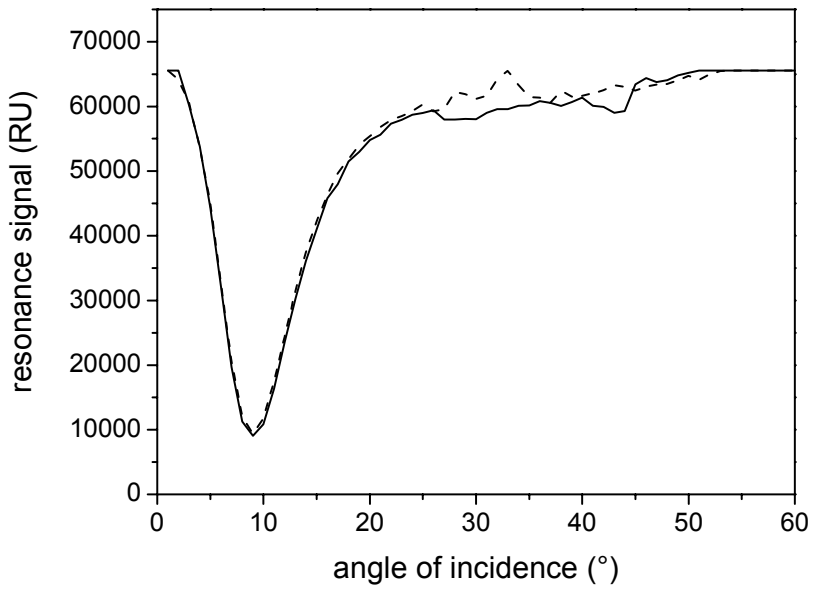


**Figure 6: Reflected light intensity in dependence on the angle of the incident light.** The intensity of the reflected light is converted into the resonance signal and depicted for both serially connected flow cells (flow cell 1: bold line, flow cell 2: dashed line).

Changes in refractive index at the conductor surface are directly reflected by a shift in the angle $\theta_{min,}$ as the dispersion relation of surface plasmon is dependent on the refractive index of the medium. Changes in the concentration of a biomolecule in the interfacial region due to physisorption are monitored in the sensogram as a function of time by measuring $\theta_{min}$. The instrument used for surface plasmon resonance studies, the BIAcore X (BIAcore, Uppsala, Sweden), records a shift in θ of 0.1 ° as 1000 resonance units, which corresponds to a change in protein concentration at the surface of about 1 ng / $mm^2$ (Stenberg et al., 1991).

## 2.2 Fluorescence correlation spectroscopy

### 2.2.1 Importance of the method

Fluorescence spectroscopy enables us to observe biomolecules even inside the living cell. Different fluorescent techniques like fluorescence recovery after photobleaching (FRAP), fluorescence correlation spectroscopy (FCS) and fluorescence resonance energy transfer (FRET) emerged. FRAP and FCS allow us to determine the lateral diffusion of biomolecules in membranes. FRAP is adequate for recording slow movements in natural membranes (diffusion coefficients of proteins in the range of $10^{-2}$ $\mu m^2/s$). FCS has a broader application spectrum than FRAP. Short diffusion times of molecules in lipid bilayers or in solution (diffusion coefficients between $10^{2}$ $\mu m^2/s$ and $10^{-1}$ $\mu m^2/s$) can be resolved far better with FCS than FRAP. Even changes in the aggregation state can be analyzed by FCS. Thus FCS is not restricted to surfaces. FCS and FRET allow us to monitor molecules with single-molecule resolution. Without averaging over an ensemble, fluctuating systems (including subpopulations) can be studied under equilibrium conditions and individual steps or intermediates of biochemical reactions can be unraveled.

### 2.2.2 Autocorrelation

In autocorrelation studies, a focused laser beam illuminates a volume element in the femtoliter range. Single molecules emitting bursts of fluorescent light quanta enter and leave the confocal volume. Thus they generate fluctuations in fluorescence which are recorded by a single photon detection unit (Avalanche photodiode) in a time-resolved manner and are analyzed statistically.

The confocal volume is ellipsoidal in shape. The confocal volume can be calculated from a cylindrical approximation (Figure 7):

$$V = \omega_1^2 \cdot \pi \cdot 2 \cdot \omega_2 = 2 \cdot \pi \cdot S \cdot \omega_1^3$$

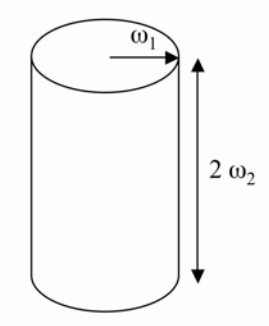


**Figure 7: Cylindrical approximation of the ellipsoidal confocal volume.**
$\omega_1$: half short axis (waist radius of the laser beam)
$\omega_2$: half long axis

The axial structural parameter S (or axial ratio AR) is introduced as $S = \omega_2 / \omega_1$ for convenience.

The particle diffusion time τ through the confocal volume can be described by

$$\tau = \frac{\omega_1^2}{4 \cdot D}$$

whereby D is the diffusion coefficient of the fluorescent molecule.

The temporal autocorrelation of the fluorescence fluctuations assuming a Gaussian distribution yields (Eigen and Rigler, 1994)

$$G(t) = 1 + \frac{1}{N} \cdot \frac{1}{1 + \frac{t}{\tau}} \cdot \frac{1}{\sqrt{1 + \frac{1}{S^2} \cdot \frac{t}{\tau}}}$$

From a fit of the autocorrelation function to the recorded correlation curve the number of molecules in the volume element and their characteristic translational diffusion times can be computed. If the size of the confocal volume is known, the molar concentration of fluorescent particles can be calculated from the particle number with regard to the Avogadro constant.

The interaction of molecules can be studied, if the diffusion time $\tau_1$ of the faster fluorescent interaction partner and the diffusion time $\tau_2$ of the slower non-fluorescent molecule differ by a factor of more than two. For dissociation rates < $10^{-1}$ $s^{-1}$ the chemical relaxation times are much larger than the characteristic diffusion times, and the interaction can be described as

$$G(t) = 1 + \frac{1}{N} \cdot \left( \frac{1 - y}{1 + \frac{t}{\tau_1} \cdot \sqrt{1 + \frac{1}{S^2} \cdot \frac{t}{\tau_1}}} + \frac{y}{1 + \frac{t}{\tau_2} \cdot \sqrt{1 + \frac{1}{S^2} \cdot \frac{t}{\tau_2}}} \right)$$

where y denotes the fraction of bound fluorescent molecule.

Considering spherical, globular molecules the diffusion coefficient can be calculated as

$$D = \frac{k \cdot T}{6 \cdot \pi \cdot \eta \cdot r}$$

k denotes the Boltzmann constant, T the absolute temperature, η the viscosity of the solution and r the hydrodynamic radius of the molecule.

The hydrodynamic radius of a spherical molecule can be described as

$$r = \sqrt[3]{\frac{3 \cdot \frac{m}{A}}{4 \cdot \pi \cdot \rho}}$$

where A is the Avogadro constant, m the molecular mass and ρ the mean density of the molecule.

### 2.2.3 Cross-correlation

In cross-correlation studies two laser beams are tightly focused in a spot and excite green- and red-fluorescent molecules upon diffusion into the illuminated volume element. The green ($\lambda_{ex}$ = 488 nm) and red ($\lambda_{ex}$ = 633 nm) fluorescence signals are dissected and recorded in time-dependent manner by two highly sensitive photodiodes. Statistical analysis of the individual green- and red-fluorescent events gives rise to two autocorrelation curves, whereas simultaneous events are merged to the cross-correlation curve. The amplitude of the cross-correlation signal indicates the ratio of co-localized green and red species to the ensemble of green and / or red species.

In cross-correlation studies the diffusion time in the confocal volume is the average of the diffusion times in the green and red detection volume. The confocal volume in the green and red channel is determined by the corresponding radii

$$V_g = \pi^{3/2} \cdot \omega_{1,g}^2 \cdot \omega_{2,g} \text{ and } V_r = \pi^{3/2} \cdot \omega_{1,r}^2 \cdot \omega_{2,r}.$$

The overlapping volume in cross-correlation is created by vectorial addition:

$$V_{gr} = \left(\frac{\pi}{2}\right)^{3/2} \cdot \left(\omega_{1,g}^2 + \omega_{1,r}^2\right) \cdot \sqrt{\omega_{2,g}^2 + \omega_{2,r}^2}\ .$$

The particle numbers are derived from the amplitudes G(0) of the two autocorrelation functions (AC,g and AC,r) and the cross-correlation function (CC)

$$G_g(0) = 1 + \frac{1}{N_{AC,g}},\ G_r(0) = 1 + \frac{1}{N_{AC,r}} \text{ and } G_{gr}(0) = 1 + \frac{1}{N_{CC}}.$$

Thus the ensemble of molecules labeled with green or red dye, respectively, can be described as

$$N_{AC,g} = N_g + N_{gr} = \frac{1}{G_g(0) - 1} \text{ and } N_{AC,r} = N_r + N_{gr} = \frac{1}{G_r(0) - 1}.$$

The number of molecules labeled with both dyes is proportional to the cross-correlation amplitude $G_{gr}(0)$

$$N_{gr} = \frac{N_{AC,g} \cdot N_{AC,r}}{N_{CC}} = \frac{\left(N_g + N_{gr}\right) \cdot \left(N_r + N_{gr}\right)}{N_{CC}}.$$

The number of molecules bearing green dye only ($N_g$) or red dye only ($N_r$) can be calculated by rearrangement of the equation above. Often the crosstalk $Q_{gr}$ of the green emission into the red channel has to be taken into consideration

$$N_g = N_{AC,g} - N_{gr} \text{ and}$$

$$N_r = N_{AC,r} - \left(Q_{gr} \cdot N_{AC,g} + N_{gr}\right)$$

$$N_{gr} = \frac{N_{AC,g} \cdot \left(N_{AC,r} + Q_{gr} \cdot N_{AC,g}\right)}{N_{CC} - Q_{gr}}.$$

The molar concentrations are calculated from the particle numbers in the corresponding confocal volumes

$$c_x = \frac{N_x}{V_x \cdot A} \text{ with x = g, r or gr,}$$

where A denotes Avogadro´s number.

### 2.3 Fluorescence resonance energy transfer

The theory of fluorescence resonance energy transfer (FRET) was developed by Theodor Förster (Förster, 1948). FRET can be described as radiationless through-space energy transfer from an excited donor (D) to and acceptor (A) fluorophore.

$$D^* + A \xrightarrow{k_T} D + A^*$$

The energy transfer results from long-range dipole-dipole interactions between the donor and acceptor. The rate of energy transfer ($k_T$) depends on the extent of spectral overlap of the emission spectrum of the donor with the absorption spectrum of the acceptor, the quantum yield of the donor, the relative orientation of the donor and acceptor transition dipoles and the distance between the donor and acceptor:

$$k_T = \frac{1}{\tau_D} \cdot \left(\frac{R_0}{r}\right)^6,$$

where $R_0$ is the Förster distance with half efficiency of FRET, $\tau_D$ the decay time of the donor in the absence of acceptor and r the donor-to-acceptor distance. Thus the rate of transfer equals the decay rate of the donor in the absence of acceptor ($\tau_D^{-1}$), if the donor-

acceptor distance r is equal to the Förster distance $R_0$. The Förster distance can be calculated by

$$R_0 = 9{,}78 \cdot 10^3 \cdot \sqrt[6]{\kappa^2 \cdot n^{-4} \cdot Q_D \cdot J(\lambda)} \quad \text{(in Å)}$$

$$\text{with } J(\lambda) = \int_0^\infty F_D(\lambda) \cdot \varepsilon_A(\lambda) \cdot \lambda^4 d\lambda ,$$

where $Q_D$ denotes the quantum yield of the donor in the absence of acceptor, n the refractive index of the medium (usually 1.4 in aqueous solution), $\kappa^2$ the orientation factor of the transition dipoles of the donor and acceptor (usually 2/3 for dynamic random averaging) and J(λ) the overlap integral of donor emission and acceptor absorption (in $cm^3M^{-1}$). The overlap integral J(λ) depends on the corrected fluorescence intensity $F_D(\lambda)$ of the donor in the wavelength range λ to λ+Δλ, the extinction coefficient $\varepsilon_A(\lambda)$ of the acceptor and the wavelength λ. Thus the Förster distance $R_0$ can be predicted from the spectral properties of the donor-acceptor pair. Förster distances range from 20 Å to100 Å.
The efficiency of energy transfer (ET) determines the fraction of photons absorbed by the donor, which are transferred to the acceptor:

$$ET = \frac{k_T}{\tau_D^{-1} + k_T} .$$

Consequently, the efficiency defines the ratio of the transfer rate to the total decay rate of the donor or

$$ET = \frac{R_0^6}{R_0^6 + r^6} .$$

The transfer efficiency displays a strong dependence on the donor-acceptor distance. Thus FRET can serve as spectroscopic ruler, but only distances ranging from 0.5 $R_0$ to 2 $R_0$ can be estimated. Consequently, FRET is applied to study distances within supramolecular assemblies and interactions between biomolecules. In practice, the transfer efficiency is derived from the relative fluorescence intensity of the donor in the absence ($F_D$) and presence ($F_{DA}$) of acceptor:

$$ET = 1 - \frac{F_{DA}}{F_D} .$$

## 2.4 Matrix-assisted laser desorption / ionization mass spectrometry

### 2.4.1 Principles

MALDI-MS determines the molecular mass of proteins by desorption of ions from an organic matrix with means of a laser pulse. The technique was developed by Michael Karas and Franz Hillenkamp from the university of Münster in 1987.

The analyte has to be cocrystallized with aromatic compounds, which are excited by UV radiation of a Nd-YAG laser or a nitrogen laser. The excitation energy leads to relaxation into the lattice and transition of molecules into the gas phase. Due to the low laser intensity ($10^6$ - $10^7$ W/cm$^2$) the analyte molecules stay intact and are protonated by the photoionized matrix. Charged molecules are accelerated in an electrostatic field (E ~ 1000 V/mm) and are separated during a drift interval because of different velocity according to their mass/charge ratio m/z. The time of flight (TOF) is measured for constant acceleration voltage and drift interval:

$$E_{kin} = \frac{1}{2} \cdot m \cdot v^2 = z \cdot e \cdot U$$

m: molecular mass of the ion

v: ion velocity after acceleration interval

z: charge factor

e: electronic charge

$$v = \frac{L}{t}$$

L: fieldless distance

t: time of flight

$$\frac{m}{z} = \frac{2 \cdot e \cdot U}{L^2} \cdot t^2$$

Thus, the mass/charge ratio is proportional to the square of the time of flight and can be calibrated with reference material.

Ion detection is accomplished with an antipolarized conversion dynode, which converts the ion flux into an electron flux (secondary electron multiplier). The analog signal of the secondary electron multiplier is subsequently amplified and digitalized by a transient recorder. With increasing ion mass secondary ions are generated by the dynode leading to temporal dispersion and thus deterioriated resolution.

### 2.4.2 Resolution and uncertainties

The resolution R = m / Δm in MALDI-TOF experiments is determined as full width at half maximum of the peak. The resolution and sensitivity of the detector decreases with higher molecular mass.

Due to uncertainties during desorption and ionization (energetic, spatial, temporal) ions with equivalent charge/mass ratio are heterogeneously distributed with respect to their kinetic energy and also time of flight. To compensate such resolution losses

1) the acceleration voltage can be increased. Then the TOF-measurement must be more precise.
2) ion reflectors can be used. A reflector introduces an antipolarized electrostatic field between two drift intervals. High-energetic ions can survive longer in this "antifield" and overcome the lag again in the subsequent drift interval. So faster and slower ions with equivalent m/z-ratio are focused at the detector position and give rise to a narrow signal.
3) delayed ion extraction can be applied. Accordingly, the electrical field is switched on with a lag to the laser pulse. High-energetic ions move farer away during the lag time and gain lower kinetic energy than low-energetic ions. So ions with identical m/z-ratio arrive simultaneously at the detector.

### 2.4.3 Fragmentation

Fragmentation can occur either during the ionization (prompt fragmentation) or in the acceleration/drift interval (metastable fragmentation, post source decay, PSD). Fragmentation is induced by collision of analyte molecules with matrix molecules and produces usually a charged fragment ion and a neutral fragment molecule. Fragment ions generated in the acceleration interval gain different kinetic energy and cause noise in the MALDI spectrum. Fragment ions produced in the drift interval cannot be separated from intact molecule ions in a linear MALDI-TOF. But in the reflector mode charged fragments are shifted to lower mass/charge values because the reflector cannot compensate for their decreased kinetic energy. This drawback is overcome by reflectors with variable voltages.

### 2.4.4 MALDI spectrum

In the MALDI spectrum several species of a molecule are analyzed. The singly charged protein ion $[M+H]^+$ dominates in the positive ion mode, but singly protonated dimer $[2M+H]^+$ and multiply protonated monomers ($[M+2H]^{2+}$, $[M+3H]^{3+}$…) are visible. The monoisotopic mass is determined from the exact atomic masses of the most frequent isotop of an element. For peptides with molecular masses <5 kDa the monoisotopic mass is determined, because it gives rise to the most intensive signal. For larger peptides and proteins the average mass is determined due to the highest signal intensity. The average mass is calculated from the average atomic distribution of the elements. Accordingly, the carbon isotopes are mainly responsible for the isotopic pattern of proteins. Due to adduct formation of peptides and proteins with water, matrix molecules and cations, e.g. $Na^+$ and $K^+$, the peaks are broadened.

# 3. Materials

## 3.1 Chemicals

| Chemicals | Manufacturer |
|---|---|
| Acetonitrile | Roth |
| Acrylamide, 30 % (w/v) mono / 0.8 % (w/v) bis | Roth |
| Agarose | Invitrogen |
| Agarose | Sigma-Aldrich |
| Alexa Fluor™ 488-$C_5$-maleimide | Molecular Probes |
| Alexa Fluor™ 594-$C_5$-maleimide | Molecular Probes |
| Alexa Fluor™ 633-$C_5$-maleimide | Molecular Probes |
| AMC | Fluka |
| Ammonium acetate | Merck |
| Ammonium peroxodisulfate | Roth |
| Ampicillin | Sigma-Aldrich |
| BSA, Fraction V | Sigma-Aldrich |
| Bromophenol blue | Roth |
| Calcium chloride | Merck |
| β-Casein, bovine, 90 % (w/w) | Sigma-Aldrich |
| Chloroacetic acid | Merck |
| Chloroform | Roth |
| Citric acid monohydrate | Fluka |
| Coomassie Brilliant Blue G 250 | Roth |
| Coomassie Brilliant Blue R 250 | Roth |
| p-Coumaric acid | Sigma |
| Cupric sulfate pentahydrate | Fluka |
| α-Cyano-4-hydroxy-cinnamic acid | Sigma-Aldrich |
| Cy3™-NHSester | Amersham Biosciences |
| Desorb solution 1 (0.5 % (w/v) SDS) | BIAcore AB |
| Desorb solution 2 (50 mM glycine, pH 9.5) | BIAcore AB |
| DMF | Merck |
| DMSO | Fluka |
| DTT | Sigma-Aldrich |

| | |
|---|---|
| EDTA | Roth |
| EDTA solution, 500 mM, pH 8.0 | Fluka |
| Ellman´s reagent | Pierce |
| Ethanol | Roth |
| Ethidium bromide | Roth |
| Fluorescein-5-iodoacetamide | Molecular Probes |
| Formaldehyde, 37 % (v/v) | Roth |
| Glacial acetic acid | Roth |
| α-D-(+)-Glucose | Roth |
| Glycerol | Roth |
| Glycine | Roth |
| HEPES | Fluka |
| $His_5$-GSGSAWRHPQGG | MPI of Biochemistry, Martinsried |
| $His_6$-Mdl1-EQ | gift from Matthias Hofacker |
| $His_6$-OpuAA | gift from Carsten Horn |
| Hydrochloric acid, 37 - 38 % (v/v) | Roth |
| Hydrogen peroxide, 30 % (v/v) | Fluka |
| Imidazole | Fluka, Merck |
| Immunoglobulin G | Sigma-Aldrich |
| Insulin, bovine | Sigma-Aldrich |
| Insulin B chain, oxidized | Sigma-Aldrich |
| Iodoacetamide | Sigma-Aldrich |
| IPTG | BTS |
| Isopropanol | Roth |
| α-Lactalbumin, bovine, type 1, 85 % (w/w) | Sigma-Aldrich |
| Luminol | Roth |
| Lysozyme, chicken | Sigma-Aldrich |
| Magnesium chloride | Roth |
| Magnesium sulfate | Merck |
| Methanol | Roth |
| Nickel chloride hexahydrate | Fluka |
| Ni-NTA Agarose | Qiagen |

| | |
|---|---|
| Ni-NTA Superflow | Qiagen |
| NTA-DODA | in house synthesis |
| NTA oligoethylene glycol thiol (NTA thiol) | in house synthesis |
| Octyl-β-D-glucopyranoside (*n*-octyl glucoside) | Fluka |
| Oligoethylene glycol thiol (matrix thiol) | in house synthesis |
| OPA-buffer | Amersham Biosciences |
| Oregon Green 488-maleimide | Molecular Probes |
| Peptone, meat | Roth |
| RRYCΨSTEL | Henklein, Charité, Berlin |
| SDS | Roth |
| Serva Blue R | Serva |
| Silver nitrate | Roth |
| Sinapic acid | Fluka |
| Sodium acetate | Roth |
| Sodium carbonate | Merck |
| Sodium chloride | Fluka, Roth |
| Sodium dihydrogenphosphate | Roth |
| Sodium iodoacetate | Sigma-Aldrich |
| Sodium thiosulfate | Roth |
| SOPC | Avanti Polar Lipids |
| Succinyl-LLVY-AMC | Bachem |
| TCEP | Molecular Probes |
| TEMED | Roth |
| Texas Red-labeled $His_6$-OpuAA | gift from Carsten Horn |
| Trichloroacetic acid | Roth |
| Trifluoroacetic acid, 98 % (v/v) | Fluka |
| Tris | Roth |
| Tween 20 | Roth |
| Uranyl acetate | Agar Scientific Ltd. |
| Yeast extract | Roth |
| Zinc chloride | Fluka |

### 3.2 Antibodies

| | |
|---|---|
| anti 20S proteasome, rabbit | gift from Drs. Erika Seemüller and Wolfgang Baumeister, MPI of Biochemistry, Martinsried |
| anti His-tag, mouse | Novagen |
| anti-rabbit, HRP-coupled, goat | Dianova |
| anti-mouse, HRP-coupled, goat | Sigma |

### 3.3 Buffers and solutions

All buffers for chromatographic purposes were sterile-filtered and degassed before use.

#### 3.3.1 Restriction analysis

One-Phor-All buffer plus (10 x):
100 mM Tris-acetate, pH 7.5
100 mM magnesium acetate
500 mM potassium acetate

#### 3.3.2 Agarose gel electrophoresis

| | |
|---|---|
| TAE-buffer : | Loading buffer (10 x): |
| 40 mM Tris, pH 8.5 | 200 mM Tris-acetate, pH 8.0 |
| 20 mM Glacial acetic acid | 10 mM EDTA |
| 2 mM EDTA | 42.5 % (v/v) glycerol |
| | 0.025 % (w/v) bromophenol blue |

#### 3.3.3 Cell culture

| | |
|---|---|
| 100 mg / ml ampicillin | 1 M IPTG |

### 3.3.4 Chromatography

#### 3.3.4.1 Immobilized metal-chelate affinity chromatography

Lysis buffer:
50 mM $NaP_i$, pH 8.0
300 mM NaCl

Zinc chloride solution:
100 mM $ZnCl_2$

Running buffer:
50 mM $NaP_i$, pH 8.0
300 mM NaCl
20 mM imidazole

Elution buffer:
50 mM $NaP_i$, pH 8.0
300 mM NaCl
500 mM imidazole

Desorption buffer:
50 mM $NaP_i$, pH 8.0
300 mM NaCl
50 mM EDTA

#### 3.3.4.2 Size exclusion chromatography

HBS buffer:
10 mM HEPES, pH 7.5
150 mM NaCl

PBS buffer:
50 mM $NaP_i$, pH 8.0
150 mM NaCl

#### 3.3.4.3 Desalting

50 mM Tris, pH 7.5

#### 3.3.4.4 Anion exchange chromatography

Running buffer:
20 mM Tris, pH 7.8
5 mM $CaCl_2$

Elution buffer:
20 mM Tris, pH 7.8
5 mM $CaCl_2$
300 mM NaCl

### 3.3.4.5 Reversed-phase chromatography

Buffer A:
0.1 % (v/v) TFA in $H_2O$

Buffer B:
0.1 % (v/v) TFA in acetonitrile

Buffer $A_1$:
100 mM ammonium acetate pH 8.0
300 mM NaCl

Buffer $B_1$:
100 mM ammonium acetate pH 8.0
300 mM NaCl
50 % (v/v) acetonitrile

### 3.3.5 SDS-PAGE

Separation-gel buffer:
1.5 M Tris, pH 8.0
0.4 % (w/v) SDS

Stacking-gel buffer:
0.5 M Tris, pH 6.8
0.4 % (w/v) SDS

Loading buffer (2-fold):
100 mM Tris, pH 6.8
40 mM DTT
4 % (w/v) SDS
20 % (v/v) glycerol
0.03 % (w/v) bromophenol blue

Running buffer:
25 mM Tris
192 mM glycine
0.1 % (w/v) SDS

### 3.3.5.1 Coomassie Stain

Stain solution:
40 % (v/v) methanol
10 % (v/v) acetic acid
0.25 % (w/v) Coomassie Brilliant Blue R250
or Serva Blue R

Destain solution :
40 % (v/v) methanol
10 % (v/v) acetic acid

#### 3.3.5.2 Silver Stain

Fixation solution :
30 % (v/v) ethanol
10 % (v/v) acetic acid

Thiosulfate buffer :
100 mM sodium acetate pH 6.0
30 % (v/v) ethanol
1 mg $NaS_2O_3$ / ml prior to use

Silver nitrate solution:
0.1 % (w/v) $AgNO_3$
0.025 % (v/v) formaldehyde 37 %

Developing solution:
2.5 % (w/v) $Na_2CO_3$
0.05 % (v/v) formaldehyde 37 %

#### 3.3.5.3 Western blot

Transfer buffer:
25 mM Tris
192 mM glycine
0.1 % (w/v) SDS
20 % (v/v) methanol

TBST buffer:
10 mM Tris pH 8.0
150 mM NaCl
0.1 % (v/v) Triton-X 100

Blocking buffer:
10 mM Tris pH 8.0
150 mM NaCl
0.1 % (v/v) Triton-X 100
7 % (w/v) lactalbumin
0.1 % (w/v) $NaN_3$

### 3.3.6 Liposome preparation and unique immobilization of proteasomes

HBS buffer:
10 mM HEPES, pH 7.5
150 mM NaCl

1 M imidazole, pH 7.5

### 3.3.7 Surface plasmon resonance studies

HBS-N buffer (BIAcore):
10 mM HEPES, pH 7.4
150 mM NaCl
filtered and degassed
for studies on NTA dextran surfaces 150 mM NaCl (solid) and 50 µM EDTA (from a 500 mM stock solution) were added
for studies on self-assembled thiol layers 150 mM NaCl (solid) and 5 mM imidazole (from a 1 M stock solution) were added

### 3.3.8 Activity assay

13 mM Suc-LLVY-AMC in DMF

Stopping reagent:
100 mM acetic acid, pH 4.3
100 mM chloroacetic acid

### 3.3.9 Digestion assays

Stopping reagent:
72 % (w/v) TCA

## 3.4 Media

### 3.4.1 LB medium

10 g peptone / l
5 g yeast extract / l
10 g NaCl / l
pH 7.5
The medium is autoclaved for 20 min at 121 °C, 2 bars.

### 3.4.2 SOB medium

20 g peptone / l

5 g yeast extract / l

0.5 g NaCl / l

pH 7.5

The medium is autoclaved for 20 min at 121 °C, 2 bars.

Afterwards the magnesium salts are added:

10 ml 1 M $MgCl_2$ (sterile)

10 ml 1 M $MgSO_4$ (sterile)

### 3.4.3 SOC medium

By adding 20 ml 20 % (w/v) glucose (sterile) to 1 l SOB medium the SOC medium is obtained.

### 3.4.4 Agarose plates

10 g peptone / l

5 g yeast extract / l

10 g NaCl / l

20 g low melting agarose / l

pH 7.5

The medium is autoclaved for 20 min at 121 °C, 2 bars. When the medium has cooled down to 50 °C, 100 µg / ml sterile ampicillin is added and the petri dishes are filled with 20 ml medium each. After solidification the plates are stored at 4 °C.

## 3.5 Kits

| | |
|---|---|
| Bio-Rad Protein Assay | Bio-Rad |
| Micro BCA™ Protein Assay Reagent | Pierce |
| Nucleo Spin™ plasmid kit | Macherey-Nagel |

### 3.6 Molecular weight markers

| | |
|---|---|
| DNA ladder (1 kb) | Invitrogen |
| Protein marker (14-116 kDa) | Fermentas |
| Prestained protein ladder | Fermentas |
| Prestained protein marker (20-122 kDa) | Peq-Lab |
| Silver stain molecular weight standard (wide range: 7 -180 kDa) | Sigma-Aldrich |

### 3.7 Restriction endonucleases

| | |
|---|---|
| *Bam* HI | New England Biolab |
| *Hind* III | New England Biolab |

### 3.8 Plasmids and strains

#### 3.8.1 pRSET5a and 6a

The genes for the two different subunits of the *Thermoplasma acidophilum* proteasome were cloned into the expression vectors pRSET5a and 6a from *E. coli* (4.3 kbp). The plasmid encodes the proteasomal α- and β-subunit with the His-tag attached to either the N- or C-terminus of the α-subunit or the C-terminus of the β-subunit in tandem under control of the IPTG-inducible T7-promotor. The plasmids were kind gifts from Drs. Erika Seemüller, Andreas Theß and Wolfgang Baumeister (Max-Planck-Institute of Biochemistry, Martinsried). In the inactive mutant (T1A) the catalytically active Thr1 of the β-subunit was replaced by Ala (Seemüller et al., 1995a).

#### 3.8.2 *E. coli* BL21(DE3)

$F^-$ *ompT hsd* $S_B$ ($r_B^-$ $m_B^-$) *gal dcm* (DE3)

This strain is protease-deficient, but encodes genomically T7-RNA polymerase.

### 3.9 Equipment

| Apparatus | Manufacturer |
|---|---|
| Äkta 100 Explorer | Amersham Biosciences |
| Agarose gelelectrophoresis apparatus | Institute workshop |
| Autoclave 5075 ELVC | Tuttnauer Systec |
| BIAcore X | BIAcore AB |
| Cary 50 Bio UV Vis spectrophotometer, Varian | Cary |
| Confocor 2 | Zeiss |
| Digital camera DC 290 | Kodak |
| Fluorolog-III Jobin | Yvon-Spex Instruments |
| FPLC apparatus | Amersham Biosciences |
| Gatan Megascan 2k x 2K CCD camera | Gatan, Inc., Pleasanton, CA |
| Incubator Kelvitron t | Heraeus |
| Infors Unitron | Infors AG, Bottmingen, Switzerland |
| Ino Lab pH-meter | WTW, Weilheim |
| Kern 770 microbalance | Kern |
| Liposofast Extruder | Avestin, Ottawa |
| Lumi Imager F1 | Roche |
| Lyovac GT 2 | Leybold-Heraeus |
| Magnetic Stirrer | Ikamag Ret |
| Membrane vacuum pump | Kobe, Marburg |
| Mettler PM 400 balance | Mettler |
| Mettler PM 460 balance | Mettler |
| Microwave T.D.S. | Samsung |
| Milli Q-Plus water system | Millipore |
| Oil vacuum pump | AEG |
| Philips CM 120 electron microscope | FEI, Eindhoven |
| Polarstar Galaxy | BMG |
| Power supply Elite 300 plus | Polymehr systems |
| SDS-PAGE apparatus | Institute workshop |
| SMART system | Amersham Biosciences |
| Tank blot apparatus | Institute workshop |

| | |
|---|---|
| Thermomixer | Eppendorf |
| Thermo Spectronic spectrophotometer | Helios |
| Unijet II Refrigerated Aspirator | Uni Equip, Martinsried |
| Univapo 100 H | Uni Equip, Martinsried |
| UV-Transilluminator UVT-20 M/W | Herolab |
| Vortexer | Bender & Hobein AG |
| Voyager De-Pro mass spectrometer | Perspective Biosystems, Framingham, MA |

### 3.9.1 Centrifuges and rotors

| Centrifuge | Rotor |
|---|---|
| Eppendorf Centrifuge 5417R | F-45-30-11 |
| Heraeus Sepatech Megafuge 1.0 R | BS4402/A |
| Sorvall RC 3C Plus | H6000A |
| Sorvall RC 5B Plus | SS34 |

### 3.9.2 Columns

| | |
|---|---|
| Hi Trap Chelating HP (1 ml) | Amersham Biosciences |
| Superose 6 HR10/30 (24 ml) | Amersham Biosciences |
| Sephadex G 25, PD10 (8.3 ml) | Amersham Biosciences |
| Resource Q (1 ml) | Amersham Biosciences |
| µRPC C2/C18 SC2.1/10 (0.35 ml) | Amersham Biosciences |

### 3.9.3 Sensor Chips

| | |
|---|---|
| Sensor chip HPA | BIAcore AB |
| Sensor chip NTA | BIAcore AB |
| NTA-thiol chip | Ali Tinazli |

### 3.10 Supplementary materials

| | |
|---|---|
| Cuvettes, quartz glass | Hellma |
| Cuvettes, plastic | Fisher Scientific |
| Dialysis tube (12 -16 kDa MWCO) | Biomol |
| *E. coli* Pulser™ cuvettes, 2 mm electrode gap | Biorad |
| Eppendorf tubes | Greiner |
| Filter paper | Whatman |
| Flow cell IFC5 (2.4 x 0.5 x 0.05 mm, 2 x 0.06 µl) | BIAcore AB |
| Glass slide D 263 | Präzisions Glas & Optik Iserlohn |
| Gloves, latex | Terumo Teruglove |
| Gloves, nitril | Servoprax |
| Lab-Tek chambered coverglass, 8 wells | Nalge Nunc International |
| Microliter™ syringes | Hamilton |
| Nitrocellulose membrane | Schleicher & Schüll |
| Pasteur pipettes | Merck |
| Pipettes | Abimed |
| Pipette tips | Greiner |
| Polycarbonate membranes, P.D. 100 nm | Avestin, Ottawa, Canada |
| Spectra Por™ dialysis tube (6 - 8 kDa MWCO) | Roth |
| Spin concentrators, Amicon, 30 kDa MWCO | Millipore |
| Sterile filters | Millipore |
| Sterile filters, single use | Roth |
| Test tubes, sterile, 15 and 50 ml | Greiner |

# 4. Methods

## 4.1 Biological methods

### 4.1.1 Preparation of electrocompetent cells

The cells carry no resistence genes. Therefore the following steps were performed with autoclaved pipettes, vessels and liquids.

40 ml LB medium were inoculated with *E. coli* BL21(DE3) cells and grown overnight at 37 °C in a shaker. 500 ml LB medium were inoculated 1 : 100 with the overnight culture. Cells were grown up to the midlogarithimc phase ($A_{600}$ = 0.5) before harvesting (5000 g, 20 min, 4 °C). The cell pellet was washed several times in glycerol to remove ions. For this purpose, the cells were resuspended in 10 % (v/v) glycerol and recentrifuged (5000 g, 20 min, 4 °C), thus reducing the suspension volume from 500 ml to 500 µl in three steps (250 ml, 50 ml and 500 µl). The final suspension was snap-frozen in aliquots of 50 µl and stored at -80 °C.

### 4.1.2 Transformation

100 ng plasmid DNA and 50 µl electrocompetent *E. coli* BL21(DE3) cells were pulsed in an electroporation cuvette (U= 2.5 V, C = 25 µF, time constant ~ 5 s) after twofold dilution with $H_2O$. The transformants were afterwards grown for 1 h at 37 °C in 1 ml SOC medium in order to express the ampicillin resistence gene. By plating 100 µl medium on agarose with 100 µg ampicillin / ml and overnight incubation at 37 °C, positive transformants were selected.

### 4.1.3 Mini preparation

A mini preparation is the rapid, small-scale preparation of pure plasmid DNA.

Pelleted bacterial cells are lysed in the alkaline milieu by addition of SDS in the presence of RNase A. SDS disrupts the membranes and induces release of the cell contents. DNA and proteins are denatured in the alkaline medium. RNase A digests the liberated RNA. The lysate is neutralized. High-salt conditions lead to precipitation of SDS, denatured proteins and cellular debris. Chromosomal DNA, which adheres to the cellwall, is co-precipitated, whereas plasmid DNA renatures and remains in the supernatant. In the absence of SDS, the supernatant is loaded on a pre-equilibrated anion exchange column. Only plasmid DNA binds, while degraded RNA and proteins appear in the flow through.

By washing with ethanolic buffer non-specific hydrophobic interactions are disrupted, thus removing remaining contaminations. In the last step pure plasmid DNA is eluted repetitively with $H_2O$ at pH 8.5.

5 ml LB medium with 100 µg ampicillin / ml were inoculated with an ampicillin-resistent transformant from a plate and grown overnight at 37 °C in a shaker. The plasmids were isolated according to the Nucleo Spin$^{TR}$ plasmid kit manual. The eluted plasmid DNA was sequenced after quantification of DNA.

### 4.1.4 Restriction endonuclease cleavage

Restriction analysis is applied to characterize, identify or isolate double-stranded DNA molecules via enzymatic digestion. Type II-restriction enzymes are endonucleases of bacterial origin. Their recognition sites are palindromic and comprise 4-8 nucleotides. These restriction endonucleases cleave phosphodiester bonds at or near the recognition site and generate sticky ends or blunt ends with a 3´-hydroxyl group and a 5´-phosphate group. Simultaneous or subsequent restriction with multiple endonucleases allows to localize their recognition sites on the original fragment after gel-electrophoretic size determination of generated overlapping fragments.

pRSET6a-plasmids encoding the proteasomal subunits (500 ng) were digested for 1 h at 37 °C with 5 U *Bam* HI or / and 5 U *Hind* III in OPA-buffer (Amersham Biosciences). The digested samples were dissolved in loading buffer and applied to an agarose gel.

### 4.1.5 Agarose gel electrophoresis

The length of linear double-stranded DNA can be estimated by gel electrophoresis. Rapid quantitation of plasmid DNA is possible by simultaneous calibration. After cleavage of plasmid DNA with restriction endonucleases the sequence of the cleavage sites can be determined.

Agarose or polyacrylamide gels are conventionally used for electrophoretic separation of DNA. The negative charge of nucleic acids is generated by the phosphate groups of the DNA-backbone and therefore maintained over a wide range of pH. The molecular mass / charge ratio is constant for nucleic acids and without influence on the separation. The electrophoretic mobility of linearized nucleic acids < 10 kb can be explained by two theories. According to Ogston-sieving nucleic acids adopt a globular conformation, which

leads to collisions with the pores of the gel and thus retention. The reptation theory implies that nucleic acids are arranged end-on in the electric field and migrate according to their size by slower or faster reptation.

The nucleic acid length in bp can be calibrated with length standards. By increasing the agarose concentration of the gel, the separation range of linear double-stranded DNA is shifted to smaller molecules. 1 % (w/v) agarose is optimal for nucleic acids of 0.5 kb–6 kb. The electrophoretic mobility of nucleic acids is dependent on the conformation. Superhelical DNA migrates faster than linearized DNA and relaxed DNA slower.

For DNA-staining in gel or after electrophoresis, ethidium bromide is used because of intercalation between the stacked heteroaromatic ring systems of the bases. The dye can be excited by UV-light (254 - 366 nm) and emits orange light (590 nm). The binding to DNA enhances the fluorescence, thus surpassing the background signal. With ethidium bromide 10 – 20 ng double-stranded DNA can be detected.

For preparation of the gel, 1 % (w/v) agarose was molten in TAE buffer. After equilibration to 50 °C, ethidium bromide (6 $*10^{-5}$ % (w/v)) was added and the gel was poured in a horizontal minigel apparatus. The comb for the samples was immediately placed at one end of the gel. After 20 min, the samples dissolved in loading buffer were applied to the gel. DNA marker X was used as standard. The agarose gel was run for 1 h at 100 V and photographed for documentation.

### 4.1.6 DNA sequence analysis

The dideoxy method was developed by Sanger in 1975 to determine the primary structure of DNA. After denaturation of double-stranded DNA and neutralization, a primer is hybridized with the single-stranded DNA. A new complementary strand is synthesized by a thermostable DNA polymerase, thus elongating the primer. Each sample contains besides DNA, 2′-deoxynucleotides (d NTP), DNA polymerase and primer 2′,3′-dideoxy-nucleotides (dd NTP), which terminate the DNA strand synthesis because of their missing 3′-hydroxyl group. The four different 2′,3′-dideoxynucleotides are each labeled with a fluorophore possessing distinct emission characteristics. As the ratio of d NTP / dd NTP is 200 : 1, the labeled dd NTP terminates the strand synthesis at all possible stages. After denaturation of the DNA strands, they are electrophoretically separated in a capillary gel

according to their size. The DNA sequence can be determined from the emission of the fluorescent DNA strand during elution.
200 ng pure plasmid DNA and primer, which hybridizes with the T7-promotor, were necessary for analysis of the proteasome α-subunit sequence in the pRSET6a-plasmid.

### 4.1.7 Cryostocks

4 ml LB medium with 100 µg ampicillin / ml were inoculated with the transformants from the plate and grown overnight at 37 °C. Cells from 1.5 ml medium were spun down in cryotubes. After discarding the supernatant, the cells were resuspended in 500 µl LB medium containing 50 % (v/v) glycerol, snap-frozen and stored at – 80 °C.

### 4.1.8 Cell culture

40 ml LB medium with 100 µg ampicllin / ml were inoculated either with ampicillin-resistent transformants from the agarose plate or a cryostock and grown overnight at 37 °C in a shaker. 1 l LB medium with 100 µg ampicllin / ml was inoculated with the overnight culture. Cells were grown up to the midlogarithmic phase ($A_{600}$= 0.6) for induction of protein expression with 1 mM IPTG. Before induction and after proteasome expression 500 µl cell medium were removed for SDS-PAGE, respectively. After 4 h or overnight expression, cells were harvested in the Sorvall RC 3C Plus centrifuge (20 min at 4000 g, 4 °C). The pelleted cells were resuspended in residual LB medium and recentrifuged in the Heraeus Sepatech Megafuge 1.0 R (15 min at 4000 g, 4 °C). The pellet was snap-frozen and stored at – 80 °C.

## 4.2 Biochemical methods

### 4.2.1 Purification of His-tagged proteasomes

#### 4.2.1.1 Cell lysis

During cell lysis the protecting outer walls of the cytosol are disrupted to yield the posttranslationally assembled proteasome. Lysozyme hydrolyzes the β-1,4-glycosidic bonds of the peptidoglycane murein, which forms one layer of the cell wall in *E. coli*. Subsequent ultrasonification disrupts the plasma membrane ending up in the cell lysate.
The cell pellet was thawn on ice in 5 ml lysis buffer and incubated in the presence of a spatula tip lysozyme for 30 min at 4 °C. The cells were lysed by ultrasonification

(12 pulses of 15 s at 40 % continuous output of the Branson sonifier). The lysate was cleared from cell debris by centrifugation (37,000 g, 30 min, 4 °C, SS34-rotor).

#### 4.2.1.2 Immobilized metal-chelate affinity chromatography

The 'IMAC' is applied to separate His-tagged biomolecules via complex formation from the rest of low-affine binders or non-binders. The column material consists of agarose crosslinked with the tridentate ligand iminodiacetate. After loading with transition metal ions like $Zn^{2+}$ an octahedral complex is formed with molecules, e.g. proteins, bearing two vicinal histidines. The binding specificity is enhanced in the presence of low concentrations of imidazole, which competes with histidines for metal binding sites. His-tagged proteins are eluted in the order of increasing complex stability with an imidazole gradient or a pH gradient.

The supernatant from the centrifugation step was applied to a Hi Trap metal chelating column at the Äkta system. Previously the column was loaded with 2 ml 100 mM zinc chloride at a flow rate of 200 µl/min, excessive metal ions were removed with $H_2O$ and the column was equilibrated with 10 column volumes (CV) of phosphate buffer containing 20 mM imidazole at a flow rate of 3 ml/min. The supernatant (~ 6 ml) was injected in three fractions followed by washing with the double volume of running buffer at a flow rate of 1 ml/min, while the flow through was collected. After washing the column with 10 CV of running buffer, His-tagged proteasomes were eluted at a flow rate of 2 ml/min by applying a step gradient of imidazole (0 – 20 % B for 10 CV, 35 % B for 3 CV, 35 – 100 % B for 20 CV). Protein absorption was recorded at 280 nm, 260 nm and 216 nm. The zinc ions were desorbed with the EDTA of the desorption buffer (5 CV) and the column was washed with $H_2O$ (5 CV) before equilibrating it with 20 % ethanol (5 CV) for longterm storage.

#### 4.2.1.3 Size exclusion chromatography

The 'SEC' separates molecules according to their molecular mass due to different permeation of analytes in a porous matrix. High-molecular-weight compounds are impeded from diffusing into pores and elute in the void volume $V_0$ with the solvent. Low-molecular-weight substances move according to their size in the internal pore volume and the inter-bead volume. Thus they are retained on the column and are eluted within a characteristic elution volume $V_e$.

For separation of contaminating proteins the obtained fractions from the IMAC were concentrated in Centriplus (MWCO: 30 kDa) to a final volume of 500 µl in the presence of 2 mM EDTA and loaded at the Äkta system on a Superose 6 column pre-equilibrated with 50 mM NaPi, 150 mM NaCl, pH 7.5 (phosphate buffer) or 10 mM HEPES, 150 mM NaCl, pH 7.5 (HEPES buffer) (2 CV). While recording the absorbance at 280 nm, 260 nm and 216 nm, the protein was eluted with 1.5 CV at a flow rate of 500 µl/min.
For column calibration 500 µl of a solution containing 0.5 % (w/v) each of aldolase (158 kDa), katalase (232 kDa) and thyroglobulin (669 kDa) in phosphate buffer were loaded after sterile filtration and eluted under the same conditions. For each standard substance the logarithm of its molecular mass was plotted against the elution volume. The corresponding molecular mass of the His-tagged proteasome was derived from a linear fit.

#### 4.2.1.4 Storage

C- and N-terminally His-tagged proteasomes could be stored in HEPES buffer at 4 °C for 8 weeks and 4 weeks, respectively. The activity towards fluorogenic tetrapeptides (4.2.7.1) was checked weekly and stayed constant over the respective period. In phosphate buffer, the peptidolytic activity of proteasomes dropped much faster, i.e. after two weeks. For surface plasmon resonance studies the proteasomes were snap-frozen after addition of 10 % (v/v) glycerol as cryoprotectant and stored at -80 °C.

### 4.2.2 Purification of lactalbumin and casein

#### 4.2.2.1 Anion exchange chromatography

The ion exchange chromatography is applied to selectively bind proteins due to their charge to a countercharged matrix and desorb the molecules with increasing ionic strength of the mobile phase in a subsequent step. A protein is negatively charged mainly due to deprotonated side chains of aspartic acid or glutamic acid residues, if the pH of the medium is more than two pH-units above the isoelectric point of the protein. In this state the protein can be bound to a matrix bearing quaternary ammonium groups (anion exchanger) by Coulomb attraction, although it has to compete with other anions. After washing, the protein is eluted from the column by running a gradient of sodium chloride or a pH gradient.

At the Äkta system a Resource Q column (Amersham Biosciences) was flushed at a flow rate of 3 ml/min with 10 CV of running buffer to remove the ethanol. Afterwards elution buffer was run through the column until the $A_{280}$, $A_{260}$ and $A_{216}$ were negligible. Now the anion exchange column was equilibrated with 8 CV of running buffer before 500 µl of a solution containing 7 mg lactalbumin or 15 mg casein in running buffer were injected onto the column at a flow rate of 1 ml/min. The unbound sample was removed with 2 CV of running buffer. The bound protein was eluted with elution buffer at a flow rate of 1 ml/min by applying a linear gradient (0 – 100 % B, 50 CV). Lactalbumin or casein eluted in the first $A_{280}$ peak at 75 mM or 165 mM NaCl, respectively. Additional 12 CV of elution buffer were run through the column at a flow rate of 3 ml/min. The anion exchange column was washed with 12 CV of running buffer before flushing it with 20 % ethanol for storage.

#### 4.2.2.2 Dialysis

The dialysis is used to remove salts or to change the buffer composition. The sample is stirred in the fastened tube at 4 °C in water or buffer while repetitively exchanging the medium. The diffusion rate through the membrane is dependent on the concentration gradient of the diffusing molecules, the diffusion constant, the membranous surface and the temperature. The cutoff-value (characterizing the pore size, e.g. of regenerated cellulose) determines the molecular mass of globular proteins, which are excluded to 90 % from the membrane.

Lactalbumin and casein fractions, respectively, were filled without air bubbles in a dialysis tube, which was previously swollen in water to remove heavy metal ions, and dialyzed overnight against the 200-fold volume of $H_2O$ in Spectra Por dialysis tubes (Roth, MWCO: 6-8 kDa).

#### 4.2.2.3 Lyophilization

By lyophilization proteins can be dried without denaturation. The solvent is sublimated in the vacuum from a frozen solution and the vapour is condensed simultaneously in the apparature. The lyophilized proteins can be attributed a high surface/mass ratio. Thus they are lyophilic and very hygroscopic.

The dialyzed lactalbumin or casein was fractionated and snap-frozen. The frozen solvent was sublimated in the oil vacuum (~ 10 Pa), while the vapour was deposited at a cooled

condenser. The lyophilization was finished when the pressure in the chamber ceased to rise. The lyophilized protein was stored at -20 °C in a sealed cup.

### 4.2.3 Liposome preparation

#### 4.2.3.1 Preparation of lipid films

Vials were thoroughly rinsed with $H_2O$, methanol and chloroform. Lipid films were prepared by injecting 180 nmoles SOPC, 20 nmoles NTA-DODA with or without 20 nmoles $NiCl_2$ in a vial and evaporating the solvents (chloroform and methanol) in the vacuum. Dried lipid films were stored at -20 °C.

#### 4.2.3.2 Lipid extrusion

Intermediate-sized unilamellar vesicles (IUVs) are obtained by passing liposomes through membrane filters of a defined pore size (100 nm pore diameter). “Nucleation track” membranes consist of a thin sheet of polymer e.g. polycarbonate with straight-sided pore holes. Due to laser irradiation and chemical etching the pores are uniform in diameter. During extrusion liposomes display flexibility in squeezing through the pores. Large liposomes are broken up and decrease in size after resealing. Finally, after multiple passes through the membrane, the average diameter of the rather homogenous liposome population is slightly smaller than the membrane pore diameter and the liposomes are unilamellar.

For vesicle preparation lipid films were swollen for 1 h at 30 °C in 1 ml degassed HBS-N buffer (BIAcore). Lipid extrusion was performed repetitively (21 times) through polycarbonate membranes (100 nm pore diameter) with a LiposoFast Extruder (500 µl-syringes). Liposomes without $NiCl_2$ were directly used for SAM formation and proteasome immobilization at the BIAcore system. Liposomes with $NiCl_2$ were tested at the BIAcore system before performing activity studies at the fluorescence spectrometer.

### 4.2.4 Uniform immobilization of proteasomes

#### 4.2.4.1 Orientated immobilization of proteasomes at lipid interfaces

Different His-tagged proteasomes were incubated with nickel-loaded liposomes for 3 h at 4 °C in HBS-N buffer on a shaker before recording substrate degradation.

For experiments with fluorogenic tetrapeptides, His-tagged proteasomes (11 nM) were incubated with nickel-loaded liposomes in molar chelator lipid / proteasome ratios of 909 : 1, 140 : 1, 56 : 1 and 14 : 1 in the presence or absence of 250 mM imidazole. The sample volume amounted to 70 µl after adding 125 µM Suc-LLVY-AMC for reaction onset.
For experiments with fluorescein-labeled casein, the proteasomes were dialyzed overnight into HEPES buffer and incubated at a final concentration of 160 nM with nickel-loaded liposomes in a molar chelator lipid / proteasome ratio of 80 : 1 in the presence or absence of 100 mM EDTA.

#### 4.2.4.2 Immobilization of proteasomes to NTA agarose material

'Ni-NTA Superflow' material was supplied nickel-loaded as a 50 % stock solution in ethanol (nominal binding capacity: 1 mg His-tagged protein/ml). Prior to docking of proteasomes the beads were pre-equilibrated with 50 mM NaPi, 150 mM NaCl, pH 8.0 (phosphate buffer, pH 8.0) by washing the pellet (500 g, 5 min, 4 °C) three times with an equal volume of buffer and discarding the supernatant after centrifugation. The final pellet was diluted twofold with phosphate buffer, pH 8.0. 40 µl 'Superflow' material with a binding capacity of 20 µg His-tagged protein were incubated with 6.7 µg His-tagged proteasomes for 3 h at 4 °C on a shaker before measuring substrate degradation at the fluorimeter.

### 4.2.5 Protein and sulfhydryl determination

#### 4.2.5.1 Micro-BCA assay

Proteins are oxidized by $Cu^{2+}$ in the alkaline milieu to $Cu^{+}$, which forms a violet complex with two bicinchonic acid (BCA) molecules. Complex formation is read out at 562 nm. The method is applied to protein concentrations of 1 - 15 µg/ml. BSA is used as calibration standard. Reducing substances and high amounts of detergents interfere with the reaction.
At first BSA was diluted (six concentrations in the range of 1 – 15 µg/ml). The working reagent was prepared by mixing 4 % (w/v) $CuSO_4 * 5\ H_2O$ and 4 % (w/v) bicinchonic acid in a ratio of 1 : 24. Afterwards the volume was diluted twofold by adding an alkaline solution of sodium tartrate. For the onset of the reaction 1 ml working reagent was added to 1 ml sample. Standards and blanks were handled accordingly. Incubation proceeded for 60 min at 60 °C. After equilibration to room temperature the absorption of all samples was

measured at λ = 562 nm in triplicate against the blank. The averages of the standard absorptions were plotted against the standard concentrations. The sample concentrations were calculated from a linear fit.

#### 4.2.5.2 Bradford assay

Due to binding of Coomassie Brilliant Blue G 250 to aromatic and basic regions of a protein the absorption maximum of the dye is shifted from 465 nm to 595 nm. The reaction is finished after 2 min, and the absorption at 595 nm is stable for up to 1 h, until the dye-protein complex aggregates. By application of the micromethod 1 – 20 µg/ml protein can be quantified in a sample. The quality of the method depends on the amino acid composition of the protein and on an optimal standard (usually BSA). Alkali and high detergent concentrations disturb the reaction.

At first, BSA as protein standard was diluted (seven concentrations in the range of 1 - 20 µg/ml). For the reaction, 200 µl Biorad reagent were added to 800 µl sample. Standards and blanks were handled accordingly. After 5 min incubation at room temperature, the absorption of all samples was measured in triplicate against the blank at λ = 595 nm. The averages of the standard absorptions were plotted against the BSA-concentration. The sample concentrations were determined from a linear fit.

#### 4.2.5.3 Ellman´s assay

Sulfhydryl groups are quantitated in solution by reaction with the homodisulfide 5,5-dithio-bis(2-nitrobenzoic acid), abbreviated DTNB (Ellman, 1959). The nucleophilic substitution yields a mixed disulfide and 2-nitro-5-mercaptobenzoate as a yellow product ($\varepsilon_{412}$ = 14,150 l $mol^{-1}$ $cm^{-1}$ at pH 7.6 - 8.6). The merit of Ellman was to introduce carboxyl groups in the well-known bis(p-nitrophenyl)disulfide in order to attain a water-soluble educt at alkaline pH. The reaction is generally applicable to physiological fluids. It is highly specific for sulfhydryl groups, very sensitive, and needs only short reaction times.

At first, calibration standards were prepared by diluting *D*-cysteine in 0.1 M $NaP_i$, pH 8.0 (nine concentrations in the range of 10 - 800 µM cysteine). In the next step, Ellman´s reagent solution was prepared by dissolving 4 mg Ellman´s reagent in 1 ml 0.1 M $NaP_i$, pH 8.0 and diluting it 51-fold in the same buffer. Subsequently 25 µl of each sample (standards and blanks accordingly) were pipetted in duplicate in a microtiter plate. The

reaction was started by adding 255 µl Ellman´s reagent solution in each well. After 15 min incubation at room temperature the absorbance was measured at $\lambda$ = 405 nm in the ELISA-Reader. The averaged standard absorptions were plotted against the sulfhydryl concentrations. The sulfhydryl concentrations of the samples were determined from a linear fit.

### 4.2.6 SDS-PAGE and Western Blotting

#### 4.2.6.1 SDS-PAGE

SDS treatment of the samples dissociates non-covalent protein complexes into single subunits. Reducing agents like 2-mercaptoethanol of DTT are necessary to reduce disulfide bonds. Hence the secondary, tertiary and quaternary structures of the protein are destroyed and polypeptide chains are unwound to filaments. As proteins associate with anionic SDS, the netto charge of the protein is overcome producing identical charge-mass ratios and uniform ellipsoidic forms. In the electrical field polyanions are separated according to their molecular mass by the meshes of the polyacrylamide gel.

The discontinuous separation with separate stacking / separation gels and glycine in the electrode buffer was first described by Lämmli (Lämmli and Quittner, 1974). Electrophoresis was performed at room temperature in a vertical flat bed apparatus (Studier, 1973) with a plate size of 120 mm x 80 mm and a gel thickness of 0.75 mm. In a gel chamber eight stacked minigels were prepared simultaneously. For lower molecular masses (15 -30 kDa) separation gels containing 15 % (w/v) acrylamide are adequate.

*Separation gel* (15 % (w/v) acrylamide)

| | |
|---|---|
| $H_2O$ | 18.75 ml |
| Separation gel buffer (4x) | 18.75 ml |
| Acrylamide solution (30 % (w/v)) | 37.5 ml |
| APS (10 % (w/v)) | 300 µl |
| TEMED | 70 µl |

The components were mixed, finally adding APS (radical initializer) and TEMED (radical stabilizer) to catalyze the polymerization. The liquid was immediately overlaid with a

cushion of isopropanol to form a uniform border line. After polymerization (approximately 1 h), the isopropanol was decanted and washed off with $H_2O$.

*Stacking gel* (4.5 % (w/v) acrylamide)

| | |
|---|---|
| $H_2O$ | 21 ml |
| Stacking gel buffer (4x) | 8.75 ml |
| Acrylamide solution (30 % (w/v)) | 5.25 ml |
| APS (10 % (w/v)) | 210 µl |
| TEMED | 70 µl |

The stacking gel was poured in the same manner. Combs for the samples were inserted before polymerization (30 min). Wetted minigels can be stored for up to two weeks at 4 °C without severe effects on the resolution.
Samples were dissolved in 2x-loading buffer adding 40 mM DTT and incubated for 5 min at 95 °C. Only whole cells and pellets were incubated in sample buffer with DTT for 10 min at 95 °C and centrifuged afterwards (20,800 g, 10 min). 20 µl of the supernatants were applied to the gel. For molecular mass calibration 3 - 8 µl of protein marker were used. The gel was run at 80 V in the stacking gel and for 100 min at 150 V in the separation gel.

#### 4.2.6.2 Coomassie Stain

After electrophoretic separation of the proteins, the bands were fixed with acetic acid and stained by incubating the gel for at least one 1 h in a solution of Coomassie Brilliant Blue R250 or Serva Blue R. Excessive dye was removed with acetic acid until distinct protein bands were visible. The sensitivity of the method depends on the amino acid composition of the protein (100 ng – 1 µg).

#### 4.2.6.3 Silver Stain

The Silver Stain is 10 fold - 100 fold more sensitive than the Coomassie Stain and can detect less than 10 ng protein. After fixation of the protein bands with acetic acid, contaminations are reduced with $Na_2S_2O_3$. Rinsing of the gel with $H_2O$ is required to remove excessive $Na_2S_2O_3$ which would otherwise react with the silver reagent to form

black silver sulfide. In the next step, the protein (functional groups and peptide bonds) reduces silver ions to silver nuclei. Harsh reductive agents like formaldehyde initiate reduction of all silver ions in the gel, but the silver nuclei dominate in growth and stain the protein bands black. The reaction is terminated by shifting the pH with acetic acid.

For a Silver Stain, the gel is incubated for 15 min in 50 ml fixation solution. In the next step the gel is shaken for 15 min in 50 ml thiosulfate buffer. Afterwards the gel is rinsed with $H_2O$ (4 x 5 min). For staining it is incubated for 30 min in 50 ml silver nitrate solution. After rinsing the gel with $H_2O$ the developing solution (100 ml) is added stepwise (2 x 20 ml, 1 x 60 ml) to enhance the contrast. The development of the gel is stopped with 1 ml glacial acetic acid. Prior to scanning the gel is incubated for 5 min in $H_2O$.

#### 4.2.6.4 Western Blotting

The transfer of proteins from a SDS-gel to a nitrocellulose membrane with subsequent immunodetection is termed ‘Western Blotting’. The principles were described previously (Renart et al., 1979; Towbin et al., 1979). After separation of proteins with SDS-PAGE, they are blotted via electrotransfer or capillary transfer on a membrane. During electroblotting (Tankblotting, Semidry-Blotting) the SDS is separated from the protein due to different migration. The protein adheres to the membrane by hydrophobic interactions which are enhanced in the presence of methanol. The Tankblotting (Bittner et al., 1980) applied here is performed in vertical buffer tanks containing platinum wires as electrodes on both sides. According to a sandwich-like technique the immunodetection is accomplished by adding at first an antibody against the blotted protein (antigen) followed by an antibody coupled to a reporter system like HRP. The enzyme catalyzes the oxidation of luminol and the emitted chemiluminescence is enhanced in the presence of phenols like p-coumaric acid, naphthols or amines.

After electrophoresis, the gel was soaked in transfer buffer and placed on wet Whatman paper. A reinforced nitrocellulose membrane was wetted in the same buffer and laid without air bubbles on top of the gel. A soaked Whatman paper was put on top of the stack. The sandwich was mounted inside a cassette in a tank filled with transfer buffer. The proteins were blotted overnight at 18 V on the nitrocellulose membrane with stirring the solution. The membrane was rinsed with TBST buffer and incubated for at least 6 h in blocking buffer. Afterwards the blot was incubated for 1 h with rabbit antiserum directed

against the α- and β-subunits of the 20 S proteasome (1:500 dilution in TBST). After careful washing of the membrane with TBST (30 min), the proteasome subunits were identified with a polyclonal HRP-coupled goat-anti-rabbit antiserum (1:30,000). After rinsing the membrane for 30 min, the blot was developed with the standard system (luminol/coumarin/hydrogen peroxide) and chemiluminescence was visualized at the Lumi-Imager. The blot was stripped off antibodies with 50 mM glycine, pH 3.0 in an acidic environment and incubated afterwards for 1 h in blocking buffer. The His-tagged subunits were detected via chemiluminescence with a monoclonal mouse antibody against the His-tag (1:1000, overnight incubation) and a polyclonal HRP-coupled goat-anti-mouse antiserum (1:30,000, 1 h incubation).

### 4.2.7 Proteasomal digestion of peptides and proteins

#### 4.2.7.1 Fluorogenic tetrapeptides

His-tagged proteasomes were tested for their activity towards small peptidic substrates by terminated incubation with a fluorogenic tetrapeptide at a favorable temperature. The tetrapeptide bears a chymotryptic proteasome cleavage site prior to a fluorogenic group yielding fluorescence upon release.

Soluble proteasomes (7.3 nM) were incubated with Suc-LLVY-AMC (10 – 350 μM) for 30 min at 60 °C in HEPES buffer before quenching the reaction with the 10-fold volume of 100 mM chloroacetic acid, 100 mM acetic acid, pH 4.3. Proteasomes (11 nM), which were immobilized at lipid interfaces or desorbed from these with imidazole (4.2.4.1), were incubated with Suc-LLVY-AMC (125 μM) for 15 min at 60 °C before adding the 9-fold volume of stopping reagent. The release of 7-amino-4-methylcoumarin was measured ($\lambda_{ex/em}$ = 380 / 440 nm). The fluorescence emission was quantified with AMC (1 – 16 μM) as standard.

The data were plotted according to Michaelis-Menten, Eadie-Hofstee and Lineweaver-Burk with the following presumptions:

1) Pre-existing equilibrium between enzyme E and substrate S leads to formation of the Michaelis-Menten complex ES.
2) Steady-state equilibrium of ES: d[ES]/dt = 0, because substrate is in large excess of enzyme.

Michaelis-Menten plot: $v = \frac{v_{max} \cdot [S]}{K_M + [S]}$

v: reaction velocity

$v_{max}$: maximal reaction velocity

$K_M$: Michaelis-Menten constant

Lineweaver-Burk plot: $\frac{1}{v} = \frac{K_M}{v_{max}} \cdot \frac{1}{[S]} + \frac{1}{v_{max}}$

Eadie-Hofstee plot: $v = -K_M \cdot \frac{v}{[S]} + v_{max}$

The reaction velocity is defined as $v = \frac{d[P]}{dt} = \frac{d[AMC]}{1800s}$.

The catalytic constant $k_{cat}$ (turnover number) determines the number of reaction cycles at each catalytic center per second:

$$k_{cat} = \frac{v_{max}}{[E]_T \cdot n}$$

$[E]_T$ : total enzyme concentration

n: number of catalytic centers per enzyme

$$k_{cat}(proteasome) = \frac{v_{max} \cdot 685{,}000 \cdot l}{5 \cdot 10^{-3} \cdot 14 \cdot mol} = 9.79 \cdot 10^6 \cdot v_{max} \cdot l \cdot mol^{-1}$$

#### 4.2.7.2 Fluorescein-labeled casein

35 µl fluorescein-labeled casein (1 – 20 µM, 5 different concentrations) were incubated with α N $His_6$, β C $His_6$ or β T1A proteasome (7 nM) for 30 min at 60 °C before diluting the sample 1 : 20 with 100 mM chloroacetic acid, 100 mM acetic acid, pH 4.3. The fluorescence emission ($\lambda_{ex/em}$ = 491 / 521 nm) was recorded at the fluorescence spectrometer (Fluorolog III, Horiba). The emission obtained with the inactive proteasome mutant as well as the emission of fluorescein-labeled casein (1 - 20 µM) without proteasome was subtracted from the emission in the presence of the active proteasomes. Kinetic parameters were derived from Michaelis-Menten plots and Eadie-Hofstee plots of the fluorescence increase against the substrate concentration, as the fluorescence increase is a measure for proteasomal activity.

#### 4.2.7.3 Alexa 594-labeled insulin B chain

Alexa 594-labeled insulin B chain (5 µM) was incubated for 1 h at 60 °C with β C $His_6$ proteasome (100 nM) in HEPES buffer before stopping the reaction with a final concentration of 7.2 % (w/v) TCA (1 h at 4 °C). After centrifugation (10 min, high speed, 4 °C), 50 µl of the supernatant were loaded on a µRPC C2/C18 column pre-equilibrated with buffer A (0.1 % (v/v) TFA in $H_2O$) and separated with a gradient of buffer A to buffer B (0.1 % (v/v) TFA in acetonitrile), while recording the absorption at 280 nm and 594 nm.

#### 4.2.7.4 S-carboxymethyl-lactalbumin and casein

S-carboxymethyl-lactalbumin or casein (90 µM each) was incubated at 60 °C with His-tagged proteasomes (37 nM or 184 nM, respectively) in 50 mM Tris, pH 7.5. At certain time points (after 0 - 90 min in case of S-carboxymethyl-lactalbumin and after 0 – 4 h in case of casein) samples of 70 µl were withdrawn. Immediately, proteasomes and non-digested substrates were precipitated with 7.2 % (w/v) TCA following 1 h incubation at 4 °C. After centrifugation (10 min, high speed, 4 °C), 50 µl of the supernatant were applied to a reversed-phase column (µRPC C2/C18) pre-equilibrated with buffer A (0.1 % (v/v) TFA in $H_2O$) and the generated fragments were separated running a gradient to buffer B (0.1 % (v/v) TFA in acetonitrile), while recording the absorption at 216 nm and 280 nm.

### 4.3. Chemical methods

#### 4.3.1 Carboxymethylation of lactalbumin

For proteasomal digestion studies lactalbumin was reduced and carboxymethylated to ensure denaturation and to prevent disulfide bond formation (Akopian et al., 1997). Lyophilized lactalbumin, which was previously purified by anion exchange chromatography, was dissolved to a final concentration of 1.38 mM in degassed phosphate buffer containing 8 M urea and 5 mM EDTA and reduced with 100 mM DTT for 45 min at room temperature. The sample was chilled on ice before adding a 2 M solution of sodium iodoacetate up to a final concentration of 120 mM. The carboxymethylation of reduced lactalbumin proceeded for 1 h at 4 °C in the dark.

Low-molecular weight contaminations like carboxymethylated DTT, urea and iodoacetate were immediately removed with a desalting column. A Sephadex G-25 column (PD-10,

Amersham Biosciences) was equilibrated with 30 ml 50 mM Tris pH 7.5 by gravity flow. The sample containing S-carboxymethylated lactalbumin was diluted to a final volume of 500 µl by adding running buffer and subsequently applied to the column. The protein was eluted with 12 ml running buffer and fractionated (fraction size: 500 µl). The $A_{280}$ of the fractions was determined photometrically. The modification was quantified with Ellman´s reagent and MALDI-MS.

### 4.3.2 Reduction of insulin and separation of the reaction products

Insulin was reduced to open the two disulfide bonds between the insulin A chain and insulin B chain (Cys7 (A) - Cys7 (B), Cys20 (A) - Cys19 (B)). Insulin B chain was isolated by reversed-phase chromatography in order to label it via both cysteines with fluorophores. Bovine insulin was dissolved to a final concentration of 120 µM in 800 µl degassed citrate buffer, pH 3.0 and reduced with 20 mM TCEP (30 min at room temperature). The sample was centrifuged and subsequently separated by reversed-phase chromatography. The supernatant was loaded on a µRPC C2/C18 column, which was pre-equilibrated with 0.1 % (v/v) TFA in $H_2O$. Subsequently, a gradient of acetonitrile was applied (0 - 28 % B within 9 min, 28 - 42 % B within 24 min, 42 - 100 % B within 5 min; B: 0.1 % (v/v) TFA in acetonitrile) and fractions of 100 µl were collected during the second gradient interval. Reduced insulin B chain eluted in one peak at 33 % (v/v) acetonitrile (the fourth peak of altogether five $A_{280}$ peaks) and was identified by MALDI-MS (M/z = 3400).

### 4.3.3 Fluorescent labeling of the insulin B chain

Cross-correlation studies required two photostable, fluorescent substrates, which can be excited at 488 nm and 633 nm, respectively, without exhibiting a spectral overlap. Thiol-specific labeling was chosen, as it guarantees a defined stoichiometry and site-specificity. Insulin B chain fractions (4.3.2) were concentrated twofold in a vacuum centrifuge to remove acetonitrile, and the pH was adjusted to pH 7.5 with 1 M Tris, pH 8.0. In the presence of 10 % (v/v) DMSO, the fluorophore (Oregon Green 488-maleimide, Alexa Fluor 488-$C_5$-maleimide, Alexa Fluor 594-$C_5$-maleimide or Alexa Fluor 633-$C_5$-maleimide) was added (800 µM) to insulin B chain (250 µM). The sample was incubated for 90 min at room temperature, centrifuged to remove precipitated dye, and subsequently separated by reversed-phase chromatography. The supernatant was loaded on a µRPC

C2/C18 column, which was pre-equilibrated with 0.1 % (v/v) TFA in $H_2O$. Subsequently, a gradient of acetonitrile was applied (0 - 30 % B within 10 min, 30 - 50 % B within 24 min and 50 – 100 % B within 5 min; B: 0.1 % (v/v) TFA in acetonitrile) and fractions of 100 µl were collected during the second gradient interval. Labeled insulin B chain eluted at 38 % (v/v) acetonitrile (absorption at 491 nm, 594 nm or 600 nm due to instrumental limitations). MALDI-MS confirmed two fluorophores per polypeptide chain (M/z = 4329, M/z = 4796, M/z = 5175 and M/z = 5580 for Oregon-Green 488-labeled insulin B chain, Alexa 488-labeled insulin B chain, Alexa 594-labeled insulin B chain and Alexa 633-labeled insulin B chain, respectively). Labeled insulin B chain was adjusted to pH 7.5 by adding 1 M Tris, pH 8.0 and the acetonitrile was evaporated in the vacuum centrifuge. Aliquots were stored at -20 °C. Substrate concentration was determined fluorimetrically assuming two fluorophores per molecule and verified in the autocorrelation mode of the Zeiss ConfoCor 2.

### 4.3.4 Fluorescent labeling of the proteasome

His-tagged proteasomes, which were isolated by affinity chromatography, were concentrated in Centriplus (MWCO: 30 kDa) to a final concentration of about 3 µM in phosphate buffer and subsequently diluted 1 : 1 in 100 mM $Na_2CO_3$, pH 9.0. Directly, the proteasome (1.5 µM) was incubated for 30 min with a 30-fold molar excess of Cy3-NHS ester or a 60-fold molar excess of Cy5-NHS ester at 25 °C in the dark. The labeled proteasome was immediately dialyzed overnight against HEPES buffer (MWCO: 14 kDa) to remove unreacted dye. Finally the labeled proteasome was concentrated in Centricons (MWCO: 30 kDa) and separated on a Superose 6 column as described in 4.2.1.3. The identity of the fractions absorbing at 552 nm or 650 nm was verified by SDS-PAGE. The labeling ratio was determined photometrically to one fluorophore per proteasome.

## 4.4 Biophysical methods

### 4.4.1 MALDI-MS

For sample preparation 10 – 100 pmoles of analyte are necessary. The analyte has to be very pure, because high buffer, salt or detergent concentrations disturb the co-crystallization of analyte and matrix or contribute to the signal. The matrix is dissolved to a

concentration of approximately 100 mM in a water/organic solvent mixture. Thus the molar matrix/analyte ratio is in the range of $10^4$-$10^5$ in order to preserve lattice formation.
0.5 µl matrix dissolved in 67 % (v/v) acetonitrile, 33 % (v/v) $H_2O$, 0.1 % (v/v) TFA (saturated solution) were mixed with 0.5 µl of analyte on the target. The solvent was dried with an air stream. For peptides α-cyano-4-hydroxy-cinnamic acid served as matrix, whereas proteins were scanned after co-crystallization with sinapic acid. Peptides with molecular masses < 5 kDa were recorded in the reflector mode, whereas larger peptides and proteins were monitored in the linear mode at the Voyager De Pro instrument (Perspective Biosystems, Framingham, MA). MALDI mass spectra were evaluated with Grams software 4.14.

### 4.4.2 UV/Vis spectroscopy

#### 4.4.2.1 Purity of double-stranded DNA

Due to interactions between the electronic system of complementary bases, the absorption maximum of double-stranded DNA is located at λ = 260 nm. The absorption ratio $A_{260}$ / $A_{280}$ is constant for double-stranded DNA ($A_{260}$ / $A_{280}$ = 1.8). Thus it serves for quality control of isolated plasmid DNA. If the absorption ratio exceeds the threshold, the sample is contaminated with single-stranded molecules e.g. RNA. A lower value for the absorption ratio can be explained by protein contaminations, as the local absorption maximum of proteins is located around λ = 280 nm due to aromatic residues like tryptophane, tyrosine and, to a lesser extent, phenylalanine.

#### 4.4.2.2 Quantification of DNA and protein

The concentration of DNA or protein can in principal be determined photometrically according to the law of Lambert-Beer.

$$A(\lambda) = \varepsilon(\lambda) \cdot c \cdot d$$

A: absorption at a certain wavelength

c: mass concentration (g/l)

ε: specific extinction coefficient (l $g^{-1}$ $cm^{-1}$), wavelength-dependent

d : light path length (cm)

Theoretical extinction coefficients are listed in the Internet (ExPasy-Tools). Extinction coefficients of proteins can also be determined experimentally by calibration with a conventional protein determination kit. If the extinction coefficient of a protein is rather low, a colorimetric determination should be prefered.

A spectrum (200 – 350 nm) of diluted DNA or protein was recorded at the spectrophotometer to locate the absorption maximum ($\lambda \sim 260$ nm for DNA and $\lambda \sim 280$ nm for protein) and to derive the absorption in the local maximum. The concentration was calculated by the law of Lambert-Beer taking the dilution factor into account.

Double-stranded DNA was diluted 30-fold and quantitated according to the law of Lambert-Beer with a specific extinction coefficient of $\varepsilon_{260} = 20\ l\ g^{-1}\ cm^{-1}$.

For lactalbumin and casein quantification the extinction coefficients were taken from experimental data.

Lactalbumin: $\varepsilon_{280} = 2.01\ l\ g^{-1}\ cm^{-1}$ (Brodbeck et al., 1967; Kuwajima et al., 1985)

Casein: $\varepsilon_{280} = 0.46\ l\ g^{-1}\ cm^{-1}$ (Stothart, 1984)

The extinction coefficient for the proteasome resulted from calibration of the protein concentration with the Micro-BCA assay (4.2.5.1) and the Bradford assay (4.2.5.2).

Proteasome: $\varepsilon_{280} = 0.629\ l\ g^{-1}\ cm^{-1}$

#### 4.4.2.3 Determination of the labeling ratio

The dye/protein ratio can be dissected for subpopulations by MALDI-MS. For larger proteins, e.g. the proteasome, the average degree of labeling is estimated with respect to the law of Lambert-Beer. Molar concentrations of dye and protein are derived from the absorbances of the labeled protein at the extinction maximum of the dye and protein. The concentration ratio is the average number of dye molecules coupled to each protein molecule (labeling ratio, LR). The calculation is corrected for the absorbance of the dye at the extinction maximum of the protein.

Accordingly, the degree of Cy3- or Cy5-labeling of the proteasome can be derived:

$$c_{Cy3} = \frac{A_{552}}{\varepsilon_{552} \cdot d}$$

$$c_{proteasome} = \frac{A_{280} - 0.08 \cdot A_{552}}{\varepsilon_{280} \cdot d}$$

$$LR(Cy3-proteasome)=\frac{c_{Cy3}}{c_{proteasome}}=\frac{A_{552}\cdot\varepsilon_{280}}{\varepsilon_{552}\cdot(A_{280}-0.08\cdot A_{552})}$$

$\varepsilon_{552\,(Cy3)} = 150{,}000\ \mathrm{l\ mol^{-1}\ cm^{-1}}$

$\varepsilon_{280\,(proteasome)} = 430{,}865\ \mathrm{l\ mol^{-1}\ cm^{-1}}$

$$LR(Cy3-proteasome)=\frac{2.87\cdot A_{552}}{A_{280}-0.08\cdot A_{552}}$$

$$c_{Cy5}=\frac{A_{650}}{\varepsilon_{650}\cdot d}$$

$$c_{proteasome}=\frac{A_{280}-0.05\cdot A_{650}}{\varepsilon_{280}\cdot d}$$

$$LR(Cy5-proteasome)=\frac{c_{Cy5}}{c_{proteasome}}=\frac{A_{650}\cdot\varepsilon_{280}}{\varepsilon_{650}\cdot(A_{280}-0.05\cdot A_{650})}$$

$\varepsilon_{650\,(Cy5)} = 250{,}000\ \mathrm{l\ mol^{-1}\ cm^{-1}}$

$\varepsilon_{280\,(proteasome)} = 430{,}865\ \mathrm{l\ mol^{-1}\ cm^{-1}}$

$$LR(Cy5-proteasome)=\frac{1.72\cdot A_{650}}{A_{280}-0.05\cdot A_{650}}$$

### 4.4.3 Fluorescence spectroscopy

#### 4.4.3.1 Degradation kinetics of fluorescein-labeled casein

90 nM fluorescein-labeled casein in 50 mM Tris, pH 7.5 was adjusted to 60 °C in a water-jacketed cuvette at the fluorescence spectrometer (Fluorolog III, Horiba). Afterwards the proteasome immobilized on lipid interfaces or ‘Ni-NTA Superflow’ was added to a final concentration of 7 nM. As control, His-tagged proteasomes in equivalent concentration were assayed with fluorescein-labeled casein directly in solution or after desorption from lipid interfaces by addition of 100 mM EDTA. The increase in fluorescence reflecting relief of quenching monitors degradation of the substrate and was recorded for 15 min. The initial rate constants were analyzed.

#### 4.4.3.2 Degradation kinetics of Alexa 594-labeled insulin B chain

Alexa 594-labeled insulin B chain (20 nM) in HEPES buffer was adjusted to 60 °C at the fluorescence spectrometer before adding β C $His_6$ proteasome (7 nM). The fluorescence increase was recorded for 15 min.

#### 4.4.3.3 FRET studies of two differently labeled insulin B chains with the proteasome

Alexa 488-labeled insulin B chain (18 nM) and Alexa 594-labeled insulin B chain (18 nM) were pre-equilibrated to 60 °C at the fluorescence spectrometer. The fluorescence emission ($\lambda_{ex/em}$ = 450 / 670 nm) was recorded in a time-resolved manner while adding β C $His_6$ proteasome (20 nM).

### 4.4.4 Fluorescence correlation spectroscopy

FCS measurements were performed on a Zeiss ConfoCor 2. The instrument was controled by Fluorescence Correlation Microscope ConfoCor 2 software 3.2 FP1 and the auto- and cross-correlation curves were analyzed with Origin 7.0.

Two parallel laser beams of an argon-ion laser (488 nm, 25 mW) and a helium-neon laser (633 nm, 5 mW) pass via a collimator through a water-immersion microscope objective (40 x, 1.2 NA) in an epi-illumination arrangement. In the sample, the two focal spots are superimposed forming a confocal volume element in the femtoliter range. The emitted fluorescence is collected by the microscope objective, separated from the excitation light by a dichroic mirror (main beam splitter 488 / 633) and focused via a lens, a secondary beam splitter (635) and two emission filters (BP 530-600 and LP 650) onto two pinholes. The pinholes are located in the image plane of the lens and their diameters can be adjusted in the x-y-z axes. The red and green emission is refocused on two avalanche photodiodes.

The pinholes in channel 1 (633 nm, diameter: 90 µm) and channel 2 (488 nm, diameter: 70 µm) were adjusted with Alexa Fluor-633-$C_5$-maleimide or Cy5 and fluorescein, respectively. The corresponding confocal volume elements were determined from one-component fits of the respective correlation curves. For cross-correlation experiments β C $His_6$ proteasome (1.5 - 2 µM) was equilibrated in an 8-well chamber to 22 °C before adding Oregon Green 488-labeled insulin B chain (20 – 50 nM) and Alexa 633-labeled insulin B chain (20 – 50 nM). The red laser was adjusted to the triple intensity of the green laser, thereby minimizing the crosstalk of the green emission into the red channel. Seven

independent cross-correlation measurements of 2 min each were averaged. The cross-correlation curve was fitted with a two-component model, since the green fluorophore caused a minor cross-emission into the red channel. The autocorrelation data obtained in the green and red channel were fitted with a two-component model assuming fractions of free and bound substrates. The diffusion times of the free substrates were extracted from one-component fits of an analogous experiment, where Oregon Green 488-labeled insulin B chain (20 – 50 nM) and Alexa 633-labeled insulin B chain (20 – 50 nM) were monitored in both channels without proteasome. The diffusion times of proteasome-bound substrates in the first study were compared with the diffusion time of Cy5-labeled β C $His_6$ proteasome (20 – 50 nM) in the presence of Oregon Green 488-labeled insulin B chain (20 – 50 nM).

Auto- and cross-correlation curves were fitted with a one-component model or a two-component model

$$G(t) = 1 + \frac{1}{N} \cdot \left( 1 + \frac{F \cdot e^{-\frac{t}{t_0}}}{1 - F} \right) \cdot \left( \sum_{i=1}^{x} \frac{\Phi_i}{\left( 1 + \frac{t}{\tau_i} \right) \cdot \sqrt{1 + \frac{1}{S^2} \cdot \frac{t}{\tau_i}}} \right)$$

with $\Phi_i = \frac{Q_i^2 \cdot Y_i}{\left( \sum_{i=1}^{x} Q_i \cdot Y_i \right)^2}$ and $Y_i = \frac{N_i}{N}$.

x denotes the number of components (x = 1 or 2), N the total number of particles in the confocal volume, $N_i$ the number of particles of component i, t the correlation time, $\tau_i$ the diffusion time of component i in the confocal volume, F the triplet fraction, $t_0$ the triplet time, $\Phi_i$ the weighting coefficient for the $i^{th}$ component, $Q_i$ the quantum yield of component i, $Y_i$ the relative molecular fraction of component i and S the structural parameter.

Diffusion coefficients of D = 2.80* $10^{-10}$ $m^2/s$ for fluorescein, D = 1.98* $10^{-10}$ $m^2/s$ for Alexa Fluor 633-$C_5$-maleimide and D = 2.19* $10^{-10}$ $m^2/s$ for Cy5 were assumed (Carl Zeiss, Jena).

### 4.4.5 Electron microscopy of immobilized His-tagged proteasomes

To demonstrate the specific and uniform orientation of His-tagged proteasomes at metal-chelating interfaces a Teflon well was filled with 3.5 µg proteasome in 35 µl HEPES buffer. Subsequently 1 µl of 1 mM SOPC / DODA-NTA (9 : 1) in chloroform / hexane (1 : 1 / v : v) was placed on top of the solution. After incubation for 0.5 - 1 h, the lipid-proteasome assembly was covered with a carbon-coated gold grid for up to 3 min and stained with 1 % (w/v) uranyl acetate. Specimens were investigated in a Philips CM 120 electron microscope (FEI, Eindhoven) operating at 100 kV with a calibrated magnification of 58,300 x under low electron dose conditions covering a defocus rage of 1 – 2 µm. Images were recorded on a Gatan Megascan 2K x 2K CCD camera (Gatan, Inc., Pleasanton, CA) and image quality assessed by calculating Fast Fourier Transform (FFT) with Digital Micrograph 3.4.4. The experiment was established with minor alterations by (Thess et al., 2002) and performed in collaboration with Dr. Kirsten Model, Åsa Böker and Prof. Dr. Werner Kühlbrandt (Max-Planck-Institute of Biophysics).

### 4.4.6 Surface plasmon resonance studies

#### 4.4.6.1 Studies on NTA-dextran surfaces

Protein adsorption to a functionalized gold-dextran surface (Sensor chip NTA, BIAcore AB, Uppsala, Sweden) was analyzed with surface plasmon resonance at the BIAcore X instrument (BIAcore). The NTA-modified dextran surface is mounted via a linker layer to a gold film evaporated on a glass support. The headgroups were unloaded with EDTA prior to uniform loading with nickel ions. His-tagged proteins like the engineered proteasome are bound specifically to the surface in order to study substrate association and product dissociation in real time.

The NTA-dextran chip was primed with 10 mM HEPES, 300 mM NaCl, 50 µM EDTA, pH 7.5 at a flow rate of 10 µl /min (25 - 37 °C). Both flow cells were rinsed with 500 mM EDTA, before the surface of one flow cell was loaded with $NiCl_2$ (10 mM). Binding of 300 nM α N $His_6$ or β C $His_6$ proteasome was studied in both flow cells. As the buffer composition excludes loading of the reference flow cell with traces of metal ions, non-specific binding of the proteasome to the gold-dextran surface could be differentiated from specific binding via the His-tag. Subsequently, up to 2 µM S-carboxymethyl-lactalbumin or up to 20 µM casein was injected over both flow cells. Finally the

proteasome was removed with 500 mM EDTA. The chip was regenerated with 10 mM NaOH plus a programmed desorption procedure (0.5 % (w/v) SDS / 50 mM glycine, pH 9.5).

#### 4.4.6.2 Studies on self-assembled thiol layers

On clean precut glass slides (D 263, Präzisions Glas & Optik Iserlohn) chromium and afterwards gold was evaporated up to a height of 3 nm and additional 40 nm, respectively. Afterwards the gold chips were cleaned extensively and incubated for 24 h in a solution containing 1 mol % NTA-thiol and 99 mol % matrix thiol. The synthesis of the compounds is described separately (manuscript in preparation). The chips were mounted on a plastic holder and ready to use.

The BIAcore X system was initialized with degassed SPR buffer (10 mM HEPES, 300 mM NaCl, 5 mM imidazole, pH 7.5) at a flow rate of 10 µl/min. With a pulse of 100 mM EDTA multivalent cations were removed from the surface followed by uniform loading of the headgroups with 100 mM $NiCl_2$. Subsequently, 250 nM α N His-tagged proteasome or β C His-tagged proteasome was injected over the primed surface until a surface coverage of 1400 RU (β C His-tagged proteasome) or 2200 RU (α N $His_6$ proteasome) was reached. To block non-specific binding imidazole (20 mM) was added to the proteasome solution. Afterwards BSA (60 µM) was injected to minimize non-specific binding of the hydrophobic substrate to the surface. Substrate association and dissociation were recorded at 25 °C with injections of up to 20 µM casein, which had previously been denatured (60 °C, 10 min). The high salt concentration excluded electrostatic binding of the substrate to the charged proteasome surface. Finally, the proteasomes were desorbed with 1 M imidazole and 100 mM HCl. The surface was regenerated with 100 mM NaOH.

To calculate the stoichiometry of substrates per proteasome the casein signal amplitude was corrected by the refractive index shift and normalized to 1000 resonance units of immobilized proteasome, assuming no impact of the orientation parameter. The substrate/proteasome ratio weights the normalized signal amplitudes of casein per proteasome with their molecular masses. For $k_{off}$-determination the casein signal at the end of injection was normalized and fitted with a monoexponential function.

#### 4.4.6.3 Studies on self-assembled lipid monolayers

A commercial HPA chip (BIAcore) bears a self-assembled monolayer of octadecylthiols on the gold layer, so that unilamellar vesicles can be fused on the surface leading to a solid-supported lipid monolayer. Due to doping of the monolayer with metal-chelating lipids, His-tagged proteins are specifically and reversibly bound to the layer after uniform loading of the headgroups with nickel ions. To enhance the specificity of binding His-tagged proteasomes were immobilized in the presence of low imidazole concentrations, which do not trigger elution of the protein during affinity chromatography. Substrate association and dissociation were monitored with casein. Unfortunately, BSA and immunoglobulin G as blocking agents could not suppress hydrophobic interactions of the substrate with the lipids.

The HPA chip was primed with HBS-N buffer at a flow rate of 10 µl/min (22 °C). Both flow cells (FC) were carefully rinsed with 40 mM *n*-octyl glucoside before liposome injection. 100 µl vesicles containing 180 µM SOPC and 20 µM DODA-NTA were fused at a flow rate of 2 µl/min to a SAM, which was washed for 1 h at a flow rate of 10 µl/min. Afterwards, experiments with α N $His_6$ proteasomes were performed in FC 1, whereas β C $His_6$ proteasomes were subsequently examined in FC 2.

In FC 1 metal ions were removed with a pulse of 100 mM EDTA, before the doped monolayer was loaded with $NiCl_2$ (1 mM). Immediately, α N $His_6$ proteasomes (50 nM) were injected in the presence of 20 mM imidazole, until the lipid monolayer was covered with proteasomes. Substrate association and dissociation were monitored with increasing casein concentrations (100 nM, 150 nM, 200 nM). Subsequently, the flow was switched to FC 2.

After injecting EDTA (100 mM) and subsequently $NiCl_2$ (1 mM), β C $His_6$ proteasomes were immobilized in the presence of 20 mM imidazole. Several injections of 100 – 200 nM proteasome were necessary to saturate the lipid monolayer. Casein was afterwards injected at increasing concentrations (100 – 300 nM). Finally the proteasomes were desorbed with two pulses of 500 mM EDTA or 1 M imidazole. The lipid was removed with 40 mM *n*-octyl glucoside.

# 5. Results

## 5.1 Preparation of proteasomes

### 5.1.1 Identification of the plasmid

pRSET5a/pRSET6a vectors harboring the inserts for proteasome expression were checked by restriction endonuclease cleavage and subsequent agarose gel electrophoresis. Endonuclease digestion of the plasmid DNA with *Bam* HI or *Hind* III (one restriction site per plasmid each) revealed linearized plasmid DNA of similar size (4246 bp), whereas a 694 bp-fragment and a 3552 bp-fragment were detected after simultaneous *Bam* HI / *Hind* III-cleavage of the plasmid-DNA. Non-digested plasmid-DNA was separated in 2-3 different conformations. Supercoiled DNA, which ensures efficient transcription after transformation, always dominated over relaxed or linearized DNA.

### 5.1.2 Proteasome expression

Transformed *E. coli* BL21(DE3) cells were competent in transcription and translation of the engineered proteasomal genes from *T. acidophilum* as well as the assembly of distinct proteasomes from single subunits. Strains harboring plasmids for expression of the respective proteasome displayed similar growth characteristics before induction as well as during expression. Bacterial growth was more dependent on the selected clone. The T7-promotor is leaky towards transcription of the proteasomal α- and β-subunits, as demonstrated by SDS-PAGE of comparable amounts of non-induced and induced cells (Figure 9).

### 5.1.3 Proteasome purification and identification

In a first step His-tagged proteasomes could easily be purified by IMAC. An imidazole concentration of 175 mM was applied to desorb the His-tagged proteasomes with minimal buffer volume from the zinc-preloaded IDA headgroups. In a linear imidazole gradient β C His-tagged proteasomes, α N $His_6$ proteasomes and α C $His_6$ proteasomes were eluted with 110 mM imidazole, 140 mM imidazole and 170 mM imidazole, respectively. When loading the IDA material, zinc ions were superior to nickel ions, because the binding affintiy of His-tagged proteasomes was lower and aggregate formation could be minimized. If NTA material (Ni-NTA agarose or Ni-NTA Superflow, both Qiagen) was used for IMAC, His-tagged proteasomes could be obtained with high purity, but large

amounts of proteasome were wasted in the flow through. The accessibility of the His-tags during affinity purification was not restricting, as loading of the column under denaturing conditions (8 M urea in Tris-buffered saline) did not improve the yield. The binding of proteasomes was most probably critical due to the low exclusion limit of the beads (4 MDa). Accordingly, proteasomes might be excluded from the inner surface of the material, where most of the NTA headgroups are located.

The elution pattern of the Zinc/IDA column (Figure 8) always showed one or two prepeaks due to desorption of low-affine binding proteins and nucleic acid fragments. The most prominent peak corresponded to the eluted proteasome. In case of α N $His_6$ proteasomes the broad $A_{280}$-peak could be explained by heterogenous affinity to the column material, as up to seven His-tags can bind at one proteasomal end to the metal-loaded iminodiacetate headgroups. β C $His_6$ proteasomes produced a narrow $A_{280}$-peak during elution, presumably because the smaller number of binding His-tags also varied to a lesser extent.

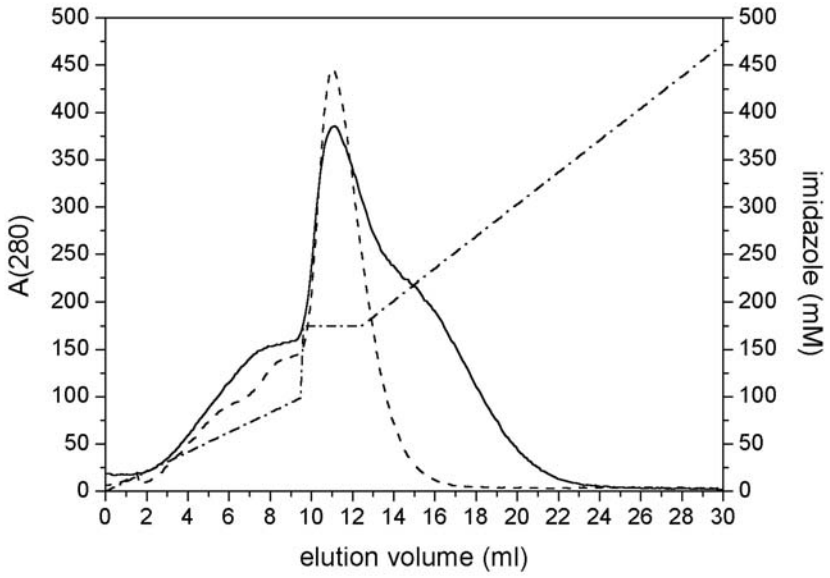


**Figure 8: IMAC-elution pattern of two His-tagged proteasomes.** α N $His_6$ proteasomes (bold line) and β C $His_6$ proteasomes (dashed line) were eluted from a HiTrap Chelating column preloaded with zinc ions. The absorption at λ = 280 nm is plotted against the elution volume. The imidazole gradient applied for elution is indicated as dash-dotted line.

According to SDS-PAGE and Coomassie Stain (Figure 9) α N $His_6$ proteasomes could be clearly separated in two different subunits (His-tagged α-subunit: 27 kDa, β-subunit: 25 kDa). In case of β C $His_6$ proteasomes, the His-tag is attached to the smaller subunit; hence the two subunits converged in one diffuse band (26 kDa).

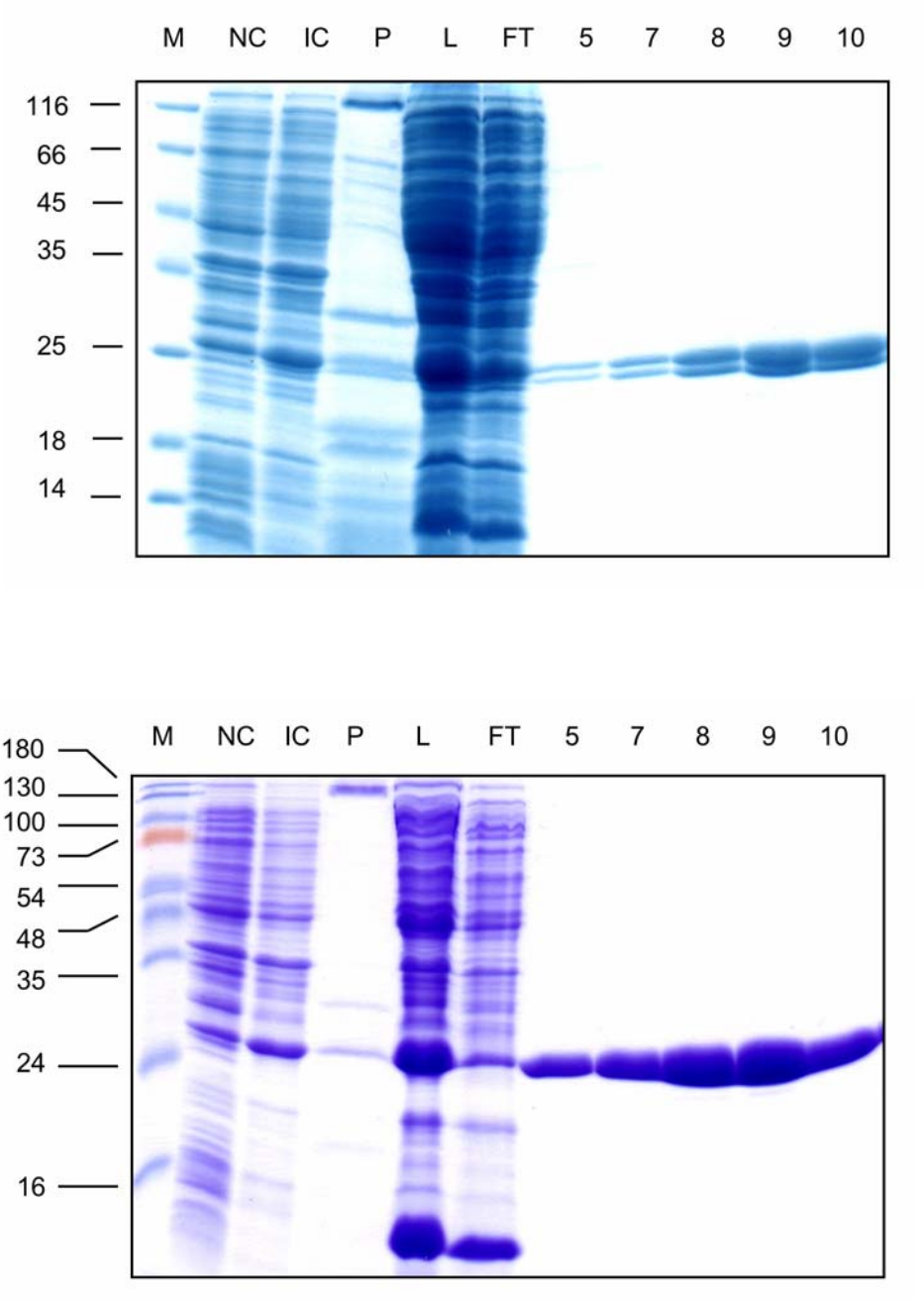


**Figure 9: SDS-PAGE after affinity purification of α N $His_6$ and β C $His_6$ proteasomes.** α N $His_6$ (top) and β C $His_6$ proteasomes (bottom) were analyzed by SDS-PAGE after purification by IMAC. Pelleted non-induced cells (NC) and induced cells (IC) in equivalent amounts ($A_{600}$ = 0.6) and the pellet after ultrasonification were extracted with 20 µl loading buffer containing 40 mM DTT each (10 min and 15 min incubation at 95 °C, respectively). 5 µl lysate (L), 10 µl flow through (FT) and 10 µl of the indicated fractions 5, 7-10 were added up to 20 µl with loading buffer containing 40 mM DTT and incubated for 5 min at 95 °C. 20 µl of the supernatants and 8 µl of boiled protein marker (M, top) or prestained marker (M, bottom) were loaded per lane. The gel was run at 80 V in the stacking gel and for 100 min at 150 V in the separation gel containing 15 % (w/v) acrylamide. The gel was stained overnight with Coomassie Brilliant Blue R250 (top) or Serva Blue R (bottom).

The flow through always contained some proteasomes, even after loading of a column with the 5-fold capacity. Especially the binding behavior of the column, but also the resolution deterioriated after frequent utilization (Figure 9, bottom). The lysate was enriched in protesomes besides lysozyme from the cell lysis. The eluted fractions were pure according to SDS-PAGE / Coomassie Stain. A Silver Stain sometimes showed minor contaminations. So generally the proteasome was purified by gel filtration in a second step, which was also necessary to remove imidazole for immobilization studies.

The elution profile of the gel filtration was similar for all proteasomes (Figure 10). Aggregates were eluted with the void volume around 5.5 ml. One single homogenous peak could be ascribed to the proteasome (elution volume: 11.1 ml).

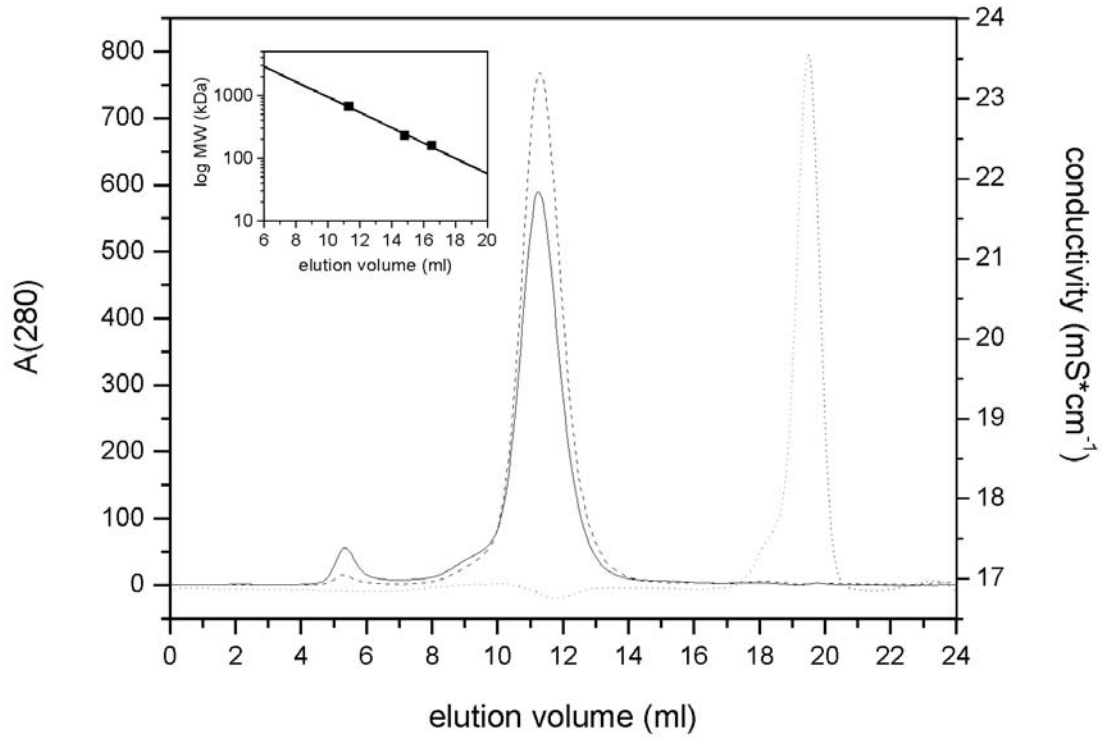


**Figure 10: Size exclusion chromatogram of α N $His_6$ and β C $His_6$ proteasomes.** The peak fractions from the affinity chromatography were pooled, concentrated in Centricons in the presence of 2 mM EDTA and applied to a Superose 6 column. During elution the $A_{280}$ of prepurified α N $His_6$ (bold line) and β C $His_6$ proteasomes (dashed line) as well as the conductivity (dotted line) were recorded. Fractions of 1 ml each were collected and examined by SDS-PAGE and Western Blot. *Inset: Calibration of the Superose 6 column with aldolase, katalase and thyroglobulin.* Aldolase (158 kDa), katalase (232 kDa) and thyroglobulin (669 kDa) were loaded on the Superose 6 column in amounts leading to similar $A_{280}$ during elution. The logarithm of their respective molecular masses was plotted against the elution volume and fitted by linear regression.

According to calibration of the Superose 6 column with aldolase (158 kDa), katalase (232 kDa) and thyroglobulin (669 kDa), the molecular mass of the His-tagged proteasome corresponded to 695 kDa (Figure 10 inset). The theoretical molecular mass of the proteasome including the 14 His-tags was calculated to 685 kDa. As Centricons with a MWCO of 30 kDa were used for concentration of the proteasome, the eluate was deficient of single subunits, which could originate from non-stoichiometric expression and specific binding to the HiTrap Chelating column. The concentration in filtration units and the gel filtration reduced the overall yield of proteasome both by 16 % each, when normalized to the yield after IMAC. Thus finally 5 – 10 mg pure, monodisperse proteasome were obtained per l LB broth.

The SDS-PAGE with subsequent Silver Stain showed no impurities of the eluted proteasome in the central fractions 12/13, which were used for the assays (Figure 11).

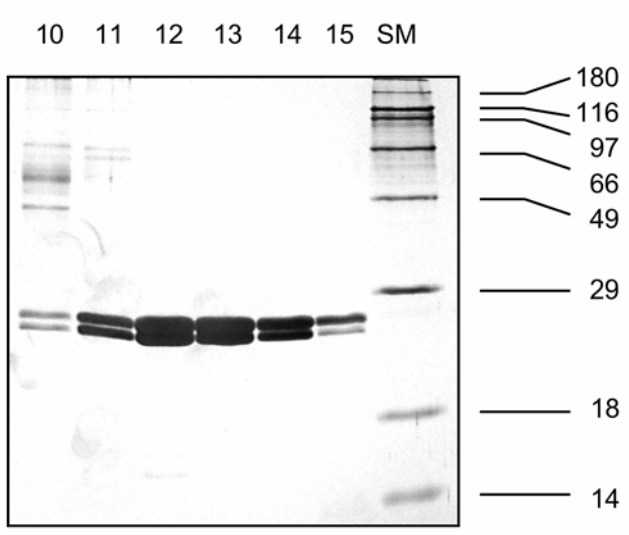


**Figure 11: SDS-PAGE with Silver Stain of α N $His_6$ proteasomes after gel filtration.** 6 µl each of fraction 10-15 from the gel filtration of α N $His_6$ proteasomes were diluted with 12 µl loading buffer containing 40 mM DTT, heated for 10 min at 95 °C and 15 µl each (as well as Silver Stain Marker) were applied to a SDS-gel.

The His-tagged α-subunits and the β-subunits could be separated according to SDS-PAGE/ Coomassie Stain after gel filtration of the α N $His_6$ proteasomes (Figure 12 A) Both bands were detected by an antibody directed against the 20S proteasome from *T. acidophilum* (Figure 12 B, left), albeit the signal caused by the larger α-subunits dominated over the

signal obtained from the smaller β-subunits. In case of the β C $His_6$ proteasomes, the α- and His-tagged β-subunits migrated as one diffuse band (Figure 12 A), which was also probed by the anti-20S proteasome antiserum (Figure 12 B, left). In addition to slight differences in electrophoretic mobility the His-tagged subunits of both recombinant proteasomes could be identified by an antibody directed against the His-tag (Figure 12 B, right). By probing the nitrocellulose membrane with this antibody, a minimum span of five consecutive histidines could be identified.

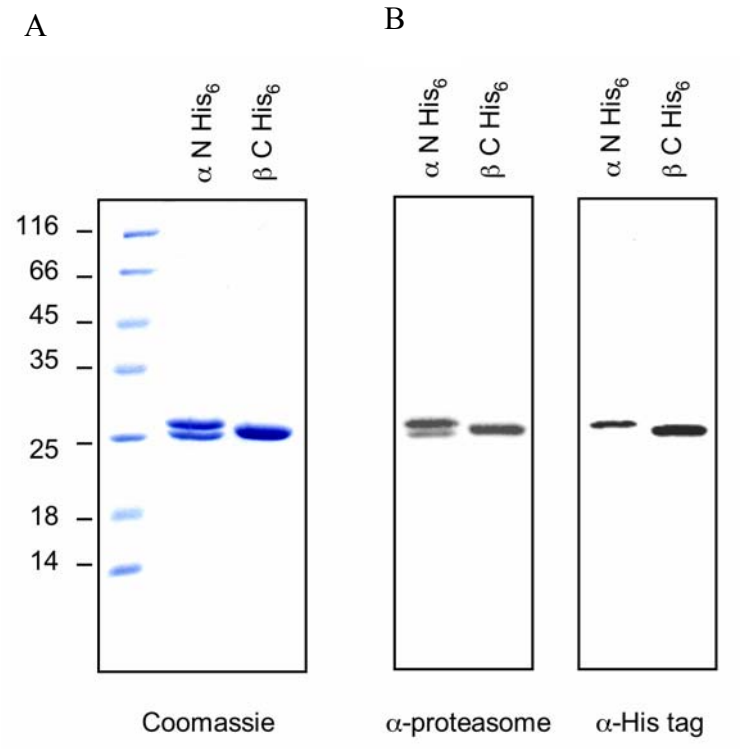


**Figure 12: SDS-PAGE and Western Blot of α N $His_6$ and β C $His_6$ proteasomes subsequent to gel filtration.** 4 µg (A) and 1 µg (B) each of α N $His_6$ and β C $His_6$ were dissolved in loading buffer and were applied to SDS-PAGE. A) The gel part was stained overnight with Serva Blue R. B) The other gel part was blotted on a nitrocellulose membrane. The proteasome was identified with a rabbit antiserum directed against the α- and β-subunits (1 : 500) and a polyclonal HRP-coupled goat-anti-rabbit antiserum (1 : 30.000). The chemiluminescence was developed with the standard system and visualized at the Lumi-Imager. After stripping, the His-tagged subunits were detected with a mouse antibody against the His-tag (1 : 1000) and a polyclonal HRP-coupled goat-anti-mouse antiserum (1 : 30.000).

## 5.2 Activity of the proteasome

### 5.2.1 Peptidolytic activity of the soluble proteasome

To demonstrate that the His-tag does not influence proteasomal function differently His-tagged proteasomes were tested for release of AMC from the fluorogenic tetrapeptide Suc-LLVY-AMC. After calibration of the fluorescence emission with AMC the experimental fluorescence signal could be converted by linear regression into proteasomal activity. The Michaelis-Menten plots for all three active His-tagged proteasomes were similar (Figure 13 A). For determination of kinetic parameters plots were linearized according to Eadie-Hofstee (Figure 13 B) or Lineweaver-Burk (not shown). Eadie-Hofstee plots allow a simple readout of $v_{max}$ (y-intercept, see 4.2.7.1) and $K_M$ (negative slope), which is superior to approximation of Michaelis-Menten plots with the Levenberg-Marquardt algorithm. All fits were run only up to substrate concentrations of 200 µM in case of α C $His_6$ and β C $His_6$ proteasomes, because substrate inhibition was observed at higher concentrations.

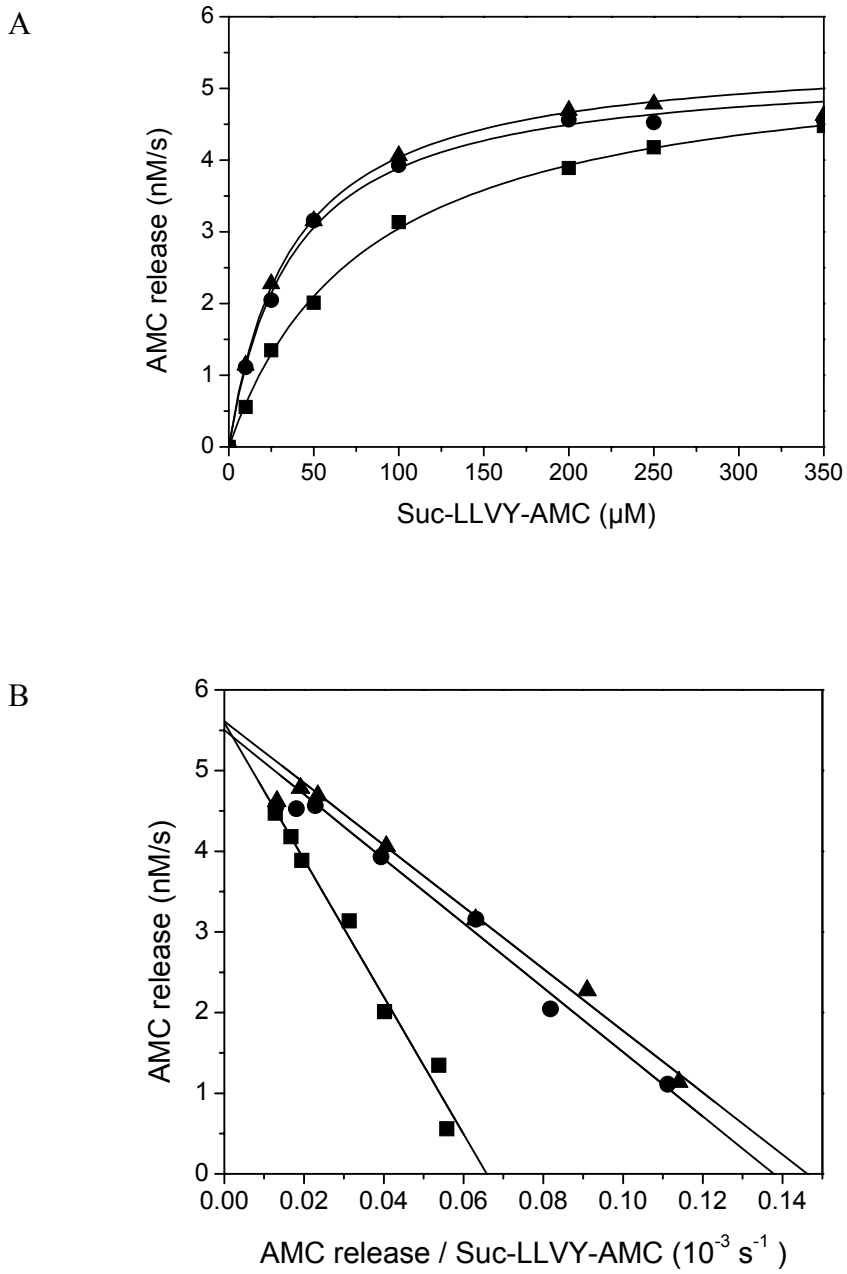


**Figure 13: Proteasomal activity against fluorogenic tetrapeptides (Michaelis-Menten and Eadie-Hofstee plot).** Soluble proteasomes (5 µg/ml) were incubated with Suc-LLVY-AMC (10 - 350 µM) for 30 min at 60 °C, before quenching the reaction with 100 mM chloroacetic acid, 100 mM acetic acid, pH 4.3 and measuring the release of AMC ($\lambda_{ex/em}$ = 380 / 440 nm). The proteasomal activity derived from the fluorescence signal was plotted against the substrate concentration (Michaelis-Menten plot, A) or against the quotient of proteasomal activity and substrate concentration (Eadie-Hofstee plot, B). The Michaelis-Menten fit was based on approximation with the Levenberg-Marquardt algorithm. The Eadie-Hofstee plot was fitted by linear regression. The activity is depicted for α N $His_6$ proteasomes (squares), β C $His_6$ proteasomes (circles) and α C $His_6$ proteasomes (triangles).

| | | α N $His_6$ proteasome | β C $His_6$ proteasome | α C $His_6$ proteasome |
|---|---|---|---|---|
| Michaelis-Menten | $K_M$ (µM) | 81.7 ± 4.2 | 37.0 ± 2.5 | 36.8 ± 1.0 |
| | $K_{cat}$ ($s^{-1}$) | 0.054 ± 0.001 | 0.052 ± 0.001 | 0.054 ± 0.000 |
| Eadie-Hofstee | $K_M$ (µM) | 85.0 ± 5.4 | 39.9 ± 2.2 | 38.4 ± 1.5 |
| | $K_{cat}$ ($s^{-1}$) | 0.054 ± 0.002 | 0.053 ± 0.002 | 0.055 ± 0.001 |
| Lineweaver-Burk | $K_M$ (µM) | 97.6 ± 2.3 | 39.2 ± 0.8 | 40.1 ± 0.7 |
| | $K_{cat}$ ($s^{-1}$) | 0.059 ± 0.006 | 0.053 ± 0.002 | 0.056 ± 0.002 |

**Table 6: Kinetic parameters $K_{cat}$ and $K_M$ of His-tagged proteasomes for fluorogenic tetrapeptides.** The kinetic parameters $v_{max}$ and $K_M$ were derived from Michaelis-Menten plots, Eadie-Hofstee plots and Lineweaver-Burk plots. $v_{max}$ was transformed into the catalytic constant $k_{cat}$ per active catalytic center as described in Methods (4.2.7.1).

According to Table 6 the catalytic constants were in the same range for all three His-tagged proteasomes indicating that the location of the His-tag has only a moderate effect on the degradation of peptidic substrates by the proteasome. The affinity for the substrate represented by the Michaelis-Menten constant was reduced in case of the α N $His_6$ proteasome. Possibly the confinement of the pores by the His-tags slightly restricts substrate entry and thus decreases the effective substrate concentration at the active centers.

For all His-tagged proteasomes the enzymatic activity is relatively stable over several weeks, when stored at 4 °C in HEPES buffer. In case of β C $His_6$ and α C $His_6$ proteasomes, the catalytic constants dropped only about 8 % within 50 days (Table 7), whereas the substrate affinity increased 10 - 20 % within the same period. Remarkably, the substrate affinity of α N $His_6$ proteasomes climbed more than 30 % within the first 22 days

after purification, whereas the catalytic constants increased gradually within this period, before aggregation caused a severe loss of activity.

| | | α N $His_6$ proteasome after 22 d | β C $His_6$ proteasome after 50 d | α C $His_6$ proteasome after 25d |
|---|---|---|---|---|
| Michaelis-Menten | $K_M$ (μM) | 65.9 ± 0.7 | 33.5 ± 1.7 | 32.5 ± 1.9 |
| | $K_{cat}$ ($s^{-1}$) | 0.057 ± 0.000 | 0.050 ± 0.001 | 0.051 ± 0.001 |
| Eadie-Hofstee | $K_M$ (μM) | 66.9 ± 0.6 | 32.3 ± 2.1 | 35.0 ± 1.2 |
| | $K_{cat}$ ($s^{-1}$) | 0.058 ± 0.000 | 0.049 ± 0.002 | 0.053 ± 0.001 |
| Lineweaver-Burk | $K_M$ (μM) | 66.5 ± 0.4 | 31.0 ± 1.0 | 35.0 ± 0.4 |
| | $K_{cat}$ ($s^{-1}$) | 0.057 ± 0.001 | 0.048 ± 0.002 | 0.053 ± 0.001 |

**Table 7: Changes of kinetic parameters $K_{cat}$ and $K_M$ of His-tagged proteasomes against fluorogenic tetrapeptides during storage.** The kinetic parameters $v_{max}$ and $K_M$ were derived from Michaelis-Menten plots, Eadie-Hofstee plots and Lineweaver-Burk plots. $v_{max}$ was transformed into the catalytic constant $k_{cat}$ per active catalytic center as described in Methods (4.2.7.1).

Additionally, the mature α N $His_6$ proteasome displayed substrate inhibition at the highest tested concentration. Maturation of α N $His_6$ proteasomes is most probably due to a reorganization of the His-tags and dilation of the pore openings, thus resembling more and more the proteasomes without His-tags at the entrances.

### 5.2.2 Proteasomal digestion of proteins

#### 5.2.2.1 Proteasomal digestion of lactalbumin

α-Lactalbumin from bovine milk was purified by anion exchange chromatography. According to MALDI-MS the peak fraction corresponded to 14,195 Da. Several reducing agents (β-mercaptoethanol, DTT and TCEP) were tested to cleave all four disulfide bonds, wherein DTT worked best (45 min, 25 °C). According to MALDI-MS the reduced species corresponded to 14,203 Da and Ellman´s reagent detected approximately eight free thiol groups. After carboxymethylation with an excess of sodium iodoacetate (45 min, 4 °C), 0.5 mol free cysteines / mol product could be determined with the Ellman´s assay. MALDI-MS of S-carboxymethyl-lactalbumin showed a major peak of the 8-fold carboxymethylated species (14,664 Da, theoretical molecular mass: 14,667 Da).

S-carboxymethyl-lactalbumin was degraded by different His-tagged proteasomes and the generated fragments were separated by reversed-phase chromatography (μRPC C2/C18 column) (Figure 14). Product formation increased linearly within the first 90 min of incubation (Figure 15). S-carboxymethyl-lactalbumin (90 μM) was degraded completely by α C $His_6$ proteasomes (36 nM) within 270 min at 60 °C, as substrate (15 μg) could not be detected in a Silver Stain after SDS-PAGE / Tricine (Schägger and von Jagow, 1987).

Differences were visible with respect to proteasomal activity, as well as the substrate and product pattern. Proteasomes harboring His-tags on their sides appeared approximately four times as active as proteasomes with His-tags located at the pore apertures. In case of α N $His_6$ proteasomes contaminating traces of peptides with a molecular mass lower than S-carboxymethyl-lactalbumin were apparently (preferentially) digested. According to the HPLC pattern also products seemed to be smaller sized or less hydrophobic compared to α C $His_6$ proteasomes. Thus His-tags around the pore apertures might slightly restrict substrate entry into the proteasome interior.

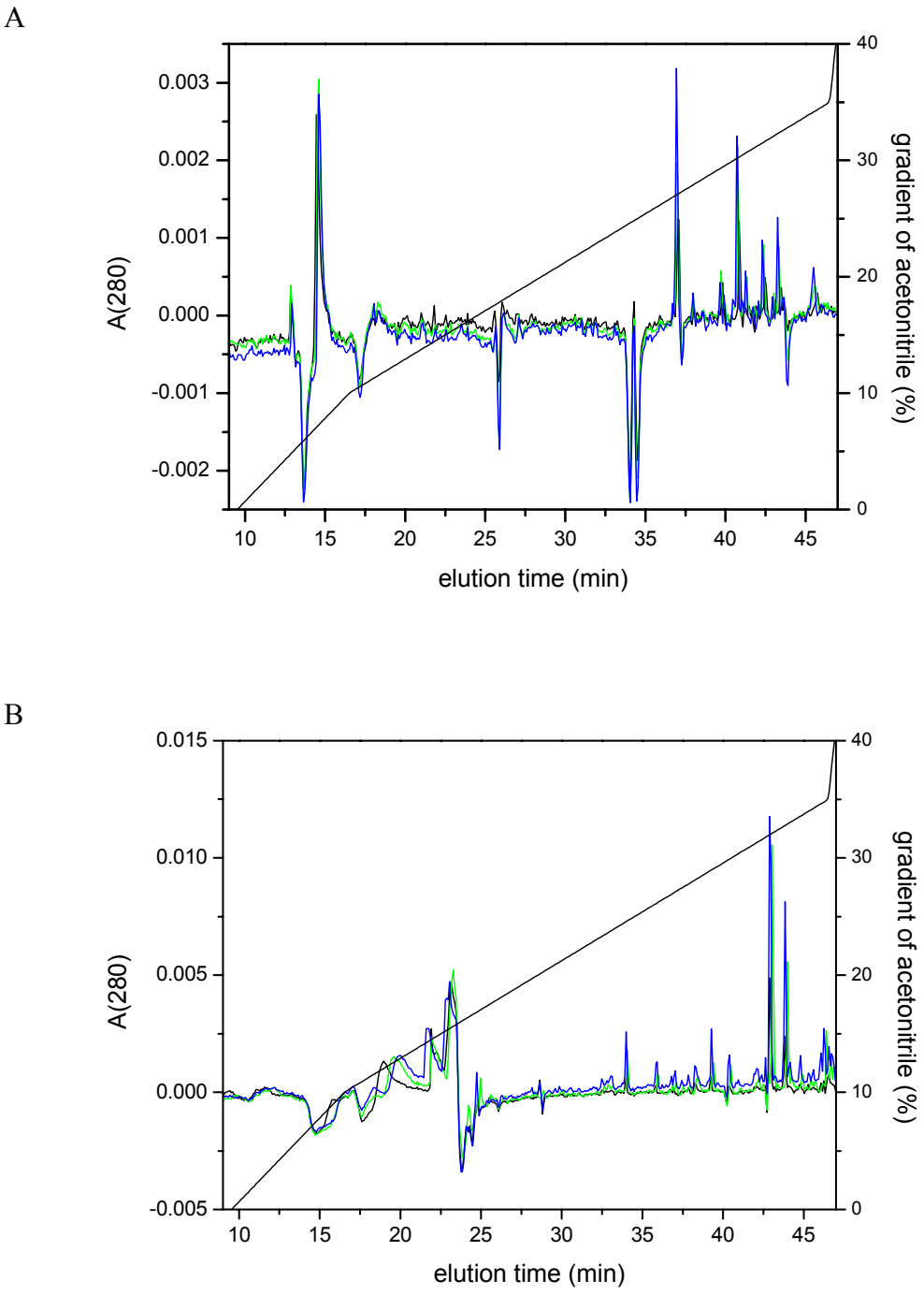


**Figure 14: Digestion pattern of S-carboxymethyl-lactalbumin with different His-tagged proteasomes.** S-carboxymethyl-lactalbumin (90 µM) was degraded by α N $His_6$ (A) or α C $His_6$ proteasome (B) (both 36 nM). Degradation proceeded for 30 min (black line), 60 min (green line), or 90 min (blue line) at 60 °C in 50 mM Tris, pH 7.5 before stopping the digestion with 7.2 % (w/v) TCA (1 h, 4 °C). 50 µl of each supernatant were applied to a µRPC C2/C18 column pre-equilibrated with 0.1 % (v/v) TFA (buffer A). Fragments were separated running a gradient of buffer A to buffer B (0.1 % (v/v) TFA in acetonitrile): 0 – 10 % B within 15 min, 10 – 35 % B within 30 min and 35 – 100 % B within 5 min. The absorption at 280 nm was recorded for the differently incubated samples and corrected by the corresponding absorption of the sample withdrawn without incubation.

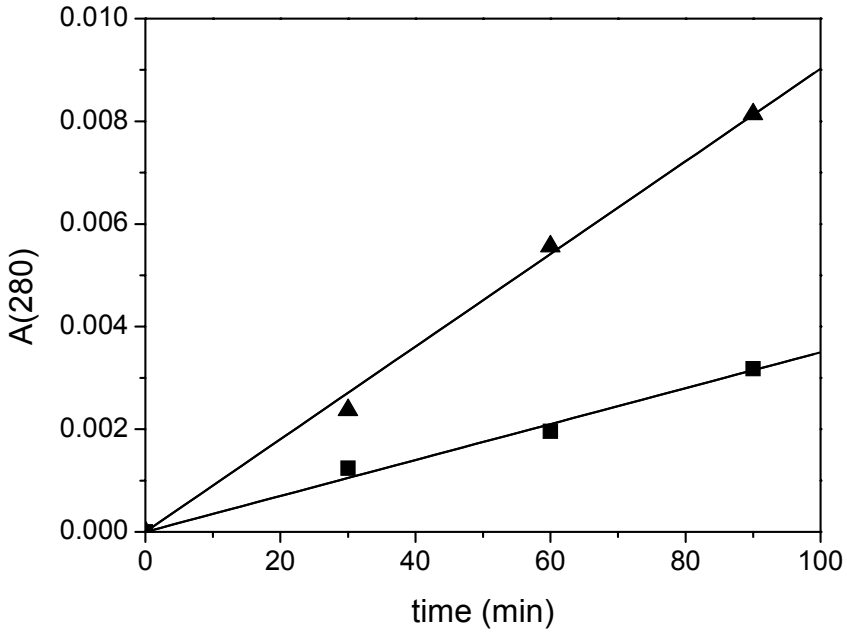


**Figure 15: Degradation kinetics of S-carboxymethyl-lactalbumin for different His-tagged proteasomes.** The data were derived from Figure 14 for fragments generated by α N $His_6$ (squares, elution time: 36.9 min), and α C $His_6$ proteasomes (triangles, elution time: 43.8 min).

### 5.2.2.2 Proteasomal digestion of casein

Purified casein (molecular mass: 23,950 Da) was analyzed by MALDI-MS (Figure 16).

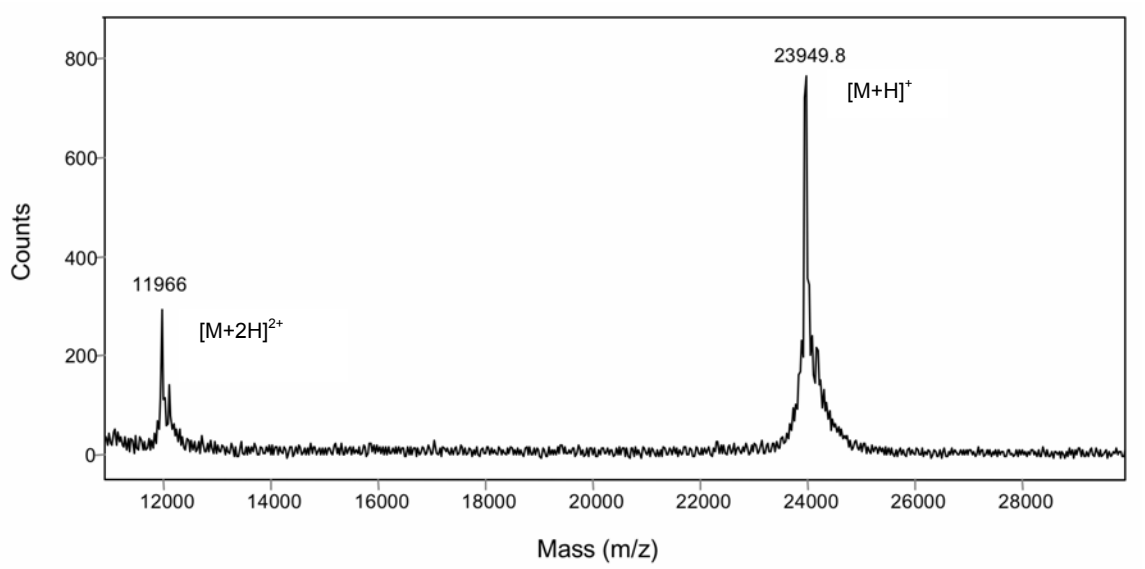


**Figure 16: MALDI-MS of casein.** Casein was purified via anion exchange chromatography, dialyzed against $H_2O$ and lyophilized. Casein and sinapic acid as matrix were dissolved separately in 67 % (v/v) acetonitrile, 0.1 % (v/v) TFA and mixed on the target.

Proteasomal degradation of casein was analyzed by reversed-phase chromatography (Figure 17). For α N $His_6$ proteasomes fragment generation increased linearly with incubation time over 4 h at 60 °C (Figure 18). The activity of the α C $His_6$ proteasomes was gradually higher than the activity of the β C $His_6$ proteasomes and exceeded the activity of the α N $His_6$ proteasomes by the same factor as in case of lactalbumin, when comparing more hydrophobic peptides. Fragment generation increased linearly with incubation time, but was almost finished after 3 h degradation in case of α C $His_6$ proteasomes. The product pattern differed considerably for proteasomes bearing His-tags at their sides or at the pore openings. The elution pattern and MALDI-MS data indicated that the fragments were in average smaller in case of α N $His_6$ proteasomes compared to α C $His_6$ and β C $His_6$ proteasomes. Thus substrates seem to be degraded more exhaustively by α N $His_6$ proteasomes than α C $His_6$ and β C $His_6$ proteasomes, presumably because the His-tags impose constraints against premature fragment release. Proteasomal activity against casein was lower than against S-carboxymethyl-lactalbumin measuring the $A_{216}$ of the fragments at identical substrate and proteasome concentrations. But proteasomal activity against casein could be enhanced twofold in the presence of 100 mM magnesium ions and 5-fold in the presence of 250 mM calcium ions. At least stimulation of α N $His_6$ proteasomes by calcium ions seemed to be mediated by pore dilation, since the fragment size was increased due to premature product release.

A

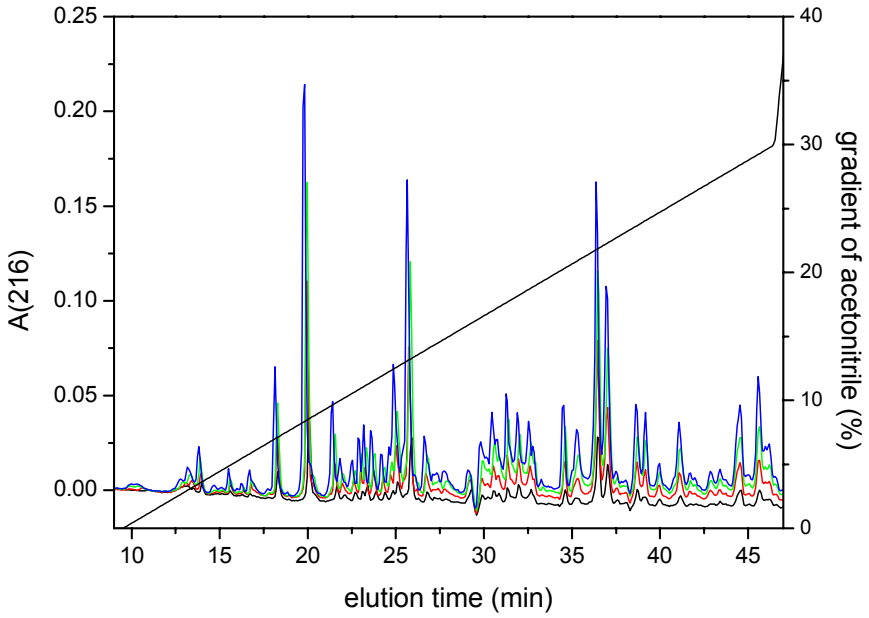


B

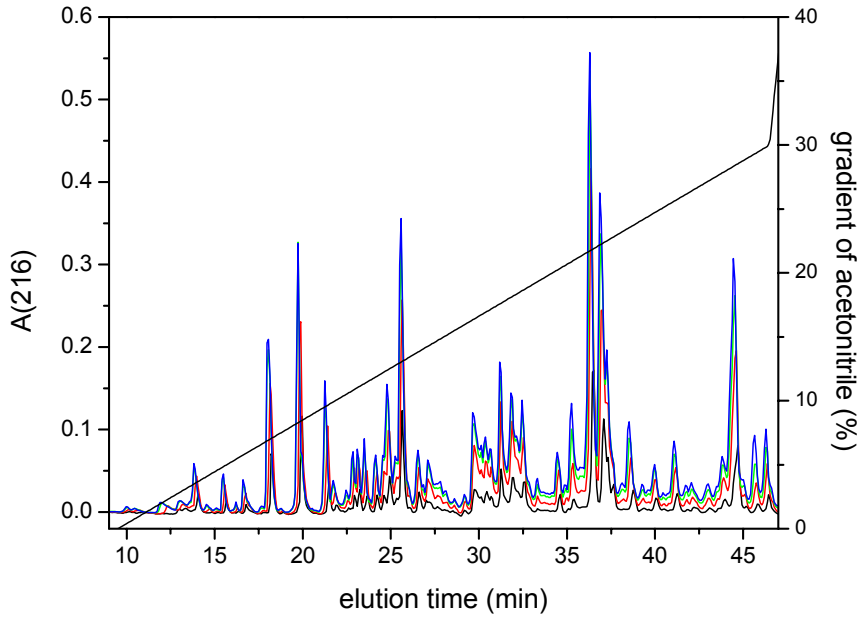


**Figure 17: Digestion pattern of casein with different His-tagged proteasomes.** Casein (90 µM) was subjected to degradation by α N $His_6$ (A) or α C $His_6$ proteasome (B) (both 182 nM) for 1 h (black line), 2 h (red line), 3 h (green line), or 4 h (blue line) at 60 °C in 50 mM Tris, pH 7.5. After precipitation with 7.2 % (w/v) TCA (1 h, 4 °C), 50 µl of each supernatant were applied to a µRPC C2/C18 column pre-equilibrated with 0.1 % (v/v) TFA (buffer A). Fragments were separated with a gradient of buffer A to buffer B (0.1 % (v/v) TFA in acetonitrile): 0 – 30 % B within 37 min and 30 - 100 % B within 5 min. Substrate degradation was evaluated by subtracting from the recorded $A_{216}$ of each sample the corresponding absorption of the sample withdrawn at time zero.

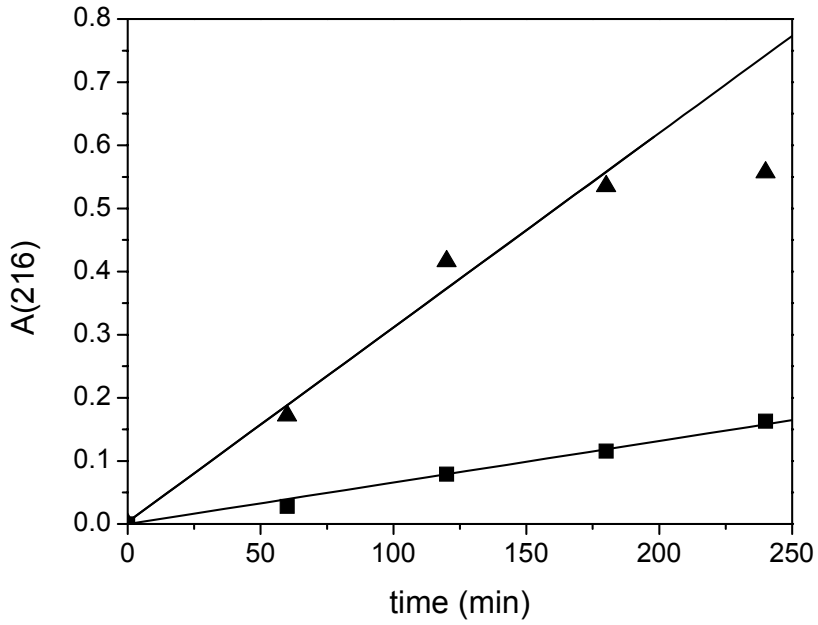


**Figure 18: Degradation kinetics of casein for different His-tagged proteasomes.** The data were derived from Figure 17 for a fragment (elution time: 36.5 min) generated by α N $His_6$ (squares) and α C $His_6$ proteasomes (triangles).

### 5.2.3 Proteolytic activity of the proteasome

#### 5.2.3.1 Proteolytic activity of the soluble proteasome

The activity of the proteasome against fluorescein-labeled casein as proteinaceous substrate was evaluated by the generated fluorescence increase (Figure 19). As the proteasome eventually cleaves between the single fluorescein molecules attached to casein, the self-quenching of the fluorophores is relieved during degradation by the proteasome. In solution all three active His-tagged proteasomes displayed similar activities against fluorescein-labeled casein. As an internal control, the β T1A proteasome mutant did not enhance the fluorescence due to a substitution of the catalytically active threonines. The fluorescence increase of α N $His_6$ and β C $His_6$ proteasomes against fluorescein-labeled casein (30 min, 60 °C) revealed similar Michaelis-Menten constants for the proteasomes (4.4 µM and 4.3 µM for α N $His_6$ and β C $His_6$ proteasome, respectively). Thus also the Michaelis-Menten constants exclude any major influence of the His-tag on proteolysis.

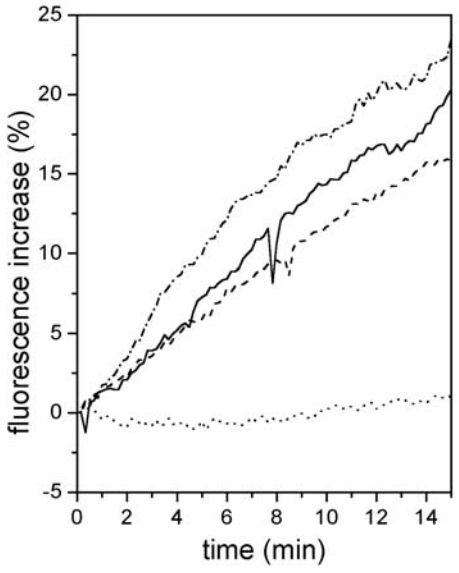


**Figure 19: Activity of different His-tagged proteasomes against fluorescein-labeled casein in solution.** 90 nM fluorescein-labeled casein were subjected to degradation (15 min, 60 °C) by 7 nM His-tagged proteasomes dissolved in 50 mM Tris, pH 7.5. The fluorescence increase reflecting proteasomal activity is expressed as percentage of the initial fluorescence. The fluorescence increase is denoted as dash-dotted line (α C $His_6$ proteasome), dashed line (β C $His_6$ proteasome), bold line (α N $His_6$ proteasome) and dotted line (β T1A proteasome).

### 5.2.3.2 Proteolytic activity of His-tagged proteasomes after immobilization on NTA agarose

Proteasomes were immobilized, presumably in different orientations, via their His-tags on NTA agarose preloaded with nickel ions. The activity against fluorescein-labeled casein was assayed afterwards by applying substrate and proteasome concentrations as in the previous experiment with soluble proteasomes (Figure 20). α N $His_6$ proteasomes did not alter their activity upon end-on immobilization. α C $His_6$ and β C $His_6$ proteasomes, which were immobilized side-on, degraded the substrate much faster than in solution. According to Figure 20 B the activity of the α C $His_6$ proteasomes was stimulated twofold, the activity of β C $His_6$ proteasomes even threefold upon immobilization. Probably the fluorescence increase attained with the active His-tagged proteasomes is in part due to substrate enrichment near the surface. The fluorescence did not change in the presence of the proteasome mutant. Therefore, fluorescence enhancement is a measure for proteasomal activity and is dependent on the orientation of the proteasome.

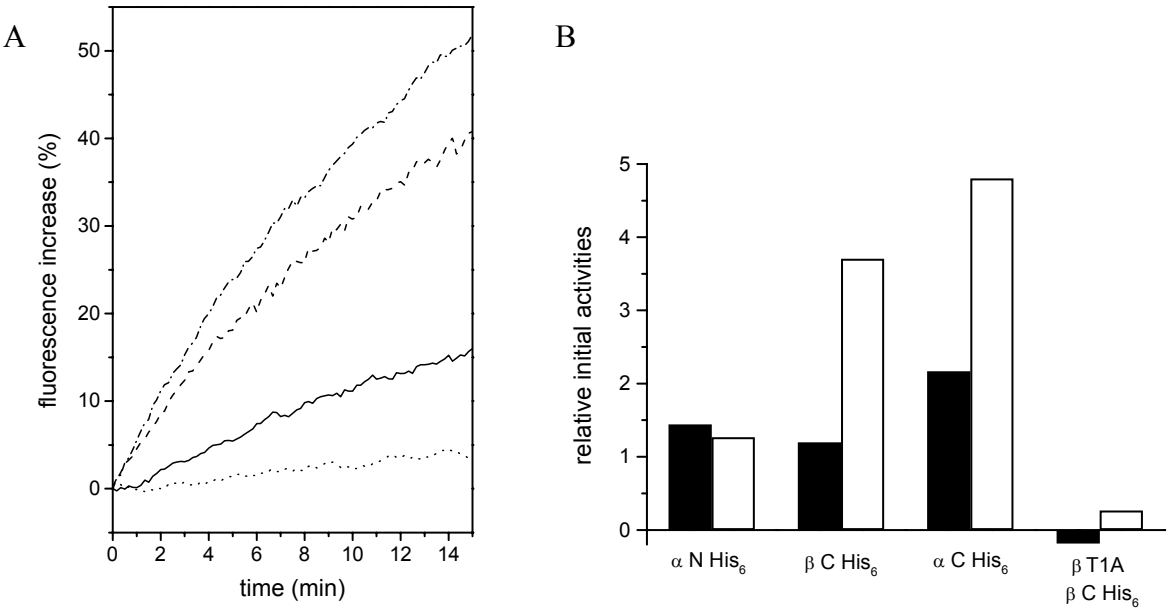


**Figure 20: Activity of different His-tagged proteasomes against fluorescein-labeled casein after immobilization on NTA-agarose**. A) 90 nM fluorescein-labeled casein were subjected to degradation (15 min, 60 °C) by His-tagged proteasomes (7 nM) which were suspended in 50 mM Tris, pH 7.5 subsequent to immobilization on NTA-agarose. The fluorescence increase reflecting proteasomal activity is expressed as percentage of the initial fluorescence. The fluorescence increase is denoted as dash-dotted line (α C $His_6$ proteasome), dashed line (β C $His_6$ proteasome), bold line (α N $His_6$ proteasome), and dotted line (β T1A proteasome). B) Initial degradation rates of the corresponding proteasomes were compared for the soluble enzyme (filled bars, see Figure 19) and NTA-agarose bound enzyme (open bars).

## 5.3 Orientated immobilization of His-tagged proteasomes at metal-chelating interfaces

Electron micrographs revealed two distinct orientations of proteasomes corresponding to the location of their His-tags (Figure 21 and Figure 22). His-tags located at the C-termini of the β-subunits enforce the proteasomes in side-on orientation at chelating interfaces (Figure 21). β C $His_6$ proteasomes appear striated due to the organization in four stacked disks (Figure 21 left). A statistical analysis revealed that 87 % of all β C $His_6$ proteasomes are immobilized side-on and only 2 % are orientated end-on at chelating interfaces (Figure 21 right).

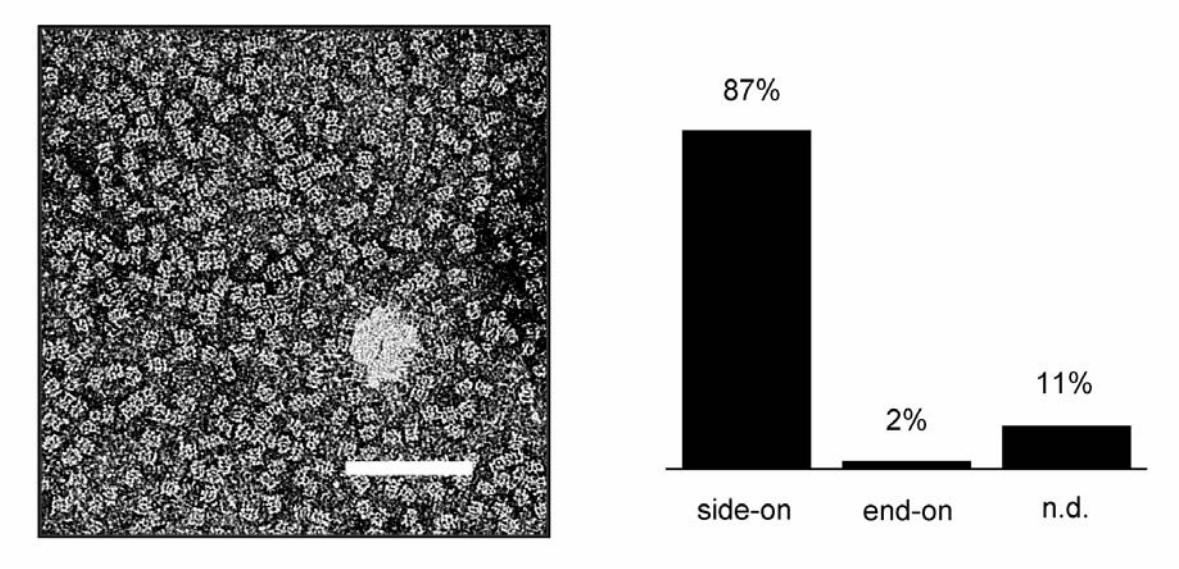


**Figure 21: Electron micrographs of β C $His_6$ proteasomes displaying uniformly one specific orientation at metal-chelating lipid interfaces.** β C $His_6$ proteasomes are enforced in side-on orientations at metal-chelating lipid films (left, scale bar, 50 nm). Statistics on the orientation of β C $His_6$ proteasomes are given in the right panel.

Proteasomes with His-tags at the N-termini of the α-subunits are immobilized predominantly end-on at chelating interfaces (Figure 22 A left, B). 76 % of all α N $His_6$ proteasomes are depicted in end-on orientation, whereas only 4 % could be detected in side-on orientation (Figure 22 A right). Longer adsorption times of the α N $His_6$ proteasomes to metal chelating lipid interfaces allow two-dimensional crystallization of the proteasomes (Figure 22 B left). In the top view, the pore apertures of α N $His_6$ proteasomes become clearly visible (Figure 22 B right).

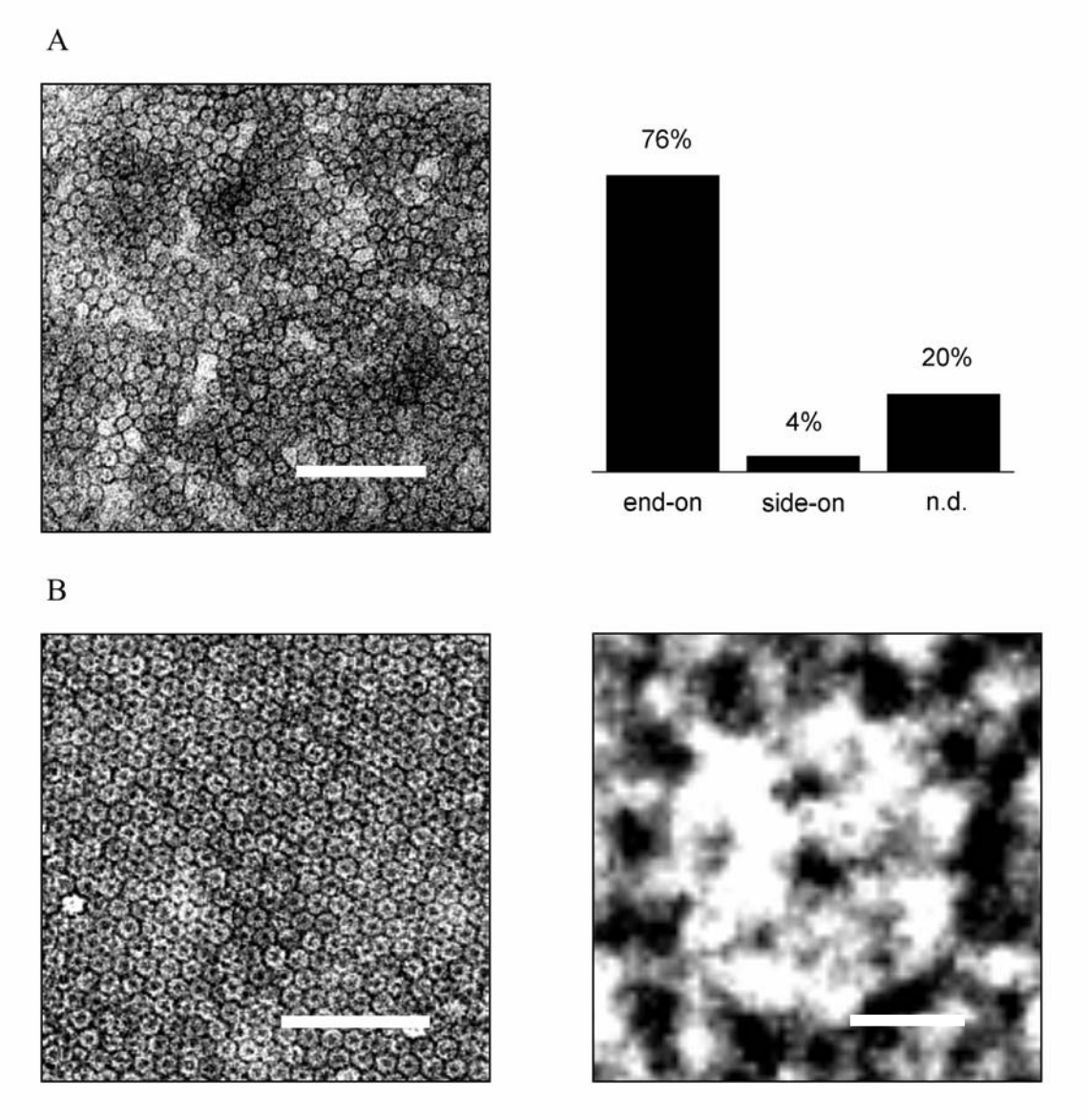


**Figure 22: Electron micrographs of α N $His_6$ proteasomes displaying uniformly one specific orientation at metal-chelating lipid interfaces.** A) α N $His_6$ proteasomes appear in end-on views at chelating interfaces (left). Statistics on the orientation of α N $His_6$ proteasomes are shown in the right panel. B) 2D-crystallization of α N $His_6$ proteasomes in uniform end-on orientations (left).The scale bars correspond to 50 nm (A, B left) and 5 nm (B right). Single α N $His_6$ proteasome in top view (right).

Wild-type proteasomes without His-tags are randomly orientated (Thess et al., 2002). Hence coordination with the chelating interface is mediated specifically via the His-tag. Random orientation is also observed, if chelating lipids or nickel ions are missing at the interface.

## 5.4 Proteasomal activity after immobilization at metal-chelating interfaces

### 5.4.1 Peptidolytic activity of the immobilized proteasome

Degradation of small substrates might be altered by site-specific orientation of His-tagged proteasomes at metal-chelating interfaces. It remains elusive whether substrates and products can enter and exit the α N $His_6$ proteasome in end-on orientation via one channel only or whether peptidic substrates can circumvent the barrier. Therefore proteasomal activity was studied after immobilization of His-tagged proteasomes on liposomes bearing 10 mol % nickel-loaded chelator lipids and subsequent to desorption (Table 8). As the interface coverage reflected by the proteasome/chelator lipid ratio might affect substrate degradation, it was kept as a variable parameter in several docking experiments.

In case of proteasome/chelator lipid ratios of 1 : 909 (proteasomal surface coverage up to 6 %), 1 : 140 (proteasomal surface coverage up to 39 %) and 1 : 56 (proteasomal surface coverage up to 98 %) the catalytic constants for fluorogenic tetrapeptides dropped only slightly following immobilization of the proteasomes. This effect might be in part due to a stimulation of soluble proteasomal activity in the presence of nickel ions. Imidazole treatment did not interfere with the activity of soluble proteasomes. Alternatively proteasomal activity decreased slightly upon immobilization. If the liposomes were overcrowded with proteasomes (His-tag/chelator lipid ratio of 1:1), the catalytic constants of α N $His_6$ proteasomes dropped significantly. Proteasomes crosslinking different lipsomes might be responsible for this phenomenon.

The proteasomal activities displayed in the presence of 125 µM tetrapeptide were converted into percentages of the respective catalytic constants (see Table 6) and compared with the theoretical value estimated from the Michaelis-Menten equation. In case of α N $His_6$ and β C $His_6$ proteasomes the deviation from the theoretical fraction of the catalytic constant amounted to ≤ 20 % and ≤ 15 %, respectively. In summary, immobilization altered the catalytic activity of His-tagged proteasomes against small substrates only very slightly. Thus it can be assumed that the blocked entrance was not tightly sealed against entry of small substrates. The validity of the assay was proven by the fact that the supernatant after precipitation of liposome-docked proteasomes via ultracentrifugation was deficient of soluble proteasomes as judged from the Micro-BCA assay.

| Proteasome / chelator lipid ratio | AMC release (nM/s) | | | | | |
|---|---|---|---|---|---|---|
| | α N $His_6$ proteasomes | | β C $His_6$ proteasomes | | T1A β C $His_6$ proteasomes | |
| | soluble | immob. | soluble | Immob. | soluble | immob. |
| 1 : 909 | 5.72 (116) | 5.28 (107) | 6.86 (111) | 6.35 (103) | 0.12 | 0.09 |
| 1 : 140 | 5.92 (120) | 5.30 (107) | 6.38 (103) | 5.28 (85) | 0.08 | 0.11 |
| 1 : 56 | 5.40 (109) | 5.18 (105) | 6.27 (101) | 5.31 (86) | 0.10 | 0.07 |

**Table 8: Activity of His-tagged proteasomes against fluorogenic tetrapeptides after immobilization at chelating interfaces and subsequent to desorption.** 180 µM SOPC and 20 µM nickel-loaded NTA-DODA were dissolved in HEPES buffer and after swelling liposomes were formed by lipid extrusion. 125 µM Suc-LLVY-AMC were subjected to degradation by 11 nM His-tagged proteasomes after immobilization on liposomes and subsequent to desorption with 250 mM imidazole (15 min, 60 °C), before terminating the reaction with the 9-fold volume of stopping reagent and measuring the AMC release. The experimental error of proteasomal activity was in the range of ± 0.2 nM AMC / s. The numbers in brackets indicate the percentage of the catalytic constant displayed at 125 µM substrate, if estimated from the Michaelis-Menten equation after extraction of the catalytic constant from the Eadie-Hofstee plot.

### 5.4.2 Proteolytic activity of the immobilized proteasome

Site-specific orientation of His-tagged proteasomes at chelating interfaces was key to understand mechanistic aspects of protein degradation. For this purpose similar amounts of proteasome were immobilized at nickel-chelating lipid interfaces, whereby adsorption was not restricted by crowding, and their activity against fluorescein-labeled casein was studied (Figure 23 A). The tight binding of the His-tags to the chelator lipids could be reversed by addition of EDTA, and substrate degradation was recorded again with the desorbed proteasomes (Figure 23 B). The activity of α N $His_6$ proteasomes immobilized end-on at the lipid interfaces was enhanced threefold upon desorption of the proteasomes (Figure 23 C). The activity of β C $His_6$ proteasomes against fluorescein-labeled casein was comparable when immobilized side-on at lipid interfaces and after complete desorption. The fluorescence increase directly reflects the activity of the proteasome. Consequently, protein degradation of proteasomes is controlled by their orientation. 'Dead-end' proteasomes are able to degrade proteins, albeit at one-third the rate of side-on immobilized or soluble proteasomes.

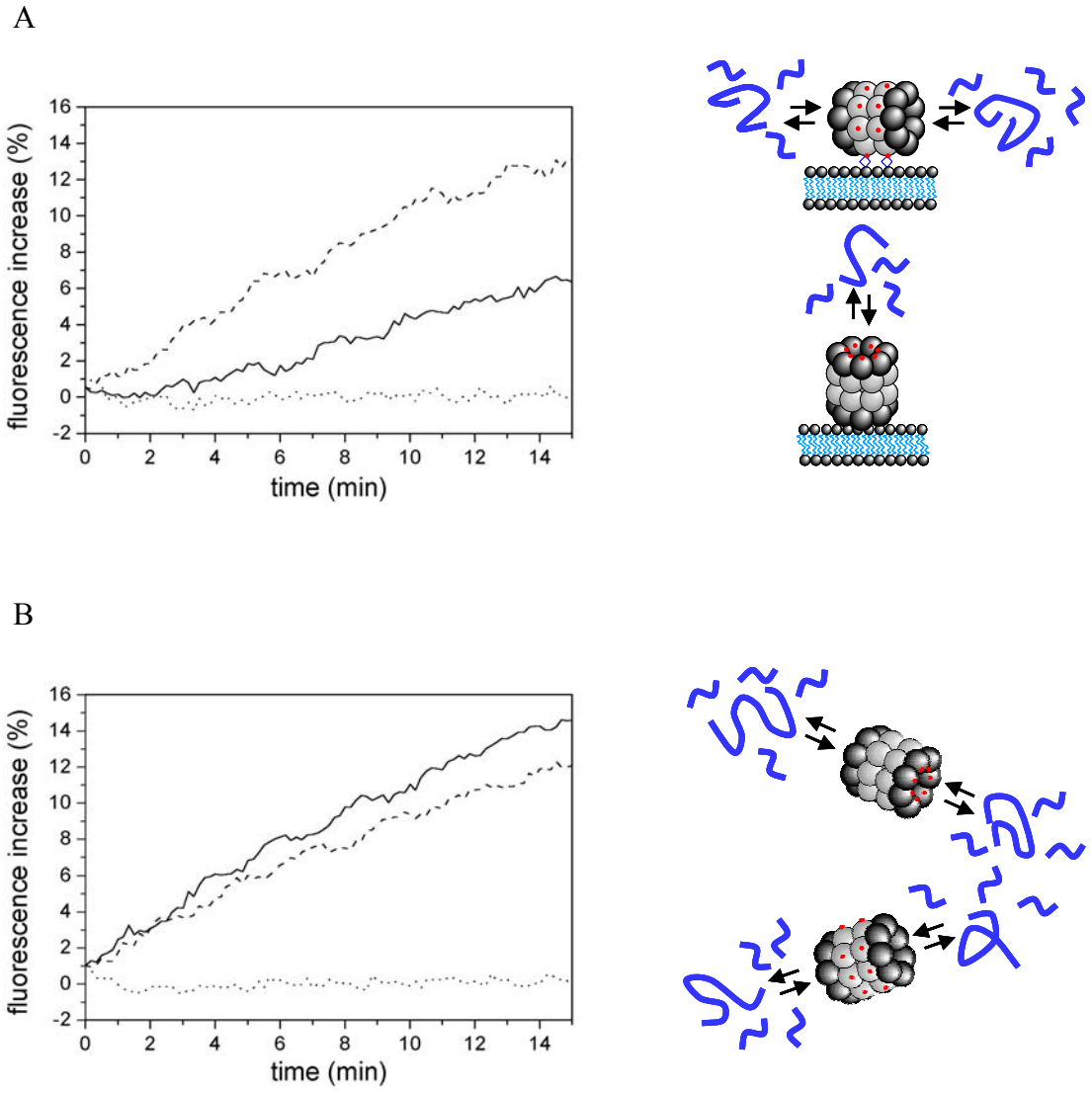


**Figure 23: Proteolytic activity of side-on and end-on immobilized proteasomes.** A) His-tagged proteasomes were immobilized on or B) desorbed from NTA-lipid vesicles (90 mol % SOPC and 10 mol % nickel-loaded chelator lipid) by addition of 100 mM EDTA. Afterwards the proteasomes were dissolved to a final concentration of 7 nM in 50 mM Tris, pH 7.5 containing 90 nM fluorescein-labeled casein. Substrate degradation was recorded fluorimetrically for 15 min at 60 °C and expressed as fluorescence increase of the initial value. The fluorescence increase is denoted as dashed line (β C $His_6$ proteasome), bold line (α N $His_6$ proteasome), and dotted line (β T1A $His_6$ proteasome). C) The initial degradation rates of the corresponding proteasomes are compared before (open bars) or after desorption (filled bars).

## 5.5 Monitoring the loading and unloading of the degradation machinery in real time

### 5.5.1 Studies on NTA-dextran surfaces

The processing of substrates by proteasomes can be dissected after defined immobilization at metal-chelating interfaces. Surface plasmon resonance spectroscopy allows to follow substrate interaction with the proteasome in real time.

At first, substrate degradation was analyzed after immobilizing the proteasome on NTA-dextran chips. The proteasome was bound specifically to the gold-dextran surface, as binding could be reversed (97 %) by addition of EDTA. Around 0.3 - 0.4 casein substrates associated with each α N $His_6$ or β C $His_6$ proteasome. But casein dissociation was always slow, and irreversible binding was high (20 - 30 %). Nonspecific binding prevailed also in the presence of detergent. In case of S-carboxymethyl-lactalbumin, association and dissociation kinetics were fast and dissociation was complete. ~ 0.6 substrates associated with each α N $His_6$ proteasome and ~ 0.8 substrates were bound per β C $His_6$ proteasome. Accordingly, no general differences in substrate processing could be detected on this surface for differently His-tagged proteasomes. This may be due to the flexibility of the dextran molecules, thus perturbing defined orientations of the proteasomes. In case of casein, the low substrate/proteasome stoichiometry arises probably from steric hindrance of protein entry via the dextran linkers. Additionally, the NTA-dextran surface has the drawback of swelling corresponding to the buffer composition. Thus signal stability could not be guaranteed.

### 5.5.2 Studies on lipid monolayers

For proteasome immobilization lipid monolayers were assembled on hydrophobic SAMs of alkylthiols. The lipid monolayers were formed by fusion of SOPC vesicles containing 10 mol % NTA-DODA as metal-chelating lipid. Vesicle fusion raised the resonance signal by ~ 3000 RU (Figure 24), thus confirming the thickness of a monolayer (Dorn et al., 1999; Dorn et al., 1998; Rädler et al., 2000).

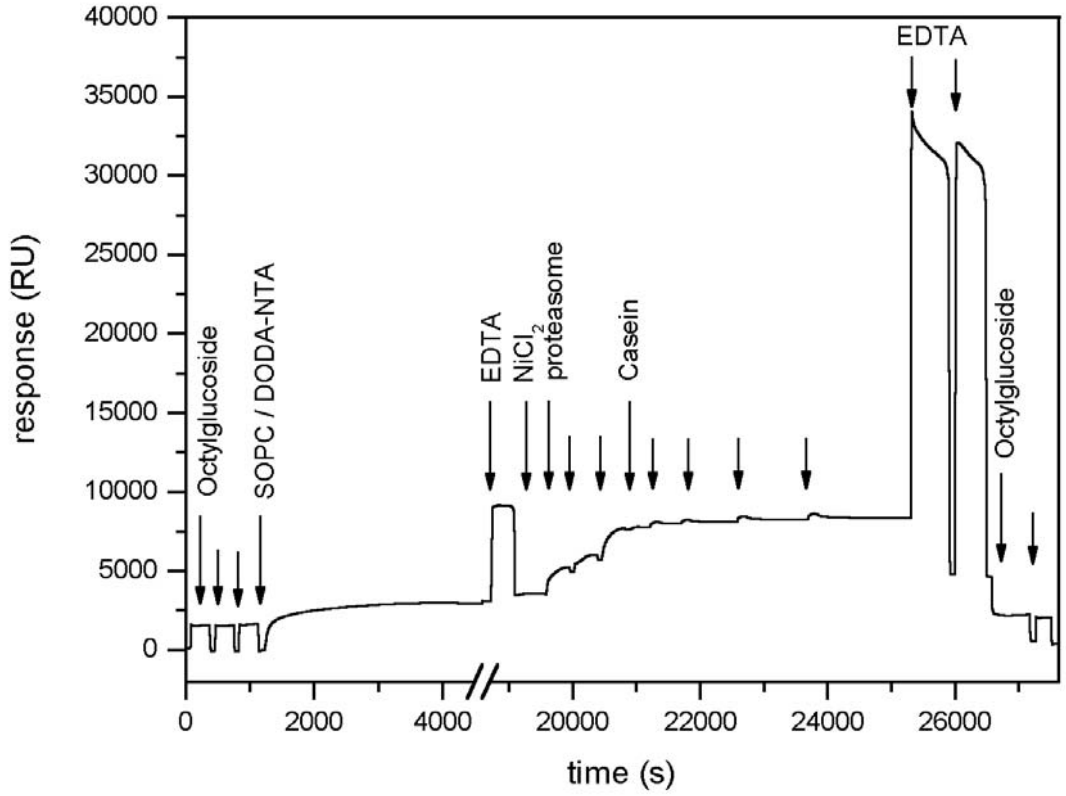


**Figure 24: Binding of casein to β C $His_6$ proteasome after immobilization on a hybrid lipid monolayer.** Lipid vesicles (180 µM SOPC, 20 µM NTA-DODA) were formed in HEPES buffer by extrusion through polycarbonate membranes (100 nm pore diameter) and assembled on a HPA chip, which was previously rinsed with three injections of octylglucoside (40 mM). The SAM was rinsed for 1 h with HEPES buffer before removing metal ions with a pulse of EDTA (100 mM) and loading the NTA headgroups with $NiCl_2$ (100 mM). Afterwards β C $His_6$ proteasome (100 – 200 nM) was injected three times in the presence of imidazole (20 mM). Five casein injections (100 – 300 nM) were recorded, before the proteasomes were removed with two injections of EDTA (500 mM) and the monolayer was washed off with three pulses of detergent (40 mM). The first injection of each type is denoted with a long arrow. A similar procedure was accomplished in the other flow cell for α N $His_6$ proteasomes.

After loading of the NTA headgroups with nickel ions, proteasomes were immobilized on the hybrid lipid monolayer. To study the effect of orientation on substrate degradation α N $His_6$ and β C $His_6$ proteasomes were immobilized in two separate flow chambers. A surface coverage of ~ 60 % was achieved for either proteasome as could be derived from the maximum binding values assuming molecular areas of 95 $nm^2$ for the α N $His_6$ proteasome and of 165 $nm^2$ for the β C $His_6$ proteasome. As substrates casein and insulin B chain were tested.

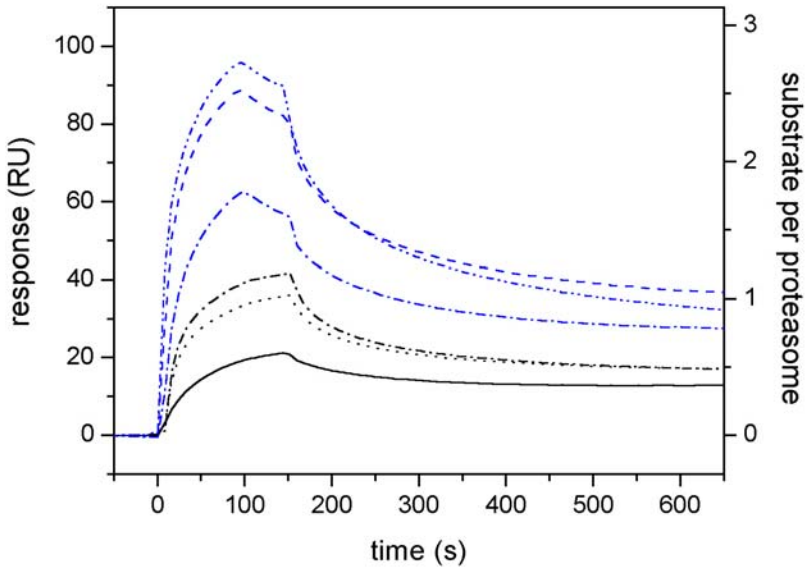


**Figure 25: Real-time analysis of casein association with two differently His-tagged proteasomes after orientated immobilization on lipid monolayers.** α N $His_6$ and β C $His_6$ proteasomes were immobilized in specific orientations at the BIAcore system on a hybrid lipid monolayer containing 10 mol % NTA-DODA and 90 mol % SOPC (see Figure 24). Subsequently, casein was added as substrate in increasing concentrations of 100 – 200 nM (α N $His_6$ proteasomes, black) and 200 – 300 nM (β C $His_6$ proteasomes, blue), where 100 nM are denoted as solid line, 150 nM as dotted line, 200 nM as dash-dotted line, 250 nM as dashed line and 300 nM as dash-dot-dotted line. Casein signals were normalized to 1000 resonance units of immobilized proteasome. The data for the β C $His_6$ proteasome were derived from Figure 24.

When increasing the casein concentration in the upper nanomolar range, the amplitudes reached rapidly saturating levels for both proteasomes, although the Michelis-Menten constants are in the micromolar range (Figure 25). This is most probably caused by the hydrophobic character of the substrate, which interacts strongly with the lipid monolayer or residual adsorbed vesicles. Due to the charged proteasome surface electrostatic interactions with casein cannot be ruled out either. But vesicle fusion was unsuccessful at higher ionic strength in order to overcome ionic interactions. Apparently the substrate/proteasome stoichiometry was double in case of β C $His_6$ proteasomes compared to α N $His_6$ proteasomes. Subtraction of the initial shift due to changes in refractive index would result in a substrate/proteasome stoichiometry of ~ 2 for the β C $His_6$ proteasome and ~ 1 for the α N $His_6$ proteasome. But these values are not reliable, as casein dissociation was impaired due to hydrophobic interactions, thus supporting non-specific binding to the lipid or proteasome.

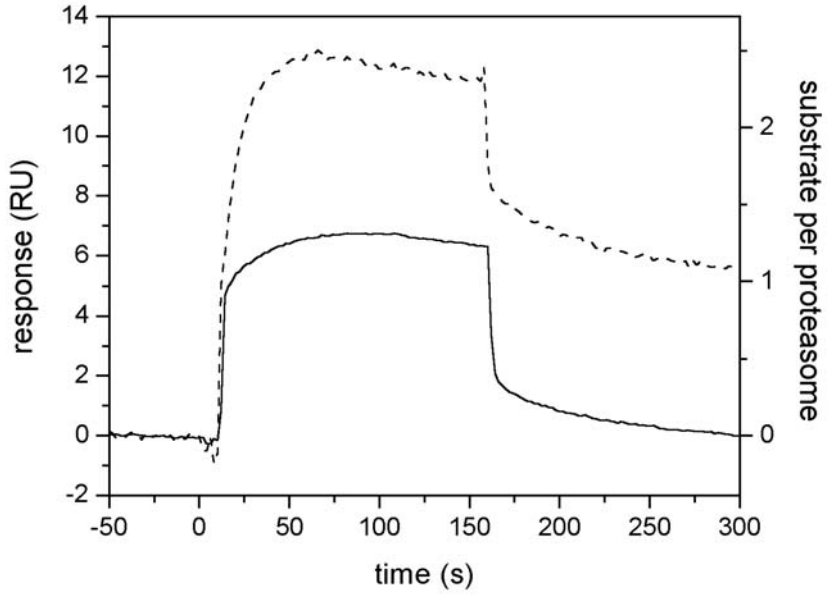


**Figure 26: Real-time analysis of insulin B chain association with two differently His-tagged proteasomes after orientated immobilization on lipid monolayers.** α N $His_6$ and β C $His_6$ proteasomes were immobilized in specific orientations on a self-assembled monolayer containing 10 mol % NTA-DODA. Insulin B chain (10 µM) was added as substrate for α N $His_6$ proteasome (solid line) and β C $His_6$ proteasome (dashed line). Insulin B chain signals were normalized to 1000 resonance units of immobilized proteasome.

Specificity of substrate association could be improved for insulin B chain binding to α N $His_6$ proteasome (Figure 26). But success was restricted to 100 % proteasomal surface coverage. At this proteasomal density substrate interactions with the lipid monolayer beneath or the proteasomal surface were obviously negligible, but interactions among the proteasomes could not be excluded. In case of β C $His_6$ proteasomes, a surface coverage of more than 60 % could not be realized, which is in agreement with side-on orientations (atomic force microscopy and electron microscopy). Consequently dissociation of insulin B chain was hampered similar to casein. The substrate/proteasome ratio again was ambiguous, but resembled the 2 : 1 stoichiometry obtained in case of casein for β C $His_6$ proteasomes : α N $His_6$ proteasomes. The proteasome was immobilized rather specifically on the lipid surface, as one imidazole injection removed 98 % of all proteasomes (Figure 27). Alternatively the 'remainder' could be explained by imidazole molecules binding to NTA headgroups. With respect to desorption, imidazole was even superior to EDTA (92 % specificity, see Figure 24), which removes the metal ions from cryptic places beneath the proteasomes.

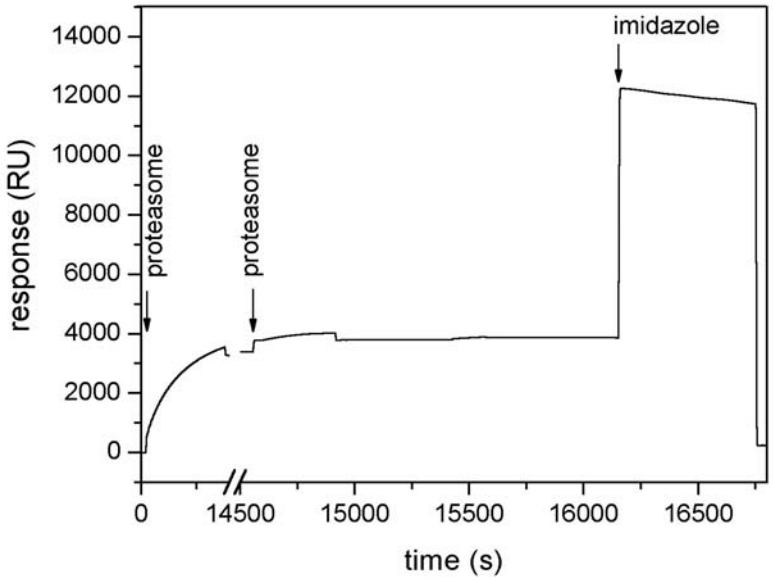


**Figure 27: Reversibility of proteasome immobilization on a hybrid lipid monolayer.** Two injections of β C $His_6$ proteasomes (300 nM and 800 nM, respectively) in the presence of imidazole (20 mM) lead to an increase in resonance signal of altogether 3690 RU on the lipid monolayer (~ 3000 RU) containing 90 mol % SOPC and 10 mol % NTA-DODA. The proteasome was removed by one pulse of imidazole (1 M).

### 5.5.3 Studies on self-assembled thiol monolayers

α N $His_6$ and β C $His_6$ proteasomes were bound site-specifically to the NTA thiols integrated in the matrix of the self-assembled thiol monolayers. The maximum binding values are consistent with a surface coverage of about 20 % assuming molecular areas of 95 $nm^2$ for the α N $His_6$ proteasome and of 165 $nm^2$ for the β C $His_6$ proteasome. Subsequently substrate loading and unloading of the 20S proteasome was recorded at increasing concentrations of casein. Substrate association is specific, as casein binding is efficiently competed out by small peptides (Karin Busch & Robert Tampé, unpublished results). The normalized casein resonance signal obtained with α N $His_6$, β C $His_6$ and β T1A β C $His_6$ proteasomes (Figure 28 A, B and C, respectively) was plotted against the substrate/proteasome stoichiometry (Figure 29).

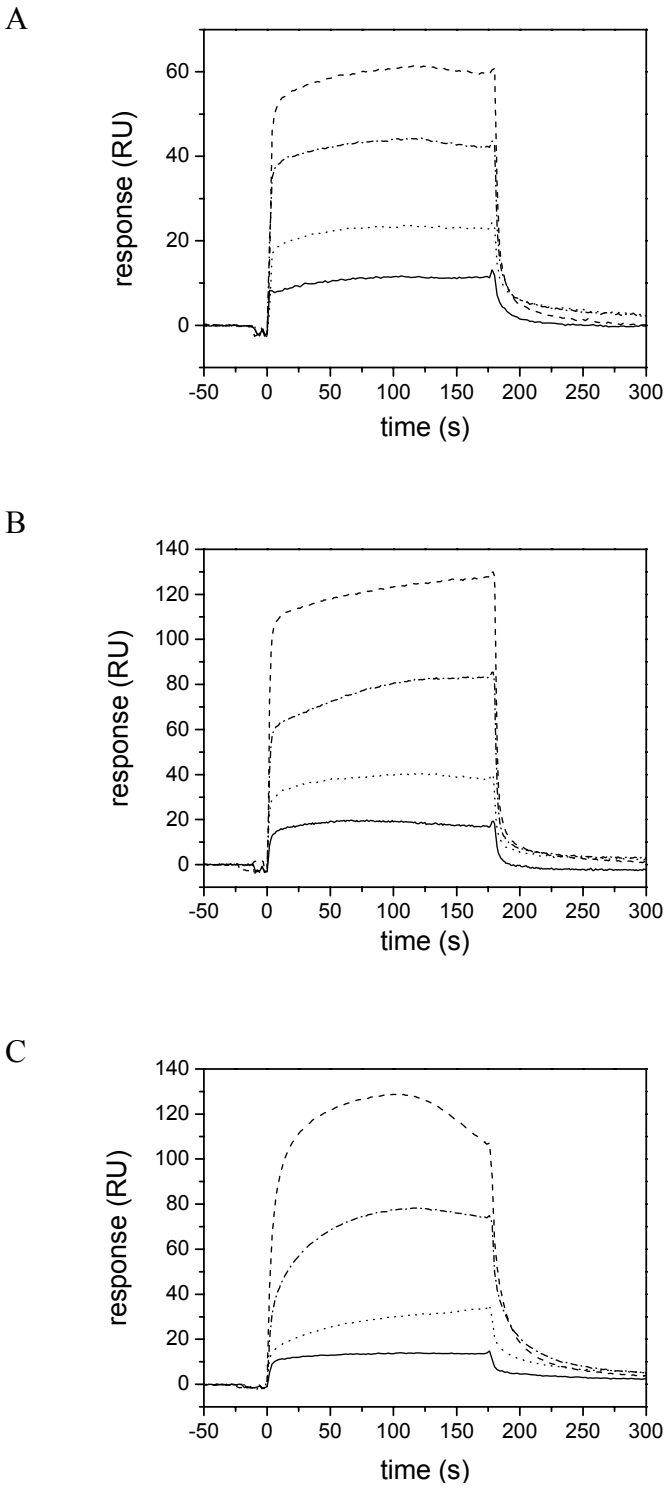


**Figure 28: Real-time analysis of casein association with two different His-tagged proteasomes after orientated immobilization on thiol layers.** α N $His_6$ proteasomes (A), β C $His_6$ proteasomes (B) and β T1A β C $His_6$ proteasomes (C) were immobilized in specific orientations at the BIAcore system on a functionalized surface doped with 1 mol % NTA thiols. Subsequently casein was added as substrate in increasing concentrations of 2.5 to 20 µM (2.5 µM, bold line; 5 µM, dotted line; 10 µM, dash-dotted line; 20 µM, dashed line). Casein signals were normalized to 1000 resonance units of immobilized proteasome.

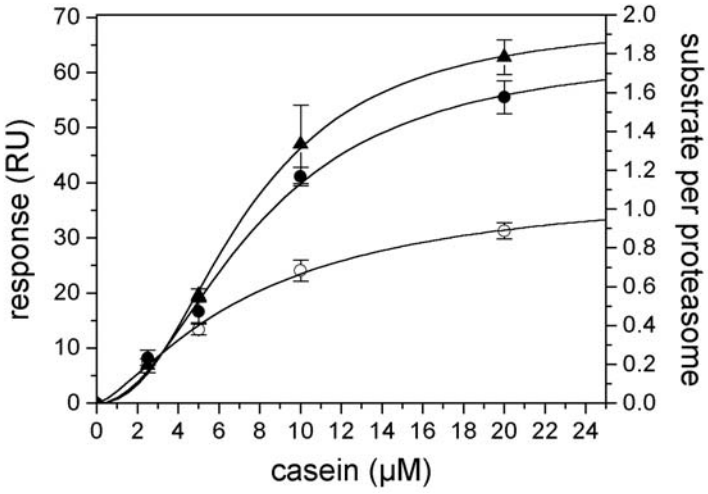


**Figure 29: Substrate/proteasome stoichiometry derived from surface plasmon resonance studies.** Stoichiometry of bound casein molecules per immobilized α N $His_6$ proteasome (open circles), β C $His_6$ proteasome (filled circles) and β T1A β C $His_6$ proteasome (filled triangles), respectively. The data were derived from Figure 28 as described in Methods. The measurements were performed in triplicate.

Strikingly, the final value of the fit for the substrate/proteasome ratio was about twofold for the β C $His_6$ and β T1A β C $His_6$ proteasome when compared with the α N $His_6$ proteasome (1.85 and 1.98 versus 1.14). Thus it can be concluded that end-on immobilized α N $His_6$ proteasome associates with one substrate, whereas side-on immobilized β C His-tagged proteasomes bind simultaneously two substrates. Fitting the substrate/proteasome binding curves with the Hill equation yielded Hill coefficients of 1.37, 1.99 and 2.25 for α N $His_6$, β C $His_6$ and β T1A β C $His_6$ proteasomes, respectively. Thus two-substrate association with β C His-tagged proteasomes underlies positive cooperativity in contrast to one-substrate association. The half-saturation constants were similar: 7.7 µM for α N $His_6$ proteasomes, 7.9 µM for β C $His_6$ proteasomes and 7.4 µM for β T1A β C $His_6$ proteasomes.

From the dissociation intervals of casein the $k_{off}$-values could be determined (Figure 30 and Table 9). β C $His_6$ proteasomes displayed a $k_{off}$ of 0.36 $s^{-1}$ for casein, whereas α N $His_6$ proteasomes could be attributed a $k_{off}$ of 0.18 $s^{-1}$, i. e. half the value. When comparing these two immobilized proteasomes, the number of exit pathways is double in case of β C $His_6$ proteasomes, indicating that the different off-rates arise from statistics. Due to a processing defect the off-rate of casein from β T1A β C $His_6$ proteasomes decreased with increasing substrate concentration (Figure 31).

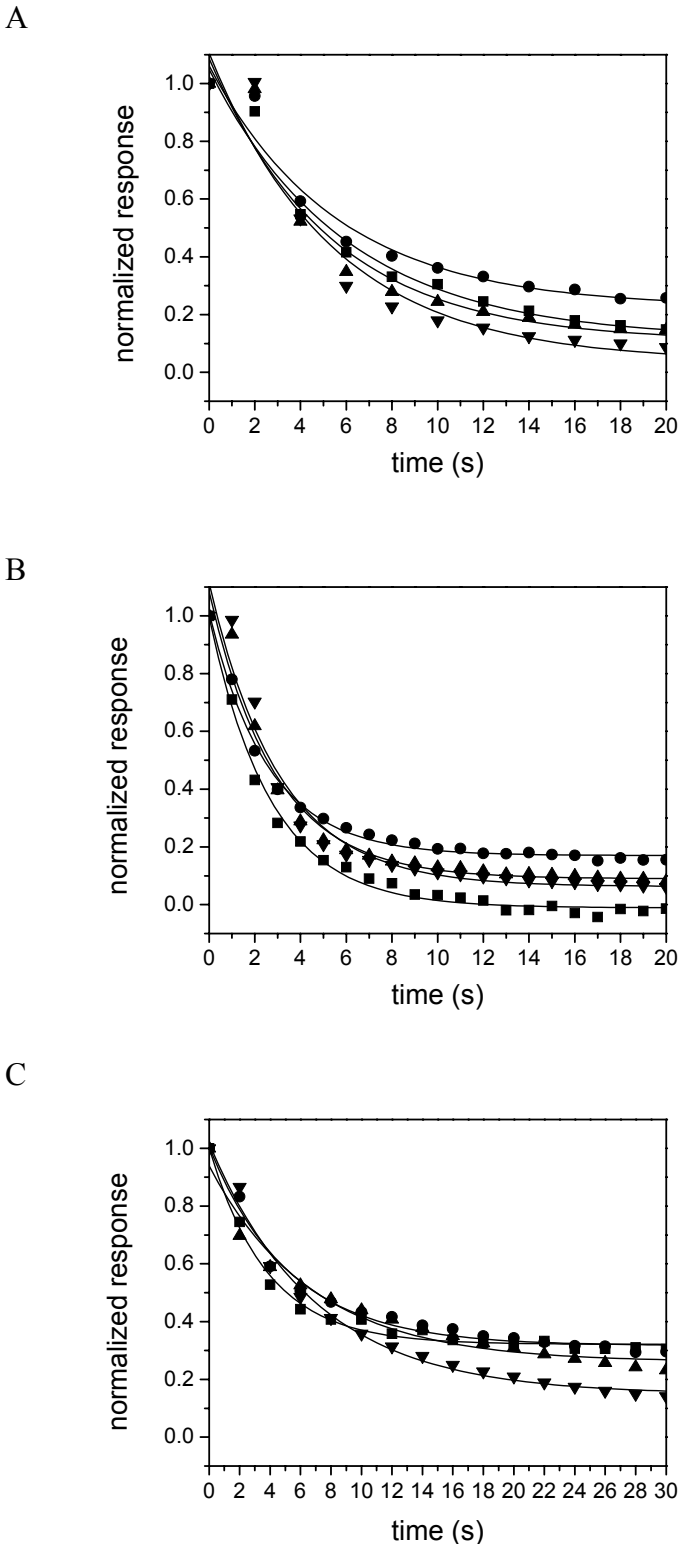


**Figure 30: Casein dissociation from immobilized proteasomes.** Casein dissociation from α N $His_6$ proteasomes (A), β C $His_6$ proteasomes (B) and β T1A β C $His_6$ proteasomes (C) is depicted after normalization of the signal. The curves are fitted with a monoexponential function within an interval of 20 s (A and B) or 30 s (C). The casein concentrations are denoted as squares (2.5 µM), circles (5 µM), upright triangles (10 µM) and downward triangles (20 µM).

| Proteasome | $k_{off}$-values at different casein concentrations ($s^{-1}$) | | | | |
|---|---|---|---|---|---|
| | 2.5 µM | 5 µM | 10 µM | 20 µM | Average |
| α N $His_6$ | 0.168 | 0.179 | 0.189 | 0.184 | 0.180 |
| β C $His_6$ | 0.368 | 0.388 | 0.348 | 0.327 | 0.358 |
| β T1A β C $His_6$ | 0.262 | 0.189 | 0.148 | 0.144 | (0.143) |

**Table 9: Off-rate constants of casein for the different proteasomes.** The off-rate constants were obtained from a monoexponential fit of the dissociation phase (see Figure 30). The number in brackets indicates the threshold of the $k_{off}$-value for the inactive proteasome mutant at infinite substrate concentration.

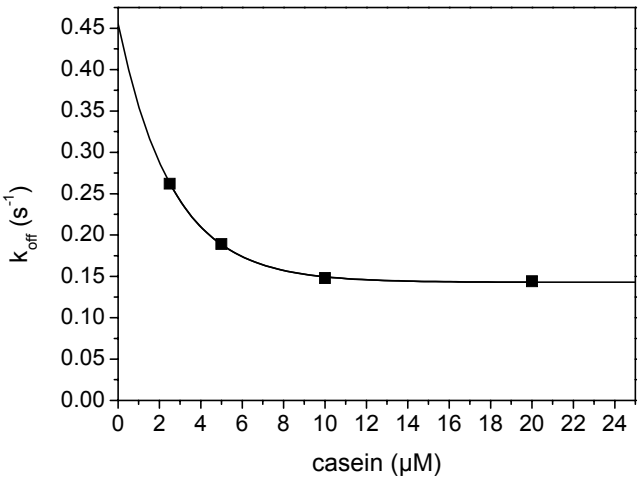


**Figure 31: Concentration dependence of the off-rate for the inactive proteasome mutant.** The off-rate of casein from β T1A β C $His_6$ proteasome was plotted against the substrate concentration and approximated with a monoexponential fit.

Around 40 % of the $k_{off}$-value (0.143 $s^{-1}$) for β C $His_6$ proteasomes could be assigned to the inactive proteasome mutant at infinite substrate concentrations. Accordingly, the two-substrate complex formed at infinite casein concentrations is associated with half up to one-third the off-rate of the one-substrate complex formed at infinite dilution.

According to a biexponential fit, the two association constants are at high casein concentration similar for α N $His_6$ and β C $His_6$ proteasomes (Table 10).

| Proteasome | $k_{on}$-values | 2.5 µM | 5 µM | 10 µM | 20 µM |
|---|---|---|---|---|---|
| α N $His_6$ | $k_1$ ($s^{-1}$) | n.d. | 0.038 | 0.142 | 0.142 |
| | $k_2$ ($s^{-1}$) | n.d. | 1.278 | 1.298 | 1.179 |
| | $k_{on}$ ($s^{-1}$) | n.d. | 1.099 | 1.109 | 0.995 |
| β C $His_6$ | $k_1$ ($s^{-1}$) | 0.125 | 0.105 | 0.095 | 0.126 |
| | $k_2$ ($s^{-1}$) | 1.082 | 1.756 | 1.051 | 1.075 |
| | $k_{on}$ ($s^{-1}$) | 0.714 | 1.368 | 0.703 | 0.748 |
| β T1A β C $His_6$ | $k_1$ ($s^{-1}$) | 0.018 | 0.043 | 0.047 | 0.089 |
| | $k_2$ ($s^{-1}$) | 0.620 | 0.947 | 0.590 | 0.458 |
| | $k_{on}$ ($s^{-1}$) | 0.358 | 0.758 | 0.442 | 0.314 |

**Table 10: On-rate constants of casein for the different proteasomes.** These were obtained from biexponential fits of the association phase (2 – 22 s after injection of casein).

The low value of the first association constant $k_1$ might indicate a rate-limiting translocation step of the substrate and the higher value of the second association constant $k_2$ could be due to substrate binding in the antechambers, assuming an open-pore mechanism for binding of the second substrate. As the His-tags around the pore apertures restrict substrate entry into the α N $His_6$ proteasome, an increase of $k_1$ with substrate concentration is expected and was observed in contrast to the β C $His_6$ proteasome. Positive cooperativity of β C $His_6$ proteasomes can be explained by drastically increasing on-rates because of omission of the rate-limiting translocation step during association with the second substrate. In case of the β T1A β C $His_6$ proteasome the first substrate does probably not facilitate entry of the second. It is rational that in case of the inactive mutant leaving substrates impede translocation of entering substrates into the proteasome as apparent from with increasing substrate concentration dropping off-rates and increasing $k_1$-values. Thus positive cooperativity of the β T1A β C $His_6$ proteasome is mainly due to a decrease in the off-rate of the forming bisubstrate:proteasome complex.

### 5.6 Two-substrate association with the proteasome

To confirm that two substrates are simultaneously bound to the 20 S proteasome single-molecule experiments were performed. By means of fluorescence auto- and cross-correlation spectroscopy one can dissect the association process at the proteasome in the first and second substrate-binding step and determine equilibrium concentrations of the different species and the corresponding binding constants. Insulin B chain served in these experiments as substrate for the proteasome. Insulin B chain labeled with two fluorophores is internally self-quenched, as degradation by the proteasome triggered a considerable fluorescence increase (Figure 32, inset). HPLC profiles of digested Alexa 594-labeled insulin B chain demonstrated fragmentation of the substrate (Figure 32).

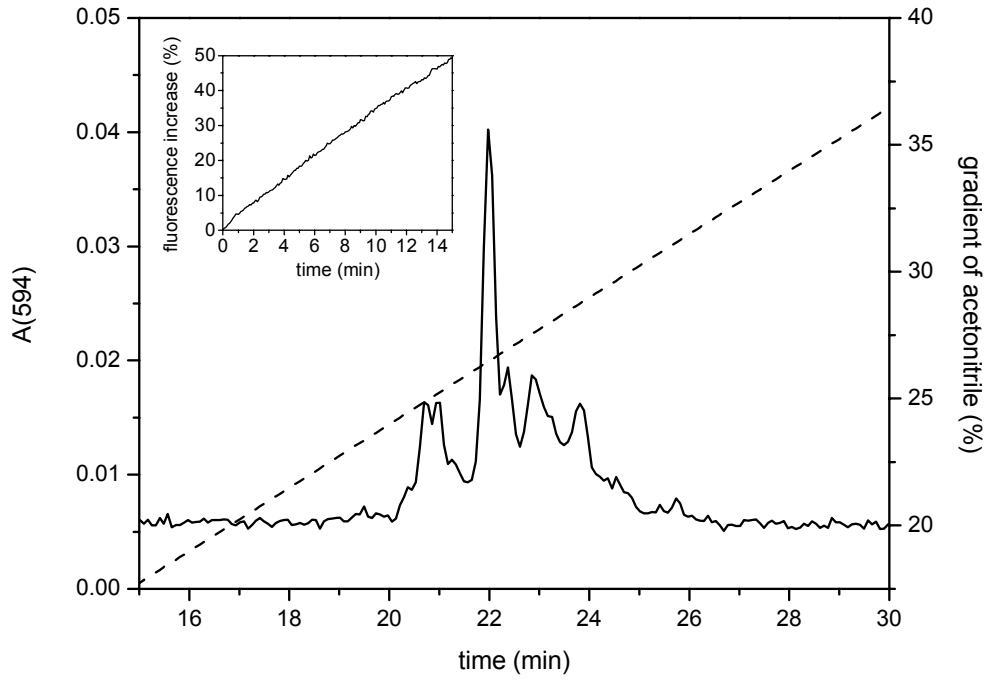


**Figure 32: Cleavage profile of digested Alexa 594-labeled insulin B chain.** Alexa 594-labeled insulin B chain (5 µM) was digested (1 h, 60 °C) by β C $His_6$ proteasome (100 nM) in HEPES buffer, before stopping the reaction with 7.2 % (w/v) TCA. 50 µl of the supernatant were separated on a µRPC C2/C18 column pre-equilibrated with 0.1 % (v/v) TFA in $H_2O$ (buffer A) by running a gradient from buffer A to buffer B (0 - 10 % B within 8 min, 10 – 40 % B within 24 min and 40 – 100 % B within 7 min, B: 0.1 % (v/v) TFA in acetonitrile). The absorption at 594 nm was recorded. *Inset: Proteasomal degradation of labeled insulin B chain.* Alexa 594-labeled insulin B chain (20 nM) was digested (15 min, 60 °C) by β C $His_6$ proteasome (7 nM) in HEPES buffer. The fluorescence increase in per cent of the initial value is shown.

Preliminary FRET studies with Alexa 488-labeled insulin B chain and Alexa 594-labeled insulin B chain indicated a fluorescence increase upon addition of β C $His_6$ proteasome. But internal quenching of the fluorophores was lost during degradation (Figure 32 inset) and enhanced also the recorded emission. Thus FRET studies in the presence of multiply labeled insulin B chain or casein suggest only ambiguously a two-substrate association with the proteasome.

In the cross-correlation experiment, auto- and cross-correlation curves of β C $His_6$ proteasome were monitored in the presence of Oregon-Green 488-labeled insulin B chain and Alexa 633-labeled insulin B chain (Figure 33). As the cross-correlation amplitude exceeded significantly the threshold value of 1.001, at least two distinct labeled substrates could be co-localized in the proteasome. Parameters derived from the cross-correlation experiment are compiled in Table 11.

In addition, equilibrium concentrations of all proteasome-bound species and dissociation constants could be determined according to the reaction scheme given in Figure 34. Oregon-Green 488-labeled insulin B chain predominantly bound to the proteasome (bound fraction: 26.3 %, $\tau_D$= 42 µs) over Alexa 633-labeled insulin B chain (bound fraction: 12.9 %, $\tau_D$= 86 µs), presumably because the smaller label imposed less steric constraints. The increased concentrations of free green substrate in comparison with free red substrate can be explained by the higher quantum yield of the green dye. Processing of both substrates was accompanied by a pronounced fluorescence increase in the green and red channel. The overall dissociation constant of the two-step process was determined from the concentration of free and bound interaction partners ($K_{D,\ overall}$ = 3 $\mu M^2$). Subtraction of double binding events with regard to the cross-correlation product concentration revealed the dissociation constants for the first binding process to the proteasome ($K_{D,Sg}$ = 4.5 µM and $K_{D,Sr}$ = 11.6 µM, Table 12) and the concentrations of the monosubstrate complexes ($c_{Sg*P}$= 15.1 nM and $c_{Sr*P}$= 0.92 nM). Based on the presumption that the proteasomal affinities of the green substrate relative to the red substrate are identical in the first and second binding step, the dissociation constants for the homo- and heterobisubstrate binding processes ($K_{D,Sg*Sg}$ = 510 nM, $K_{D,Sr*Sr}$ = 1.32 µM, $K_{D,Sg*Sr}$ = 660 nM, $K_{D,Sr*Sg}$ = 260 nM) and the concentrations of the bisubstrate complexes ($c_{Sg*Sg*P}$= 1.4 nM and $c_{Sr*Sr*P}$= 5 pM) could be calculated.

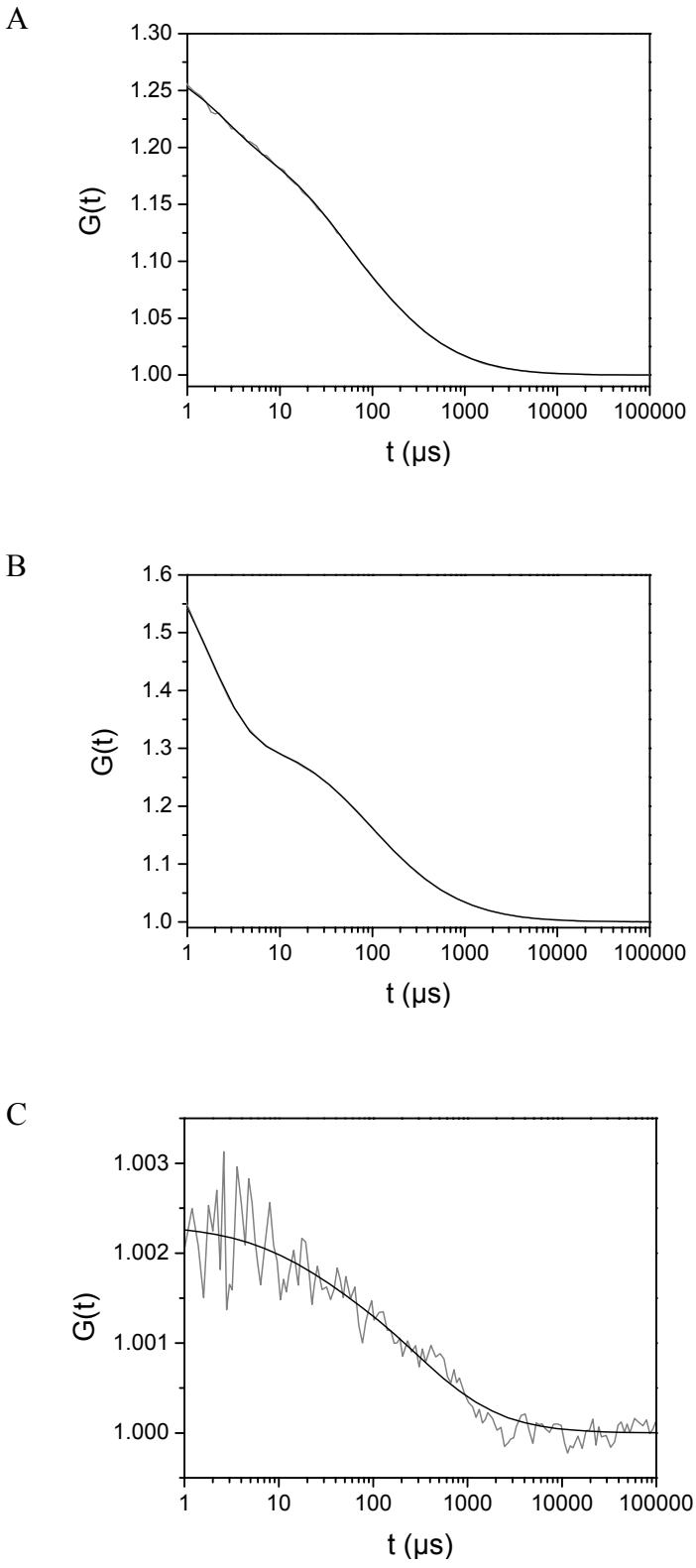


**Figure 33: Two-substrate association with the proteasome.** Autocorrelation curves ($\lambda_{ex}$ = 488 nm (A) and $\lambda_{ex}$ = 633 nm (B)) and cross-correlation curves (C) were recorded with β C $His_6$ proteasome (1.46 µM) and additions of Oregon Green 488-labeled insulin B chain (37 nM) and Alexa 633-labeled insulin B chain (22 nM). Auto- and cross-correlation curves were fitted with a two-component model.

| | AC488 | AC633 | CC |
|---|---|---|---|
| $\tau_{dye}$/µs | 21.4 | 67.2 | - |
| S | 5.6 | 7.9 | 6.7 |
| V/fl | 0.116 | 0.540 | 0.307 |
| G(0) | 1.224 | 1.319 | 1.002 |
| $N_{substrate}$ | 4.433 | 2.751 | 0.031 |
| $c_{substrate}$/nM | 63.4 | 8.46 | 0.168 |
| $\tau_{unbound\ substrate\ or\ dye}$/µs | 41.5 | 86.0 | 22.0 |
| $F_{unbound\ substrate\ or\ dye}$/% | 73.7 | 87.1 | 8.2 |
| $c_{unbound\ substrate\ or\ dye}$/nM | 46.73 | 7.37 | 0.014 |
| $\tau_{bound\ substrate}$ /µs | 290.2 ± 11.8 | 513.6 ± 27.1 | 369.2 ± 91.8 |
| $c_{substrate*proteasome}$/nM | 15.1 | 0.92 | - |
| $c_{substrate*substrate*proteasome}$/nM | 1.4 | 0.005 | 0.168 |

**Table 11: Cross-correlation data of proteasome with Oregon Green 488-labeled insulin B chain and Alexa 633-labeled insulin B chain.** Auto- (AC 488 and AC 633) and cross-correlation curves (CC) were recorded with β C $His_6$ proteasome (1.46 µM) in the presence of Oregon Green 488-labeled insulin B chain (37 nM) and Alexa 633-labeled insulin B chain (22 nM). Data were derived from the plots as described in the Method section or calculated according to the reaction scheme. The cross-correlation curve was background-corrected with regard to a crosstalk of the green emissison into the red channel ($Q_{gr}$= 8 %).

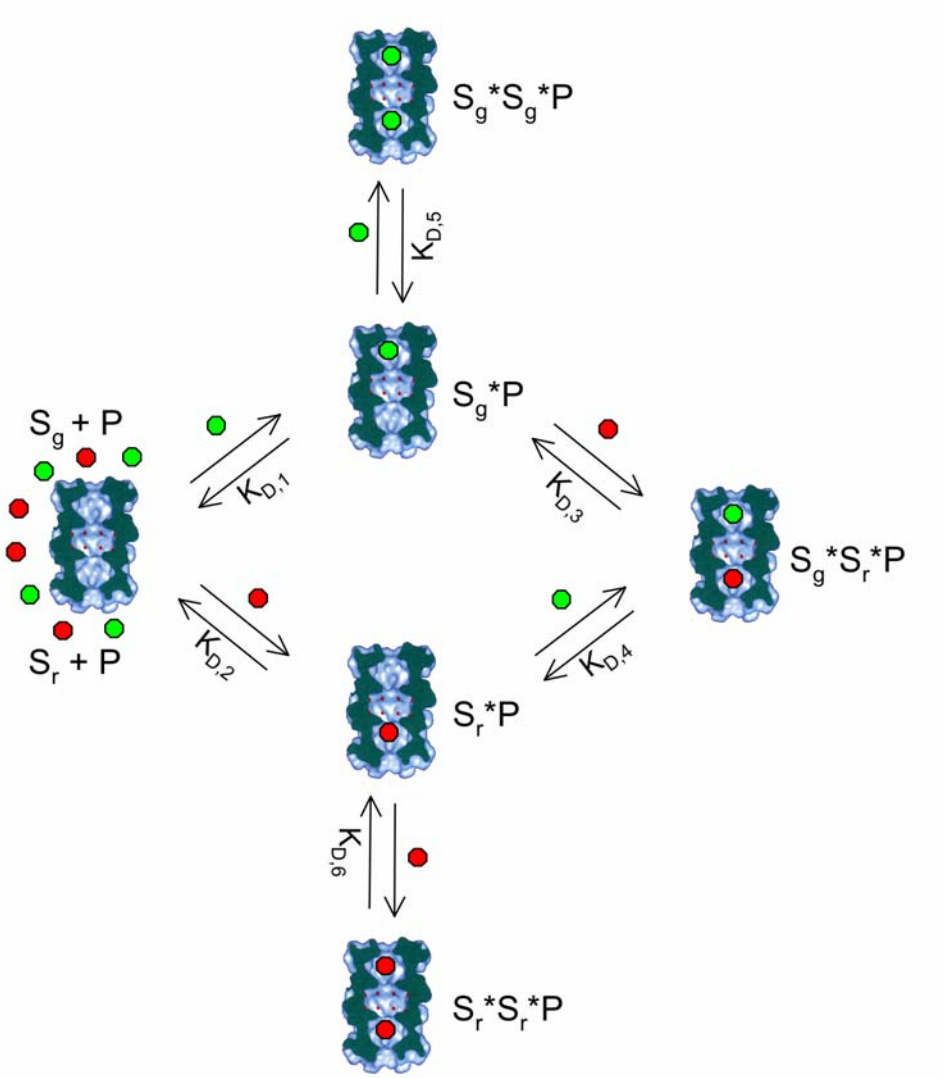


**Figure 34: Scheme of the binding events at the proteasome**. β C $His_6$ proteasome (P) binds to Oregon Green 488-labeled insulin B chain ($S_g$) and Alexa 633-labeled insulin B chain ($S_r$) generating two different single-substrate complexes ($S_g$*P and $S_r$*P) and three different binary substrate complexes ($S_g$*$S_g$*P, $S_r$*$S_r$*P and $S_g$*$S_r$*P). The dissociation constants ($K_D$) are outlined.

| | |
|---|---|
| $K_{D,1}$ | 4.5 µM |
| $K_{D,2}$ | 11.6 µM |
| $K_{D,3}$ | 660 nM |
| $K_{D,4}$ | 260 nM |
| $K_{D,5}$ | 510 nM |
| $K_{D,6}$ | 1.32 µM |

**Table 12: Dissociation constants of single and binary substrate-binding processes.** The dissociation constants were calculated according to the reaction scheme (Figure 34).

Remarkably, the affinity for the second substrate was more than a factor of 8 higher than for the first. Consequently, positive cooperativity of the two substrate binding processes could be demonstrated. In accordance with previous observations, the concentrations of green mono- and bisubstrate complexes exceeded the red mono- and bisubstrate complexes. The cross-correlation product exhibited a concentration between green-only and red-only bisubstrate : proteasome complexes ($c_{Sg*Sr*P}$= 168 pM) and according to the instrumental adjustments a diffusion time ($\tau_D$= 369 µs) between the mono- and bi-substrate*proteasome complexes detected in the green ($\tau_D$= 290 µs) and red channel ($\tau_D$= 514 µs). In summary, the proteasome processes two substrates per degradation cycle with positive cooperative binding characteristics.

A second set of cross-correlation experiments was performed with Cy5-labeled β C $His_6$ proteasome and Oregon-Green 488-labeled insulin B chain to extract the dissociation constant of the theoretical single-substrate binding state from the steady-state equilibrium. The auto- and cross-correlation curves are depicted in Figure 35. The corresponding parameters were derived as described previously (Table 13).

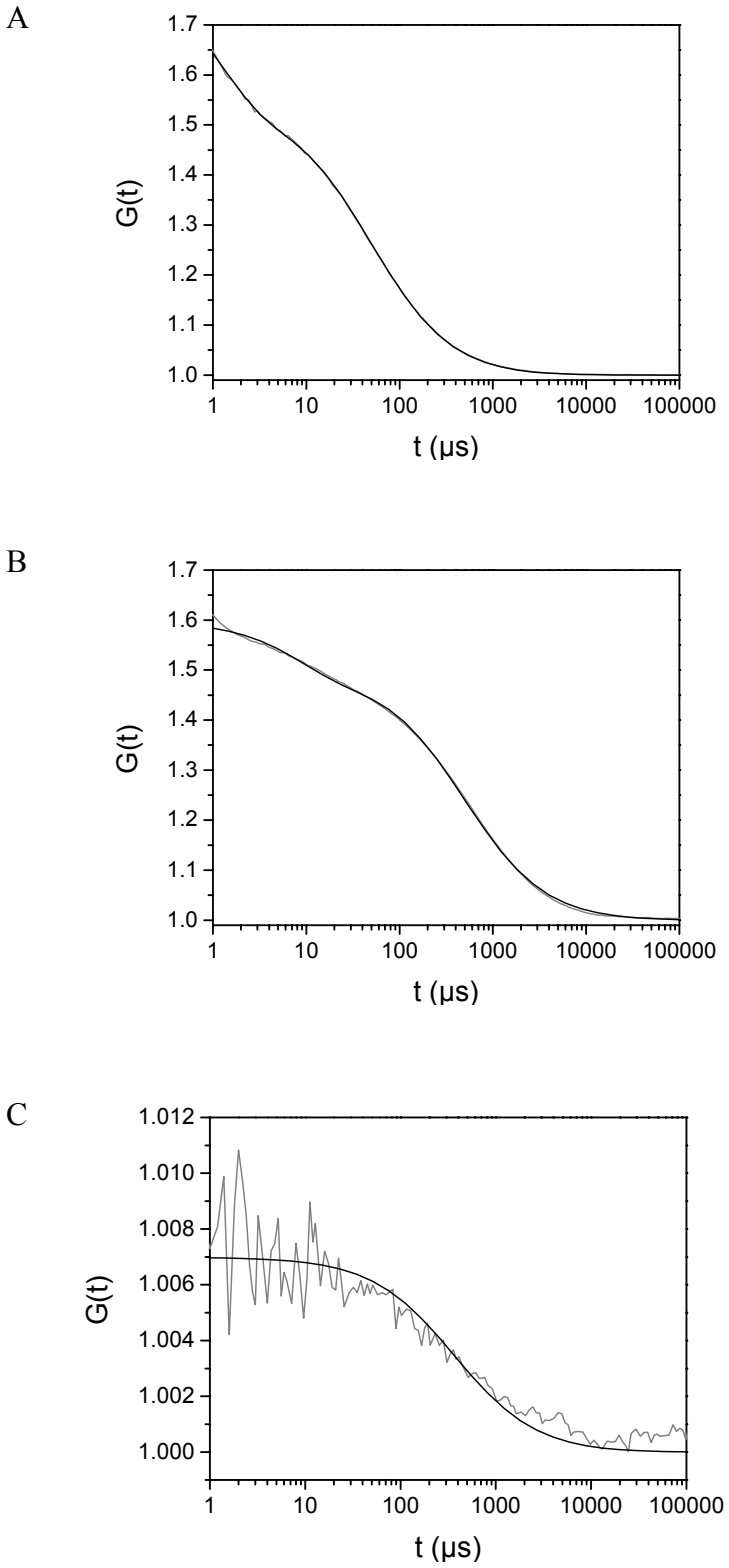


**Figure 35: Cross-correlation experiment studying the interactions of Oregon Green 488-labeled substrate with Cy5-labeled proteasomes.** Autocorrelation curves ($\lambda_{ex}$ = 488 nm (A) and $\lambda_{ex}$ = 633 nm (B)) and cross-correlation curves (C) were monitored with Cy5-labeled β C $His_6$ proteasome (32 nM) in the presence of Oregon Green 488-labeled insulin B chain (31 nM) and fitted with one-component models.

| | AC488 | AC633 | CC |
|---|---|---|---|
| $\tau_{dye}/\mu s$ | 24.9 | 52.9 | - |
| S | 6.3 | 8.4 | 7.4 |
| V/fl | 0.163 | 0.467 | 0.306 |
| G(0) | 1.533 | 1.485 | 1.006 |
| N | 1.8528 | 2.0388 | 0.0232 |
| c/nM | 18.9 | 7.25 | 0.126 |
| $\tau/\mu s$ | 49.4 ± 0.2 | 493.1 ± 5.0 | 367.5 ± 36.5 |

**Table 13: Data extracted from the cross-correlation experiment of Cy5-labeled proteasome with Oregon Green 488-labeled insulin B chain.** Auto- (AC 488 and AC 633) and cross-correlation curves (CC) were recorded with Cy5-labeled β C $His_6$ proteasome (32 nM) in the presence of Oregon Green 488-labeled insulin B chain (31 nM). Data were derived from the plots as discussed in the Method section.

The cross-correlation curve documents that labeled insulin B chain associated with labeled proteasome, but does not discriminate between single- and multiple-substrate binding states. However, the cross-correlation product exhibited a lower concentration than in the previous experiment, because the proteasome concentration had to be decreased due to detection limits. Since the cross-correlation volumes in the two studies were equally sized, the diffusion times of the substrate-bound proteasomes were comparable (~ 370 µs). According to a hypothetical one-substrate binding model the dissociation constant could be calculated ($K_D$ = 1.1 µM). As this dissociation constant is more than 4-fold lower than concluded from the previous cross-correlation experiment, binary substrate-binding events contribute to the steady-state equilibrium. An additional effect of the proteasomal Cy5-label on the dissociation constant cannot be excluded.

# 6. Discussion

## 6.1 Preparation and identification of the proteasome

The 20 S proteasome from *Thermoplasma acidophilum* was expressed heterologously in *Escherichia coli*. The expression conditions (25 °C, overnight) were favorable, as the yield was around 50 % higher than for expression at 30 °C up to the stationary phase (Akopian et al., 1997). Purification by IMAC was suboptimal for column material based on NTA agarose, presumably because the exclusion limit of the beads was relatively low. Thus purification was accomplished via binding of the proteasome to column material with higher exclusion limit as offered by IDA sepharose. Although the affinity of His-tagged proteins for IDA is reduced compared to NTA, the strategy worked better, because high elution strength due to the numerous His-tags attached to the proteasome could be bypassed and the formation of proteasome aggregates could be suppressed. In combination with IDA-material nickel ions were inferior to zinc ions. Although the affinity of His-tagged proteins is higher for the $Ni^{2+}$-complex than for the $Zn^{2+}$-complex the proteasome purification was much purer via formation of the latter complex. This might be due to the fact that the numerous His-tags trigger coelution of nickel ions which tend to form high-molecular-weight complexes with the proteasome. An aggregation tendency was never observed for zinc ions, maybe due to the lower affinity of the proteasome for zinc ions. Additionally, the tetrahedral coordination sphere of zinc ions might prevent the proteasome from forming metal complexes in contrast to the octrahedral coordination sphere of nickel ions. The proteasome preparation was always pure after IMAC, since multiply His-tagged proteins bind with high affinity to the column material. Thus gel filtration was mainly applied to remove the His-tag competitor imidazole for immobilization experiments. The concentration step for gel filtration was performed in centricons, because ultracentrifugal precipitation of the proteasome induced metal-ion mediated formation of insoluble proteasome aggregates. Spin concentrators offered the advantage of removing pre-column single proteasome subunits, which might stick non-specifically to the assembled proteasomes or clog the proteasomal apertures or the column. Sedimentation of the proteasome by ultracentrifugation also separated the single subunits, but less efficiently forming aggregates.

Gel filtration demonstrated that the proteasome was correctly assembled as the proteasome peak was homogenous and deviated only < 1.5 % from the expected molecular mass. Due

to the high molecular mass of the proteasome identification was not addressed by MALDI-MS, but by SDS-PAGE and Western Blot. Single α- and β-subunits could be detected due to their slightly different electrophoretic mobility in comparable amounts in a Silver or Coomassie Stain after SDS-PAGE. The polyclonal anti-20 S proteasome antiserum predominantly detected the α-subunits, presumably because the larger exposed surface area of α-subunits was more immunogenic. The anti-His-tag antibody identified a stretch of five consecutive histidines, thus confirming the integrity of the His-tag.

### 6.2 Degradation characteristics of the soluble proteasome

At first, activity of the soluble proteasome was studied against the fluorogenic tetrapeptide Suc-LLVY-AMC. The test represents a valid and sensitive assay for determination of the chymotrypsin-like activity, as the proteasome produces homogenously one fluorescent cleavage product. Other potential cleavage sites of the archaebacterial proteasome, e.g. behind leucine residues, cannot be ruled out, but are energetically disfavored.

The peptidolytic activity of the proteasome, which bears the His-tags at the sides, can be fitted with the Michaelis-Menten equation up to substrate concentrations of 200 µM. At higher concentrations substrate inhibition was observed. Substrate inhibition was earlier analyzed with the eukaryotic wild-type enzyme above 40 µM Suc-LLVY-AMC (Stein et al., 1996). The α C $His_6$ and β C $His_6$ proteasome can be ascribed similar Michaelis-Menten constants of ~ 39 µM and catalytic constants of ~ 0.05 $s^{-1}$ according to conventional plots (Michaelis-Menten, Eadie-Hofstee, and Linewaver-Burk plot). The kinetic parameters agree with published data (Akopian et al., 1997). Accordingly, the β C $His_6$ proteasome has a Michaelis-Menten constant of 39 µM and a catalytic constant of 0.023 $s^{-1}$ at 55 °C.

The proteasome, which harbors His-tags around the apertures, does not display substrate inhibition up to concentrations of 350 µM Suc-LLVY-AMC, presumably because the effective substrate concentration at the active centers is reduced due to the defile. This explanation is supported by the elevated Michaelis-Menten-constant of the α N $His_6$ proteasome (88 µM). The Michaelis-Menten constant is similar to the value of 85 ± 14 µM for the wild-type proteasome from *T. acidophilum* (Seemüller et al., 1995b), but not comparable as fluorescence measurements differed considerably. Consequently, it can be assumed that the wild-type enzyme can be ascribed a higher affinity in the range of the

α C $His_6$ and β C $His_6$ proteasome. The catalytic activity of the α N $His_6$ proteasome correlated with the value for the α C $His_6$ and β C $His_6$ proteasome and also with the value of 0.030 for the wild-type proteasome (Seemüller et al., 1995b). Hence, His-tags positioned at the orifices act like competitive inhibitors. They decrease proteasomal activity, if the concentration of peptidic substrate is rate-limiting ([S] << $K_M$) and lead at higher substrate concentration to wild-type enzymatic activity.

Aging of the proteasome (prior to aggregation or autoproteolysis) altered the affinity of the peptidic substrate for the proteasome, whereas the turnover numbers were maintained. Within a storage interval of 3 weeks (α N $His_6$ and α C $His_6$ proteasome) or 7 weeks (β C $His_6$ proteasome), the Michaelis-Menten constants of α N $His_6$, α C $His_6$, and β C $His_6$ proteasomes dropped by 25 %, 13 % and 18 %, respectively. Thus the affinity increase, most likely due to a displacement of the His-tags and other N-terminal residues, was most prominent for the α N $His_6$ proteasome. Probably, the pore opening is dilated and allows a more rapid substrate entry. A maturation of the active sites would enhance the catalytic constant as well and affect all engineered proteasomes.

Proteasomal digestion of proteins like modified lactalbumin with reduced and carboxymethylated cysteines revealed that constraints imposed by His-tags around the pore apertures were partiallly bypassed by breakdown of smaller cleavage intermediates. Conversely the proteasomes with His-tags at their sides obeyed uniformly a processive degradation mode. The observation that 20 S proteasomes can break strict processivity was already made for similar substrates like modified lysozyme, but was restricted to eukaryotic 20 S proteasomes from pituitary (with β1, β2 and β5 subunits) or spleen (with the corresponding immunosubunits β1i, β2i and β5i subunits) (Wang et al., 1999a).

Preferential degradation of initially released fragments might also be observed with casein. However, proteasomal digestion of casein demonstrated that constricting His-tags at the orifices lead to prolonged digestion of substrates in the central chamber; consequently the fragment size was decreased. In contrast, proteasomes with His-tags around the ‘cylinder’ degrade proteinaceous substrates less exhaustively and produce in average larger fragments. The hypothesis that the product size is determined primarily by the ease of egress from the proteasome was initially proposed for the eukaryotic 20 S proteasome (Nussbaum et al., 1998) and later verified for the regulation of PA-28 (Whitby et al., 2000). Thus one can resume that α N $His_6$ proteasomes underlie steric constraints, which

induce a specific pattern of cleaved substrates and generated products distinct from α C $His_6$ and β C $His_6$ proteasomes. According to HPLC separation of the fragments, the α N $His_6$ proteasomes seem to be less active than the α C $His_6$ and β C $His_6$ proteasomes. However, HPLC columns are blind to very small peptidic products; thus variations in proteolytic activity between the differently His-tagged proteasomes are easily overestimated.

The degradation of proteinaceous substrates can be determined fluorimetrically, since the attachment of fluorophores to the molecule, e. g. casein, triggers fluorescence self-quenching relieved during substrate degradation. His-tagged proteasomes displayed in solution similar activities against fluorescein-labeled casein. The validity of the assay was proven by the fact that the β T1A proteasome mutant did not enhance the fluorescence due to a knockout of the catalytic centers. According to the analysis the relative activities of differently His-tagged proteasomes against peptides and proteins were similar and were not affected by location of the His-tag. The fluorescence increase can also be adopted as measure of proteasomal affinity for a substrate. Accordingly, the Michaelis-Menten constant for casein could be determined uniformly to ~ 4 μM for α N $His_6$ and β C $His_6$ proteasomes, which is in agreement with the casein concentration correlated with maximum activity (25 μM) (Kisselev et al., 1998). Consequently the location of the His-tag does also not interfere with affinity of the proteasome for a proteinaceous substrate.

### 6.3 Degradation characteristics of the immobilized proteasome

A major challenge in elucidating the molecular mechanism of substrate processing is to overcome the $C_2$-symmetry of the eukaryotic proteasome or the $D_7$-symmetry of the archaebacterial proteasome. In case of success, site-directed introduction of mutations at only one pore aperture could decide about the functional necessity of two entrance channels. Surface engineering leading to unique immobilization appears to be a novel practical approach to elucidate the mechanism of highly symmetric barrel-shaped enzymes. Occlusion of one pore aperture by various techniques allows to gain insights into the handling of substrates and products. For biotinylated GroEL it could be recently shown that specific interaction with streptavidin at the pore aperture leads to enclosure of the substrate upon folding; accordingly, the ‘Anfinsen cage’ model of facilitated substrate

refolding was corroborated, while iterative annealing of the substrate could not be accepted for the majority of proteins (Brinker et al., 2001).

After immobilization on chelating supports scanning force and electron micrographs revealed predominantly end-on views of α N $His_6$ proteasomes, whereas β C $His_6$ proteasomes were imaged solely side-on; additionally the integrity of the proteasomes was ascertained after immobilization (Hutschenreiter et al., 2004; Thess et al., 2002). Hence the His-tags enforce the α N $His_6$ proteasomes in a uniform orientation where one pore was occluded by the functionalized interface. We wanted to decipher whether the size of a substrate determines the success of entry or the pathway of access into a 'dead-end' proteasome. Therefore we tested fluorimetrically the activity of immobilized proteasomes against fluorogenic tetrapeptides and fluorescein-labeled casein.

The immobilization of proteasomes at metal-chelating interfaces revealed only minor differences in peptidolytic activity for end-on and side-on orientated proteasomes. In the assay the proteasomal coverage with respect to the surface of liposomes ranged between 8 % and 98 % for β C $His_6$ proteasomes or 3 % and 57 % for α N $His_6$ proteasomes, while the proteasome/chelator lipid ratio was equal for both engineered proteasomes. Proteasomal activity was well preserved upon immobilization, when comparing the AMC release at the chosen substrate concentration (~ 2 $K_M$) with the value expected from the Michaelis-Menten plot of the soluble proteasome (Thess et al., 2002). Hence a 'dead-end' proteasome seems to be able to degrade small substrates with similar activity as in solution. Although the pore opening was not sealed tightly, a vectorial degradation model according to which substrates enter the proteasome through one pore, while products exit through the other, could be excluded.

Next we studied the proteolytic activity of proteasomes immobilized on NTA agarose beads. α N $His_6$ proteasomes retained their activity upon immobilization. The activity of α C $His_6$ proteasomes was twofold increased, the activity of β C $His_6$ proteasomes even threefold stimulated upon immobilization. Thus the degradation rate of side-on orientated proteasomes was more than double when compared with end-on immobilized proteasomes. These results indicate that substrate enrichment in proximity to the surface stimulates proteasomal degradation after immobilization, but does not override the orientational parameter, because the low substrate concentration caused no inhibition of catalytic activity. Hence it can be assumed that influx and efflux of substrates and cleavage products

is accomplished through both apertures of the soluble proteasome. Conversely, 'dead-end' proteasomes cannot or can only partially be accessed by the hidden entrance, since the substrate size imposed steric constraints. Also fragments should leave the 'dead-end' proteasome solely by the pathway of access.

To corroborate the results obtained at surfaces the proteolytic activity of the proteasomes was also tested after immobilization at metal-chelating lipid interfaces. We revealed striking differences dependent on the orientation of the proteasomes. β C $His_6$ proteasomes immobilized in side-on orientation exceeded more than twofold the activity of immobilized α N $His_6$ proteasomes. After complete desorption, the activity of released α N $His_6$ proteasomes was threefold increased, whereas β C $His_6$ proteasomes retained their activity. Therefore the reduced activity of α N $His_6$ proteasomes is solely due to their unique 'dead-end' orientation. These results document that one pore is sufficient for substrate entry and product release. In other words, the pore and antechamber can fulfil a triple function in the import and unwinding of substrates and the egress of products.

### 6.4 Monitoring the loading and unloading of the proteasome in real-time

Prerequisite for kinetic surface plasmon resonance studies with the differently His-tagged proteasomes was selection of the adequate surface for immobilization. The surface has to match the following criteria:

1) specificity of proteasomal binding
2) uniform orientation of proteasomes
3) retention of proteasomal activity upon immobilization
4) suppression of non-specific interactions of the substrate with the surface

Several surfaces were tested for immobilization of the proteasomes comprising NTA-dextran surfaces, self-assembled lipid monolayers, and self-assembled thiol layers.

NTA-dextran surfaces were easy to handle and offered a high binding specificity. However, proteasomal orientation was not preserved, presumably due to flexibility of the dextran linkers, as the tested substrates (modified lactalbumin and casein) showed no differences in association with or dissociation from the differently His-tagged proteasomes. Additionally the interaction of substrates with the surface was high as indicated by the slow dissociation. The dextran surface tended to swell corresponding to the buffer composition, thus affecting the signal-to-noise ratio.

The application of a commercial gold chip covered with an alkylthiol SAM (HPA chip) to proteasome immobilization was probed previously (Dorn et al., 1999; Rädler et al., 2000). Unfortunately, these commercial surfaces were not homogenous with respect to quality of the alkylthiol SAM. Self-assembled lipid monolayers doped with chelating lipids were generated by fusing liposomes of uniform diameter on the hydrophobic layer. The proteasome could be immobilized specifically, because binding could be reversed by imidazole (98 %) or, albeit to a lesser extent, by EDTA (92 %). More peptidic substrates like insulin B chain and proteinaceous substrates as casein were tested. For both substrates association levels with side-on immobilized proteasomes were twofold when compared with end-on orientated proteasomes. Thus paralleles to the fluorimetric experiments could be recorded with SPR. However, dissociation from the lipid interface was slow for both substrates, albeit not at 100 % proteasomal surface coverage. But densest packing of the surface could induce interactions among the proteasomes and influence proteasomal activity. A surface coverage of 60 % was acceptable as compromise on inter-proteasome interactions and substrate-lipid interactions. In comparison to the NTA-dextran surfaces fusion of lipid vesicles to a complete lipid monolayer was more tedious, but the uniformity of proteasomal orientation as prerequisite for analysis of substrate processing was guaranteed.

The optimal surface for recording substrate degradation of immobilized proteasomes proved to be the self-assembled thiol monolayer. Proteasome binding could be reversed fast and complete (98 %) thus indicating high specificity of immobilization. Uniformity of proteasomal orientation as indicated by atomic force microscopy (Ali Tinazli, unpublished results) and integrity of activity could be demonstrated, although the approach was rather simple and convenient. Most of all, interaction of the substrate with the surface was negligible, albeit the proteasomal surface coverage amounted only to 20 %. Hence the exact substrate/proteasome stoichiometry could be determined. In case of end-on immobilized $\alpha$ N $His_6$ proteasome the maximum ratio of bound casein per immobilized proteasome was approximately 1, whereas about two substrates associated with each $\beta$ C $His_6$ or $\beta$ T1A $\beta$ C $His_6$ proteasome in side-on orientation. Thus it is reasonable that one substrate entered the central chamber by each of the two pathways. Although theoretically two to three polypeptide chains can concurrently pass the internal channel in case of the end-on immobilized proteasome (Lee et al., 2002; Liu et al., 2003), these results

convincingly demonstrate that this cannot be extended to distinct polypeptides. In addition, the substrate/proteasome binding behavior indicated significant differences in substrate processing for proteasomes in end-on and side-on orientation. Substrate binding to 'dead-end' orientated proteasomes is associated with a Hill coefficient ~1, whereas side-on immobilized proteasomes show a Hill coefficient of ~2. Thus substrate association with proteasomes obeys a two-step process with positive cooperative binding behavior of the ligands, most probably in opposite antechambers of the proteasome. Consequently, immobilized 'dead-end' proteasomes cannot communicate between the *cis* side and the blocked *trans* side.

For multisubunit complexes comprising folding or disassembly machineries a crosstalk between opposite ends has already been observed. Electron microscopy studies with ClpXP revealed alternating translocation of proteinaceous substrates from both ends of the protease and only rare events where both substrates entered the degradation chamber simultaneously through opposite channels (Ortega et al., 2002). For the chaperone GroEL negative cooperativity upon substrate binding in one of the cavities could be demonstrated directly (Falke et al., 2001). In case of the 20S proteasome, the observed positive cooperative binding behavior of the second substrate might lead to 'obstruction' of the *trans* side with an entering substrate. Hence substrates are completely digested in one cycle prior to fragment release, resulting in a unique degradation mode.

Each engineered proteasome could be assigned a half-saturation constant of ~ 8 μM for casein, i.e. the double value of the soluble enzyme for fluorescein-labeled casein. Hence the affinity of the proteasome for proteinaceous substrates is retained upon immobilization, as the fluorimetric assay determines the half-saturation constant of degradation, which should be significantly lower than the half-saturation constant in the SPR study measuring reversible association plus degradation with different concentration-dependences. Since substrates and degradation products are forced to exit the 'dead-end' proteasome via a single pore aperture, their dissociation is retarded by a factor of two in comparison to the free proteasome, where two distinct exit pathways are amenable. Dissociation from either proteasome is apparently not affected by cooperativity. Crevices at the interface between the α- and β-rings of the *T. acidophilum* proteasome (Groll et al., 1997) are too small for the uptake of substrates, but could serve as exits for products. However, the exact 2 : 1 stoichiometry of the off-rates for side-on and end-on immobilized proteasomes indicates

that the two terminal pores are the preferential egress pathways. The catalytically inactive proteasome mutant developed different off-rates in one-substrate and two-substrate complexes, as the off-rate decays monoexponentially with substrate concentration. The off-rate of the one-substrate complex was at least twofold higher than the off-rate of the two-substrate complex, thus indicating that binding of the second substrate blocked the alternative exit of the first substrate and vice versa. In other words, for unprocessed substrates the access pathway is identical with the egress pathway.

Substrate association of each His-tagged proteasome is most likely accomplished in two steps. According to a biexponential fit a rather slow (0.13 $s^{-1}$) and a fast association phase (1.2 $s^{-1}$) can be assigned, which might point to substrate translocation and binding, respectively. If PAN mediates substrate unfolding, the rate-limiting and energy-dependent step is apparently translocation into the 20 S proteasome (Benaroudj et al., 2003). In case of the immobilized β C $His_6$ proteasome translocation is independent of substrate concentration, presumably because saturation of channeling through the pore is reached at very low concentration. 'Dead-end' proteasomes are able to accelerate translocation up to half-saturating substrate concentration because the His-tags impose additional confinements on the pore apertures. A two-step process can be deduced only for association with the first substrate. If a second substrate associates with the side-on immobilized β C $His_6$ proteasome or soluble enzyme, the rate-limiting translocation step might be omitted, as the first substrate can open the entrance at the other end. Moreover, by deletion of the N-terminal extremities of the α-subunits, the open channel can easily be passed by unfolded proteins without dependence on PAN or ATP (Benaroudj et al., 2003). Hence positive cooperativity of two-substrate association could be explained by the drastically enhanced on-rate. In case of the inactive proteasome mutant, it can be assumed that access is impeded by the prior effusing substrate. This speculation is supported by the more or less linear increase in the translocation on-rate constant with increasing substrate concentration and the uniformly reduced binding on-rate constant. Bypass of the translocation step via an open-pore mechanism is unlikely. Hence positive cooperativity of two-substrate association arises most probably from a decrease in the off-rates of unprocessed molecules with increasing substrate concentration.

### 6.5 Two-substrate association with the proteasome

Co-localization of substrates in the proteasome can be analyzed by fluorescence resonance energy transfer or fluorescence cross-correlation spectroscopy. Without averaging over an ensemble, single-molecule analyses allow to study fluctuating systems and subpopulations under equilibrium conditions. In addition, fluorescence correlation spectroscopy gives valuable information about binding constants for each subpopulation. As prerequisite, two substrates have to be labeled with different fluorophores, which exhibit minimum spectral overlap (FRET) or, at best, no spectral overlap (cross-correlation). Since aminospecific labeling modifies substrates in a randomized manner, thiolspecific modification was chosen as labeling guarantees a defined stoichiometry and site-specificity. Unfortunately, the known natural substrates of the 20 S proteasome from *Thermoplasma acidophilum* bear no cysteines (casein) or are yielded after opening of numerous disulfide bonds (human IGF-1 with three disulfide bonds, lactalbumin and alkaline phosphatase with four disulfide bonds each). An easily easily reducible substance (insulin) was selected and a reduced insulin B chain with two cysteines was generated. After thiolspecific labeling, Alexa-488-insulin B chain and Alexa-594-insulin B chain constituted a suboptimal FRET pair in association with proteasomes, as self-quenching of the fluorophores was lost during degradation and interfered with the recorded emission.

Cross-correlation studies demonstrated that two differently labeled insulin B chains are simultaneously bound to the proteasome. Thus cross-correlation analysis is not restricted to applications, where a linkage between two labeled molecules (DNA, protein) is formed or destroyed (Kettling et al., 1998; Kohl et al., 2002; Koltermann et al., 1998). Versatility of the method relies also on independence from the distance of the fluorophores in contrast to FRET. In addition to the cross-correlation study, autocorrelation curves were recorded at the individual wavelengths. The autocorrelation data analyzed the binding processes of Oregon Green 488-labeled insulin B chain and Alexa 633-labeled insulin B chain to the proteasome in the steady-state equilibrium. Accordingly, dissociation constants for the two successive binding processes could be derived. The affinity of the second substrate for the proteasome exceeds the affinity of the first substrate by nearly one order of magnitude (700 nM versus 8 µM). A similar cross-correlation experiment with Oregon Green 488-labeled insulin B chain and Cy5-labeled proteasome allowed to monitor steady-state substrate association. As the dissociation constant of a hypothetical one-substrate binding

model ($K_D$ ~ 1 μM) is more than fourfold lower than concluded from the previous study, the two-substrate binding state is also realized in the steady-state equilibrium.

Most probably, allosteric interactions account for positive cooperativity. Allosteric transitions have already been observed for the proteasome from *Schizosaccharomyces pombe* (Osmulski and Gaczynska, 2000; Osmulski and Gaczynska, 2002). In accordance with this model, peptidic substrates may shift the equilibrium from the closed/barrel-like conformation to the open/cylinder-like conformation. Proline- and arginine-rich peptides are known as inhibitors of the allosteric transition (Gaczynska et al., 2003). For archaeal proteasomes a gating mechanism is discussed controversially. For the proteasomal α-ring from *Archaeoglobus fulgidus* an ordered open conformation could be recently shown in the absence of any activator (Groll et al., 2003), which superimposes nicely with the open conformation of the yeast proteasome. But especially the conserved YDR motif of archaeal proteasomes failed to be relevant to a conceivable closed conformation. From mutational studies it was derived that proteinaceous substrates access the archaebacterial proteasome most efficiently in an open-gate conformation (Förster et al., 2003). Moreover, PAN is assumed to regulate gate opening of the archaeal proteasome (Benaroudj et al., 2003). Since the twelve N-terminal residues of each α-subunit in the proteasome from *T. acidophilum* are disordered according to the crystal structure (Löwe et al., 1995), a gating mechanism for archaeal proteasomes cannot completely be ruled out. Additionally, long-range conformational changes are transmitted from HslU to the active site of HslV in order to turn on the proteolytic activity (Sousa et al., 2000). As the proteasomal β-subunits show conservation of residues critical in HslV, an allosteric transition between both termini of the proteasome cannot be excluded.

GroEL serves as well-known example of a molecular machine, which displays positive cooperativity in ATP-binding among the intra-ring subunits and negative cooperativity in substrate binding with regard to the inter-ring contacts. Cooperativity most likely propagates by switching on and off intersubunit salt bridges (Ranson et al., 2001). Thus, for example, the symmetry within the GroEL rings can be retained. However, mutations are able to convert the allosteric transition of GroEL from a concerted to a sequential mechanism (Danziger et al., 2003). Hence allostery in GroEL results from coupled tertiary conformational changes. The mechanism of substrate folding via docking of GroES to the *trans* ring of GroEL is still unknown (Chaudhuri et al., 2001; Weissman, 2001). This

conformational change over a distance of 14 nm might resemble the movement in the proteasome.

### 6.6 Mechanistic model of the 20 S proteasome

A comprehensive model for the degradation mode of the proteasome has to include the precise temporal and spatial relationship between substrate binding and product release. The results of this PhD thesis complement the data of other research groups and prompt me to propose a two binding-site model of the 20 S proteasome (Figure 36). Surface plasmon resonance studies with the end-on and side-on immobilized proteasomes proved that association with the (first) substrate is a two-step process. Obviously the slow translocation step precedes binding to the proteasome, assuming omission of the rate-determining step for association with the second substrate. Otherwise association with the second substrate would reveal two on-rate constants (one for each step) non-equivalent to the on-rate constants for association with the first substrate. It is tempting to speculate that the first substrate binds independently of its size in the antechamber and induces during subsequent degradation at the catalytic centers via conformational changes pore dilation at both termini. According to other data (Osmulski and Gaczynska, 2000; Osmulski and Gaczynska, 2002) catalytic site inhibitors for example prevent the allosteric transition. Entry of the second substrate through the dilated pore aperture means bypassing the rate-limiting translocation step and thus a significant increase in the on-rate. Binding in the antechamber is maintained with regard to the on-rate constant of this step. Hence it can be assumed that the two substrates enter the proteasome in an alternating mode. Around the temperature optimum for the proteasome the rate-limiting step in a cycle is apparently threading of the substrate into the proteasome (including translocation), but not processing, as the soluble or side-on immobilized proteasome is threefold as active as the ‘dead-end’ enzyme (see fluorimetric studies). At lower temperature, processing seems to determine the rate of one degradation cycle, since the activity of the side-on immobilized is 1.7-fold compared to the ‘dead-end’ proteasome (see SPR studies). It remains elusive, whether the two substrates are degraded simultaneously at the catalytic centers. One can envisage two alternative models. Either the second substrate is accommodated in the antechamber, until degradation of the first substrate is complete (alternating degradation, Figure 36 top) or the

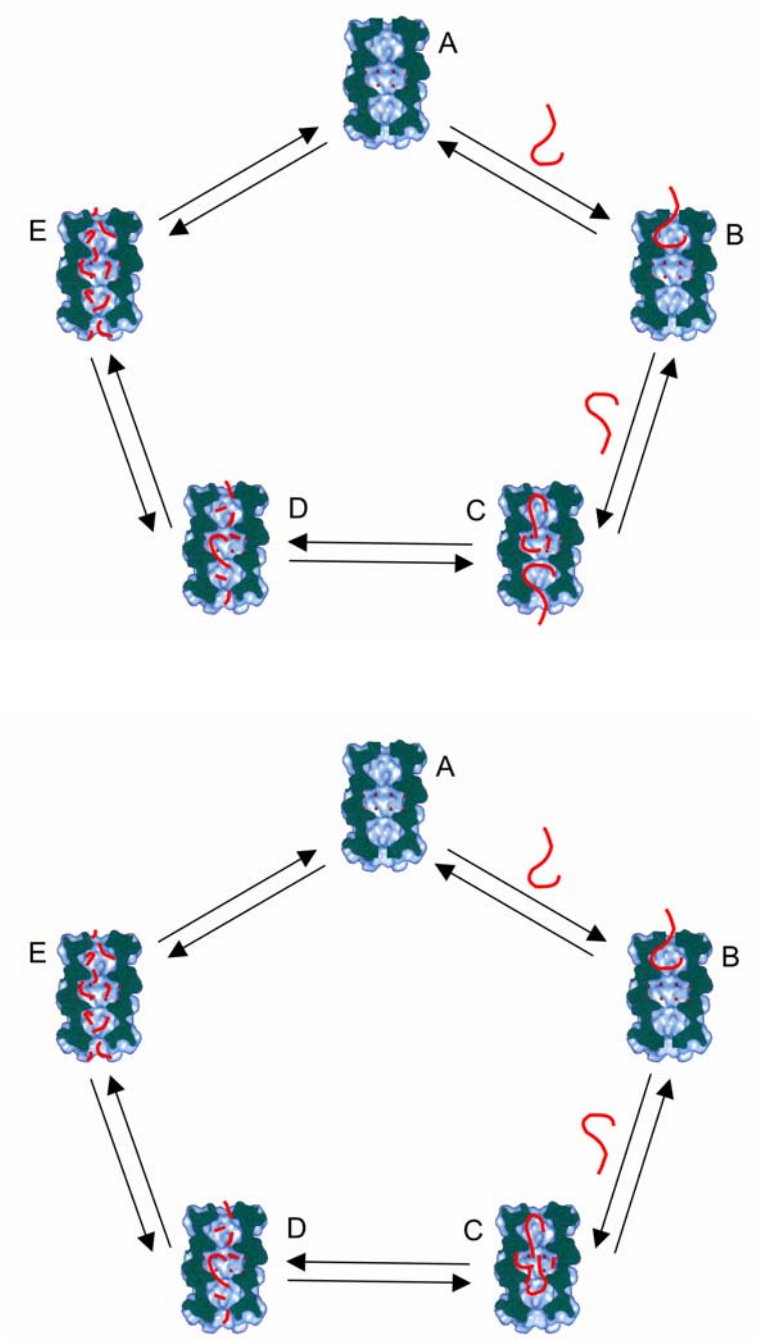


**Figure 36: Two-binding site model of the 20 S proteasome.** Top: *Alternating degradation*. The proteasome possesses constricted pore apertures in the unloaded state (A). A first substrate is translocated through the narrow pore aperture into the antechamber, where it binds (B). After transfer into the central chamber the substrate is degraded at the catalytic centers, induces pore dilation at both termini and facilitates entry of the second substrate into the antechamber (C). After finishing processing of the first substrate, the second substrate diffuses into the central chamber to be degraded there (D). Effusing fragments keep both pore apertures open until degradation is complete (E). Bottom: *Simultaneous degradation*. The proteasome posesses constricted pore apertures in the unloaded state (A). A first substrate is translocated through the narrow pore aperture into the antechamber, where it binds (B). After transfer into the central chamber the substrate is degraded at the catalytic centers, induces pore dilation at both termini and facilitates entry of the second substrate via the antechamber into the central cavity (C). Substrates are chopped down to small fragments, before autoinhibition of the exit can be bypassed (D). Fragments support opening of the pore apertures during egress (E). A new degradation cycle can be reinitiated.

second substrate enters directly, at least partially, the central cavity (simultaneous degradation, Figure 36 bottom). Fragment release is accomplished via both pores, as the off-rate for side-on immobilized β C $His_6$ proteasomes is double compared to 'dead-end' proteasomes. During egress effusing fragments might compete with entering proteins, since casein binding is inhibited by small peptides (Karin Busch & Robert Tampé, unpublished results). Occupation of non-catalytic sites mediates gating of the eukaryotic 20 S proteasome (Kisselev et al., 2002). Presumably both conceivable binding sites superimpose in the antechamber and regulate channeling of substrates to and products from the catalytic centers. Thus it is reasonable that the pore is kept in an open state until the central chamber is emptied of fragments. Simultaneously entry of unprocessed substrates is blocked. A new degradation cycle is reinitiated, when the pore closes subsequent to fragment release. Simultaneous degradation would far simpler than alternating degradation explain product egress via both pores of the proteasome. It can be assumed that the substrates are only partially threaded into the central cavity during processing. Thus the exits are obliterated, until the substrates are chopped down to small fragments. One can summarize that substrate association with the proteasome underlies an ordered alternating binding mechanism in contrast to the random mode of degradation. Moreover, the two-stroke engine offers the advantage of speeding up degradation without enhancing complexity.

### 6.7 Relevance of the mechanistic model

The mechanistic model of the 20 S proteasome from *T. acidophilum* can obviously be transferred to the eukaryotic 20 S proteasome. For degradation of hydrophobic peptides like Suc-LLVY-AMC it was concluded from kinetic data that two molecules can be bound by the two chymotrypsin-like sites with positive cooperativity (Kisselev et al., 1999a; Stein et al., 1996). Although recent studies indicate that hydrophobic peptides stimulate their own hydrolysis by binding to certain non-catalytic sites (Kisselev et al., 2002), occupation of both chymotrypsin-like sites could be ascertained (Piccinini et al., 2000). Thus it is reasonable that the two substrates enter the proteasome via opposite apertures.

The regulator PA700 binds with positive cooperativity to the 20 S proteasome (Adams et al., 1997) and enhances with positive cooperativity the peptidolytic activity of the core particle (Chu-Ping et al., 1994), irrespective of the number of capped ends (Adams et al.,

1998). The authors propose that binding of PA700 at one end of the singly capped proteasome triggers conformational changes in the outer α-subunits, which are transferred to the distal end of the core particle and facilitate substrate entry into the central cavity. My results provide an alternative explanation. Association of PA700 with the 20 S proteasome leads to gating of substrate entry into the core particle (Köhler et al., 2001; Whitby et al., 2000) and induces conformational changes in the 20 S proteasome by switching on the catalytic activity (Osmulski and Gaczynska, 2000; Osmulski and Gaczynska, 2002), thus mediating pore dilation at the distal end and binding of a second substrate (my results). Hence one can conclude that the equivalence of the two pore apertures in the 20 S proteasome is not disturbed by asymmetric binding of PA700. Consequently the two-substrate binding model could also explain regulation of the 26 S proteasome. Only hybrid proteasomes, which are capped each by one regulator PA700 and PA28, might deviate from this alternating binding mechanism and establish a vectorial model. Accordingly one pore (capped with PA700) functions as entry port for substrates, whereas the other (capped with PA28) is used as exit for products (Köhler et al., 2001; Whitby et al., 2000), thus yielding a broader size range of peptides for antigen presentation (Cascio et al., 2002).

The speculation that one PA700 cap complex per proteasome can stimulate peptidolytic activity of the proteasome via facilitated two-substrate association raises concern about activation of proteolytic activity. As most substrates are degraded by the 26 S proteasome subsequent to ubiquitination and lid subunits of PA700 are required for recognition of ubiquitinated substrates, proteolytic activity might be stimulated most efficiently by doubly capped 20 S particles. An increase in proteolytic activity of 26 S proteasomes would benefit the therapy of neurodegenerative diseases. A regulation of 20 S proteasome assembly may be achieved by exogenous supply with interferon γ, which controls proteasome maturation at the level of POMP expression. Upregulation of protein kinase activity or downregulation of phosphatase activity might help to yield doubly PA700-capped proteasomes. Additionally, a ‘modulator’ is assumed to promote proteasome-PA700 complex formation (Adams et al., 1998; Adams et al., 1997). Thus perhaps proteasomal activity can be controlled by formation of the 26 S proteasome.

# 7. Summary

## 7.1 Abstract

The detailed mechanism of the 20 S proteasome from *Thermoplasma acidophilum* is unknown. Substrates are degraded processively to small fragments without the release of intermediates, but the basis for this unique degradation mode remains obscure. The proteasome is a molecular machine, but how the different nanocompartments interplay and whether more than one substrate can be treated simultaneously has not been elucidated yet.

To address these questions we had to disable the functionality of one aperture in order to dissect whether the other pore can compensate for the loss. As it is challenging to introduce mutations solely around one pore aperture of the highly symmetrical construct, we chose a novel approach by unique orientation of the proteasome at interfaces. For this purpose we purified recombinant 20 S proteasomes, where hexahistidine tags were fused either around the entrances or at the sides. According to electron microscopic studies we immobilized these constructs uniformly either end-on or side-on at metal-chelating interfaces (lipid vesicles, lipid monolayers and self-assembled thiol monolayers). Degradation of small fluorogenic peptides and large proteins like casein was analyzed. Small substrates were degraded with comparable activity by free and immobilized proteasomes, irrespective of their orientation. Thus it can be assumed that peptides can pass the sealed entrance of the 'dead-end' proteasome. However, larger substrates like fluorescently labeled casein were processed near the temperature optimum by side-on immobilized and soluble proteasomes with threefold activity compared to end-on immobilized proteasomes. Hence it can be concluded that one pore is sufficient for substrate entry and product release. In other words, the pore and antechamber can fulfil a triple function in the import and unwinding of substrates and the egress of products.

With means of surface plasmon resonance the exact substrate/proteasome stoichiometry could be determined to ~1 for 'dead-end' proteasomes and ~2 for side-on immobilized (active and inactive) proteasomes. Most importantly, a fit with the Hill equation revealed positive cooperativity for side-on immobilized (Hill coefficient ~2) in contrast to end-on immobilized proteasomes (Hill coefficient ~1). Thus in case of soluble proteasomes two substrates bind presumably in opposite antechambers with positive cooperativity. The off-rate of casein as substrate is twofold for the active side-on immobilized proteasome in comparison to the end-on immobilized proteasome. The exact 2:1 stoichiometry of the off-

rates equals the ratio of exit pathways amenable in case of side-on orientated versus 'dead-end' immobilized proteasomes. Thus crevices along the cylindrical body of the 20 S proteasome seem not to participate in the egress of small products. An inactive proteasome mutant displays a concentration-dependent off-kinetic against casein. Accordingly, the off-rate of the bisubstrate:proteasome complex can be attributed around half the value of the monosubstrate:proteasome complex. Consequently, substrates exit the inactive proteasome via the route of access due to obstruction of the *trans* side with an entering substrate. Hence the active proteasomes have to chop substrates down to small fragments prior to release through both pores. Thus the processive degradation mode might result from positive binding cooperativity.

The on-rate constants for casein suggested that substrate association represents a two-step process comprising a rate-limiting translocation step and a fast binding step. As fluorescence cross-correlation revealed that two substrates can be co-localized in the proteasome and bind successively with increasing affinity ($K_{D,1}$ = 8 µM versus $K_{D,2}$ = 700 nM), an allosteric transition in the proteasome can be assumed. Combining our results with the data from other research groups led to a mechanistic model for the 20 S proteasome. Accordingly, the first substrate undergoes a slow translocation step, binds in the antechamber and diffuses subsequently to the catalytic centers, where it is degraded. By switching on the catalytic activity, the pores at both termini are dilated via conformational changes. Hence entry of the second substrate into the proteasome is facilitated due to omission of the rate-determining translocation step. The second substrate is either accommodated in the antechamber before it is processed (alternating degradation) or, most probably, is directly threaded into the central cavity (simultaneous degradation). As effusing peptides compete with entering proteins for binding in the antechamber, the pores are kept in an open state. After finishing digestion the pores are closed and a new degradation cycle can be reinitiated. In summary, substrate association with the proteasome underlies an ordered alternating binding mechanism in contrast to the random mode of degradation. Thus the two-stroke engine offers the advantage of speeding up degradation without enhancing complexity.

## 7.2 Zusammenfassung

Der detaillierte Mechanismus des 20 S Proteasoms von *Thermoplasma acidophilum* ist unbekannt. Substrate werden prozessiv ohne Freisetzung von Intermediaten degradiert, aber die Grundlage für diesen einzigartigen Degradationsmodus bleibt unklar. Das Proteasom ist eine molekulare Maschine, aber wie die verschiedenen Nanokompartimente miteinander interagieren und ob mehr also ein Substrat gleichzeitig berarbeitet werden kann, ist noch unerforscht.

Zur Beantwortung dieser Fragen musste die Funktionalität einer Öffnung ausgeschaltet werden, um herauszufinden, ob die andere Pore den Verlust kompensieren kann. Da es eine Herausforderung darstellt, Mutationen nur um eine Porenöffnung des hochsymmetrischen Konstruktes einzuführen, wählten wir mittels einzigartiger Orientierung des Proteasoms an Grenzflächen einen neuartigen Zugang. Zu diesem Zweck reinigten wir rekombinante 20 S Proteasomen auf, an denen entweder um die Porenöffnungen herum oder an den Seiten Hexahistidinsequenzen fusioniert wurden. Wir immobilisierten diese Konstrukte eletronenmikroskopischen Untersuchungen zufolge einheitlich entweder aufrecht oder seitlich an metall-chelatisierenden Grenzschichten (Lipidvesikel, Lipidmonolayer und selbstassemblierte Thiolschichten). Die Degradation kleiner fluorogener Peptide und grosser Proteine wie Casein wurde untersucht. Kleine Substrate wurden, ungeachtet ihrer Orientierung, mit vergleichbarer Aktivität von löslichen und immobilisierten Proteasomen degradiert. Folglich kann angenommen werden, dass Peptide die versiegelte Eintrittsöffnung des „Sackgassen"-Proteasoms passieren können. Grössere Substrate jedoch, wie fluoreszenzmarkiertes Casein, wurden nahe des Temperaturoptimums von seitlich immobilisierten und freien Proteasomen mit dreimal so hoher Geschwindigkeit prozessiert wie von aufrecht immobilisierten Proteasomen. Daraus kann gefolgert werden, dass eine Pore für den Substrateintritt und die Produktfreisetzung ausreichend ist. Mit anderen Worten, Pore und Vorkammer erfüllen eine dreifache Funktion beim Import und der Entfaltung von Substraten sowie dem Austritt von Produkten.

Über Oberflächenplasmonresonanz konnte die exakte Substrate/Proteasomstöchiometrie zu ~1 für „Sackgassen"-Proteasomen und zu ~ 2 für seitlich immobilisierte (aktive und inaktive) Proteasomen bestimmt werden. Bedeutsamerweise ergab ein Fit mit der Hill-Gleichung positive Kooperativität für seitlich immobilisierte (Hill-Koeffizient ~2) im

Gegensatz zu aufrecht immobilisierten Proteasomen (Hill-Koeffizient ~1). Also binden im Falle freier Proteasomen zwei Substrate mit positiver Kooperativität vorzugsweise in gegenüberliegenden Vorkammern. Die Dissoziationsrate von Casein als Substrat ist zweimal so hoch für das aktive seitlich immobilisierte Proteasom wie für das aufrecht immobilisierte Proteasom. Die exakte 2 : 1- Stöchiometrie der Dissoziationsraten gleicht dem Verhältnis der Austrittswege, die im Falle des seitlich immobilisierten gegenüber dem „Sackgassen"-Proteasom zugänglich sind. Folglich scheinen kleine Seitenöffnungen entlang dem zylindrischen 20 S Proteasom nicht am Austritt kleiner Produkte beteiligt zu sein. Eine inaktive Proteasommutante zeigt eine konzentrationsabhängige Dissoziationskinetik gegenüber Casein. Dergemäss nimmt die Dissoziationsrate des Zweisubstrat-Proteasomkomplexes die Hälfte des Wertes des Einsubstrat-Proteasomkomplexes an. Folglich verlassen Substrate das inaktive Proteasom wegen Blockade der *trans*-Seite mit einem eintretenden Substrat über ihren Eintrittsweg. So müssen die aktiven Proteasomen Substrate vor ihrer Freisetzung zu beiden Poren vollständig zu kleinen Fragmenten abbauen. Daher resultiert der prozessive Degradationsmechanismus möglicherweise aus der positiven Bindungskooperativität.

Die Assoziationsratenkonstanten für Casein lassen vermuten, dass die Substratassoziation einen Zweistufenprozess darstellt, der einen geschwindigkeitsbestimmenden Translokationsschritt und einen schnellen Bindungsschritt umfasst. Da Fluoreszenz-Kreuzkorrelation aufdeckte, dass zwei Substrate im Proteasom kolokalisiert werden können und nacheinander mit steigender Affinität binden ($K_{D,1}$ = 8 µM gegenüber $K_{D,2}$ = 700 nM), kann ein allosterischer Übergang im Proteasom angenommen werden. Kombiniert man unsere Resultate mit den Daten anderer Forschungsgruppen, kommt man zu einem mechanistischen Modell für das 20 S Proteasom. Demgemäss unternimmt das erste Substrat einen langsamen Translokationsschritt, bindet in der Vorkammer und diffundiert danach an die katalytischen Zentren, wo es degradiert wird. Beim Anschalten der katalytischen Aktivität werden die Poren an beiden Enden aufgrund eines Konformationswechsels erweitert. So wird der Eintritt des zweiten Substrates in das Proteasom wegen Aufhebung des geschwindigkeitsbestimmenden Translokationsschrittes erleichtert. Das zweite Substrat wartet in der Vorkammer, bevor es prozessiert wird (alternierende Degradation) oder, wahrscheinlicher, es wird direkt in die Zentralkammer eingefädelt (simultane Degradation). Da entlassene Peptide mit eintretenden Proteinen um

Bindung in der Vorkammer konkurrieren, werden die Poren in einem geöffneten Zustand gehalten. Nach Beendigung des Abbaus werden die Poren geschlossen, und ein neuer Degradationszyklus kann reinitiiert werden. Zusammengefasst unterliegt die Substratassoziation mit dem Proteasom einem geordneten alternierenden Bindungsmechanismus im Gegensatz zum ungeordneten Degradationsmodus. Folglich bietet der Zweitaktmotor den Vorteil, die Degradation zu beschleunigen, ohne die Komplexität zu erhöhen.

# 8. Supplement:

# Interaction of receptor peptides with His-tagged biomolecules

## 8.1 Introduction

Recognition processes are determined by a complex superposition of many weak long- and short-range forces (electrostatic, van der Waals, and hydrogen bonds) as well as entropic constraints, which in concert are difficult to predict and to control. Alternatively, ligands can be coordinated precisely in a three-dimensional arrangement by complex formation. For example, ($Ni^{2+}$: nitrilotriacetic acid)$_n$ derivatives of cyanine fluorochromes can function as FRET acceptors for fluorescein-labeled histidine-tagged DNA-protein complexes and proteins in a distance-dependent manner (Kapanidis et al., 2001). Metal-chelating amino acids as building blocks have the potential to bind subsequent to loading with metal ions histidine residues located in a target molecule (Figure 37). An adjacent fluorophore might act as sensor for metal-ion loading and binding to His-tagged biomolecules.

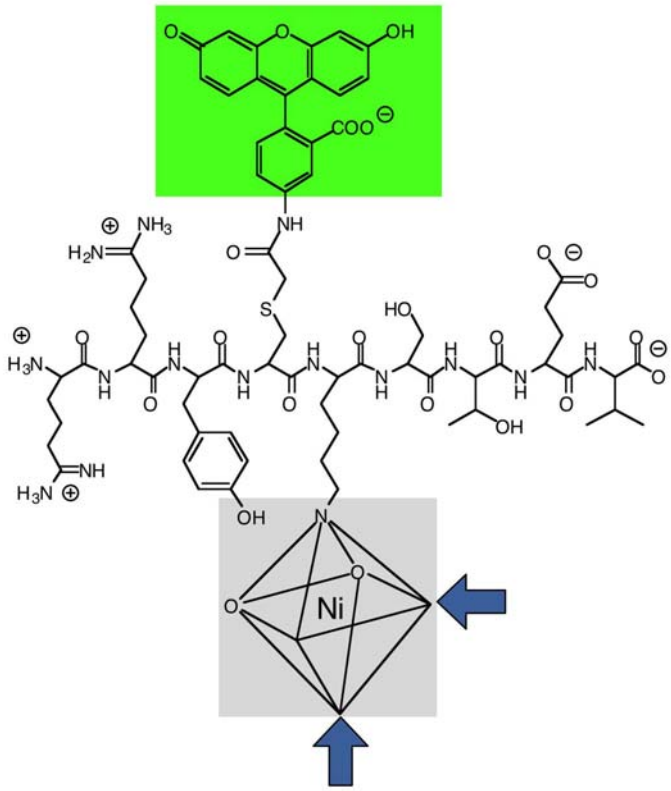


**Figure 37: Metal-chelating amino acid within a polypeptide.** Metal-chelating amino acids can serve as building blocks for synthetic receptors sensing metal ions and histidine-tagged proteins (adapted from Hutschenreiter et al., 2003).

## 8.2 Methods

### 8.2.1 Carboxamidomethylation of the IDA-peptide

The interactions between IDA-peptide (RRYCΨSTEL) and His-tagged peptides were studied with reversed-phase chromatography. For this purpose IDA-peptide was synthesized by solid-phase technique using conventional Fmoc-chemistry (see 3.1) and analyzed by MALDI-MS (M/z = 1271). To prevent disulfide bond formation via cysteines, free thiol groups of the IDA-peptide were blocked with a 12-fold molar excess of 2-iodoacetamide in 10 mM $NaP_i$, 150 mM NaCl, pH 6.5 (2 h at room temperature). The carboxamidomethylation was verified with MALDI-MS (M/z = 1329).

### 8.2.2 Fluorescent labeling of the IDA-peptide

For FRET and other fluorescence studies the IDA-peptide was labeled with fluorescein via the cysteine (Hutschenreiter et al., 2003). RRYCΨSTEL was incubated with the 1.2-fold molar excess of fluorescein-5-iodoacetamide in 50 mM $NaP_i$, 150 mM NaCl, pH 6.0, 20 % (v/v) dimethylformamide for 90 min at room temperature. After pelleting precipitated dye, the supernatant was applied to a µRPC C2/C18 column, pre-equilibrated with 0.1 % (v/v) TFA in $H_2O$ (buffer A). Subsequently a gradient from buffer A to buffer B (0.1 % (v/v) TFA in acetonitrile) was run (0 – 12 % B within 10 min, 12 – 26 % B within 20 min, 26 – 100 % B within 10 min). The absorption at 216 nm, 280 nm and 491 nm was monitored. Fractions of 80 µl were collected during the second gradient interval. The first peak corresponds to the fluorescein-labeled IDA-peptide (M/z = 1658) according to mass spectrometry (MALDI and ESI).

### 8.2.3 Complex formation between IDA-peptide and His-tagged peptide

Interactions between IDA-peptide (RRYCΨSTEL) and His-tagged peptide (HHHHHGSGSAWRHPQGG) were studied in the presence of $Cu^{2+}$ or $Ni^{2+}$ and in the absence of metal ions. For this purpose carboxamidomethylated IDA-peptide (1 mM, 8.2.1) was incubated for 1 h at 25 °C with His-tagged peptide (2 - 5 mM) in the presence of 10 mM $CuSO_4$ or 10 mM $NiCl_2$ in 100 mM ammonium acetate, 300 mM NaCl, pH 8.0 (buffer $A_1$). After centrifugation 50 µl of the sample were separated on a reversed-phase column (µRPC C2/C18) pre-equilibrated with buffer $A_1$. A linear gradient (0 – 100 % $B_1$) was run over 15 min from buffer $A_1$ to buffer $B_1$ (100 mM ammonium acetate, 300 mM

NaCl, 50 % (v/v) acetonitrile, pH 8.0), while fractions of 80 µl were collected. The absorption at 216 nm, 260 nm and 280 nm was recorded. The same experiment was also performed in the absence of metal ions, i.e. after addition of 5 mM EDTA. The second peak was due to the His-tagged peptide and in the presence of metal ions shifted to higher acetonitrile concentration. Peptides eluting in the second peak were pooled, cleared from acetonitile in the vacuum centrifuge and loaded on the same column subsequent to equilibration with 0.1 % (v/v) TFA in $H_2O$ (buffer A). Thus metal ion-mediated interactions between the functionalized peptides were disrupted. A linear gradient from buffer A to 50 % buffer B (buffer B: 0.1 % (v/v) TFA in acetonitrile) was run over 15 min. Fractions of 80 µl were collected. Peptides absorbing at 216 nm and 280 nm were examined by MALDI-MS.

### 8.2.4 Kinetic studies with fluorescein-IDA-peptide and His-tagged reporter molecules

The binding of metal ions to the IDA-head group can be sensed by the adjacent fluorescein residue. Fluorescence quenching of fluorescein-RRYCΨSTEL was recorded ($\lambda_{exc\ /\ em}$ = 470 / 514 nm) with 10 µM metal ions (nickel chloride, cupric sulfate) at 20 °C in 40 mM HEPES, 1 M NaCl, pH 6.9. Afterwards the fluorescence intensity was checked in the presence of 1 mM calcium chloride. Subsequently, interactions with the metal-loaded IDA-head group of fluorescein-RRYCΨSTEL were examined in the presence of imidazole (100 mM), $His_6$-Mdl1-EQ (20 µM) or His-tagged peptide (1 mM). The fluorescence relief was overcome in the presence of 1 mM metal ions ($Ni^{2+}$, $Cu^{2+}$). The fluorescence intensity was checked again after removal of metal ions with 10 mM EDTA or in the presence of 20 mM $CaCl_2$.

### 8.2.5 Interaction of fluorescein-IDA-peptide with biomolecules

Fluorescein-IDA-peptide (50 nM) was incubated with $(GS)_{10}H_6$, $(GS)_{10}$ or RRYQKSTEL (1 mM each) or with β T1A β C $His_6$ proteasome, casein or BSA (0.35 µM each) or with $His_6$-Mdl1 NBD (5 µM) in the presence or absence of 10 µM metal choride ($NiCl_2$, $CaCl_2$, $MgCl_2$) in 40 mM HEPES, 1 M NaCl, pH 6.9 (4 h at 25 °C). Fluorescence emission ($\lambda_{ex}$ = 470 nm) was recorded within the interval of 480 – 700 nm. The fluorescence intensity was normalized to the fluorescence intensity of the fluorescein-IDA-peptide in the absence of metal ions.

### 8.2.6 FRET studies with fluorescein-IDA-peptide and Texas Red-labeled $His_6$-OpuAA

The complex formation between fluorescein-IDA-peptide and Texas Red-labeled $His_6$-OpuAA in the presence of nickel ions should establish FRET. Fluorescein-IDA-peptide (FRET donor) was generated according to 8.2.2 and Texas Red-labeled $His_6$-OpuAA (FRET acceptor) was a kind gift.

Complex formation between fluorescein-IDA-peptide (50 – 100 nM) and Texas Red-labeled $His_6$-OpuAA (2 – 4 µM) was studied in the presence of 10 µM $NiCl_2$. As negative control, fluorescein-IDA-peptide (50 -100 nM) was incubated with unlabeled $His_6$-OpuAA (2 - 4 µM) and $NiCl_2$ (10 µM). The FRET acceptor-signal was recorded after mixing Texas Red-labeled $His_6$-OpuAA with nickel ions. Before recording the fluorescence spectrum (480 – 700 nm), each sample was incubated for 25 min at room temperature in order to reach the maximal fluorescence response.

## 8.3 Results

### 8.3.1 Coordination of metal ions to fluorescein-IDA-peptide

Transition metal ions are able to quench a fluorophore in close proximity. Thus, by attaching fluorescein to a peptide adjacent to a metal-chelating unit Ψ interaction with ligands could be studied. Addition of $Ni^{2+}$ (10 µM) to the fluorescence-labeled IDA-peptide RRYC(fluorescein)ΨSTEL (50 nM) triggered online a 40 % decrease of the initial fluorescence emission within 20 min (Figure 38). The fluorescence response to 10 µM $Cu^{2+}$ was even faster and more pronounced (75 % reduction of the emitted fluorescence within 2 min, Figure 39). Calcium and magnesium ions were not able to quench the fluorescence emission of the fluorescein-IDA-peptide. When competing out the metal ions ($Ni^{2+}$, $Cu^{2+}$) with 1 - 20 mM $Ca^{2+}$ (Figure 38, Figure 39) or $Mg^{2+}$ (data not shown), no change in fluorescence emission could be detected, thus demonstrating that neither calcium nor magnesium ions were bound to the $Ni^{2+}$- or $Cu^{2+}$-loaded chelating unit Ψ. If the metal-chelating amino acid Ψ within the peptide was replaced by a lysine residue, no fluorescence quenching was observed after addition of $Ni^{2+}$ or $Cu^{2+}$ (data not shown). These results indicate a specific complex formation between $Ni^{2+}$/$Cu^{2+}$ and the chelating amino acid Ψ. According to metal-induced fluorescence quenching the apparent complex dissociation constant of the fluorescein-IDA-peptide/ $Ni^{2+}$-complex could be determined to 20 ± 3 nM (Hutschenreiter et al., 2003).

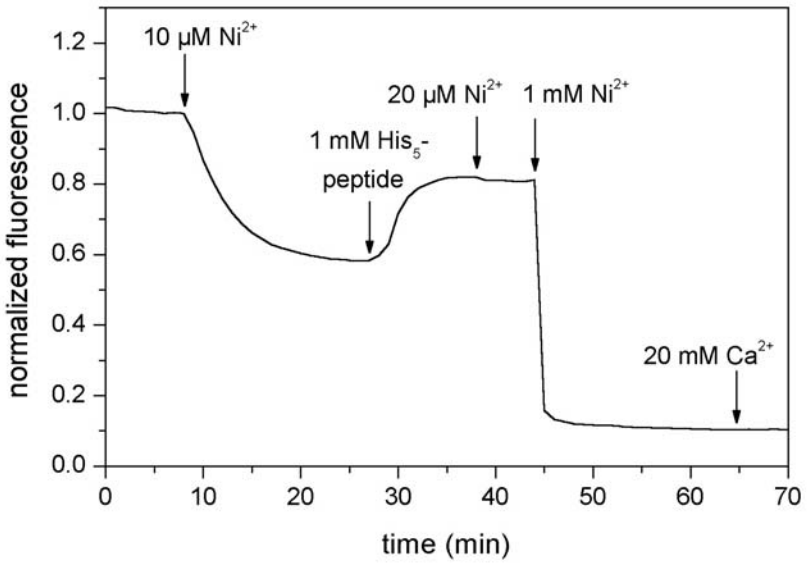


**Figure 38: Relief of nickel ion-mediated quenching of receptor peptide by His-tagged peptide.** Nickel ions (10 µM) induce quenching of RRYC(fluorescein)ΨSTEL (50 nM), which is relieved by His-tagged peptide (1 mM). Not 20 µM, but 1 mM nickel ions overcome this effect. The drastic decrease in fluorescence is not influenced by calcium ions (20 mM).

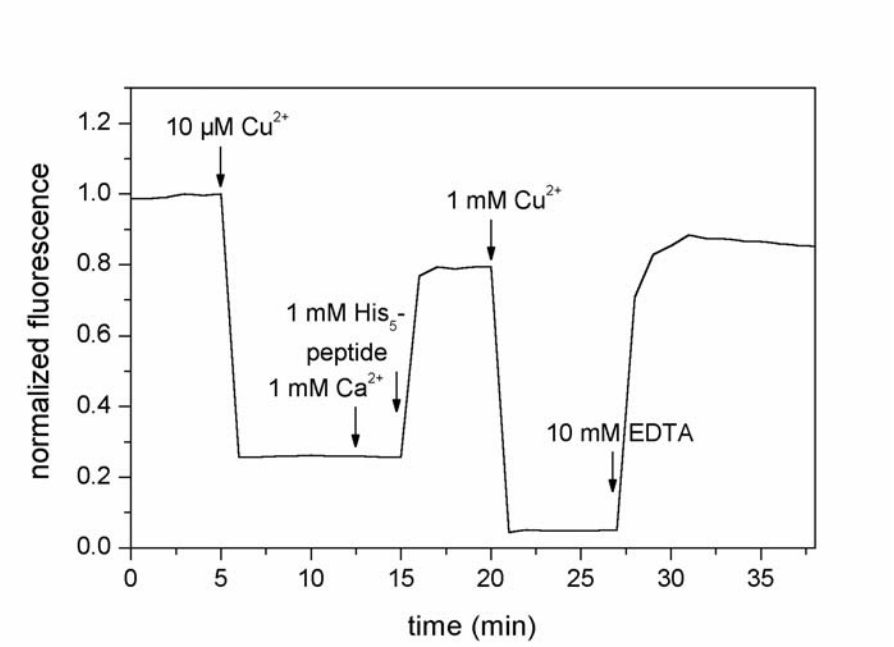


**Figure 39: Copper ion-mediated quenching of receptor peptide is reversed by His-tagged peptide or EDTA.** Copper ions (10 µM) induce rapid quenching of RRYC(fluorescein)ΨSTEL (50 nM), which is not relieved by calcium ions (1 mM), but by His-tagged peptide (1 mM). The effect is overcome by copper ions (1 mM). The drop in fluorescence is bypassed by EDTA (10 mM).

### 8.3.2 Interaction of fluorescein-IDA-peptide and His-tagged biomolecules

As the complex between the metal ion and the metal-chelating amino acid should sense the docking of imidazole and histidine, His-tagged biomolecules were tested in the micromolar and millimolar concentration range. Addition of a $His_5$-tagged peptide (HHHHHGSGSAWRHPQGG, 1 mM) to the fluorescein-IDA-peptide after metal-ion quenching resulted within a few minutes in a > 20 % (in case of $Ni^{2+}$-quenching) or > 50 % (in case of $Cu^{2+}$-quenching) recovery of the initial fluorescence (Figure 38, Figure 39) indicating formation of a ternary His-tagged peptide/$Me^{2+}$/fluorescein-IDA-peptide complex. The effect was reversible, since 1 mM $Ni^{2+}$ (Figure 38) or $Cu^{2+}$ (Figure 39) led to an almost perfect requenching of the fluorescence emission. A simple explanation for this phenomenon is that the His-tagged peptide previously abstracted the metal ion now replaced off the fluorescein-IDA-peptide instead of forming a ternary complex.

Alternatively, the kinetically disfavorable formation of a ternary complex was not finished at the stage, when metal ions were supplied in higher concentration. Thus the newly added metal ions could coordinate free fluorescein-IDA-peptide, triggered quenching, thereby surpassing the recovery of quenching due to formation of the His-tagged peptide complex with the prior metal-bound fluorescein-IDA-peptide. The later added metal ions were also trapped by free His-tagged peptide, thus controling its interaction with the metal ion/fluorescein-Ida-peptide complex. EDTA was able to abstract the metal ions off the fluorescein-IDA-peptide and restored the fluorescence almost completely (Figure 39).

His-tagged proteins could substitute for His-tagged peptides in recovering the fluorescence of the metal ion-quenched fluorescein-IDA-peptide (Figure 40). The more flexible conformation of proteins compared to peptides might permit lower concentrations (20 µM versus 1 mM) in the assay. A comparable relief of metal-ion quenching was also detected in case of imidazole (Figure 40). The sensing fluorophore ‘fluorescein’ adjacent to the metal-chelating unit could always be replaced by ‘tetramethylrhodamine’.

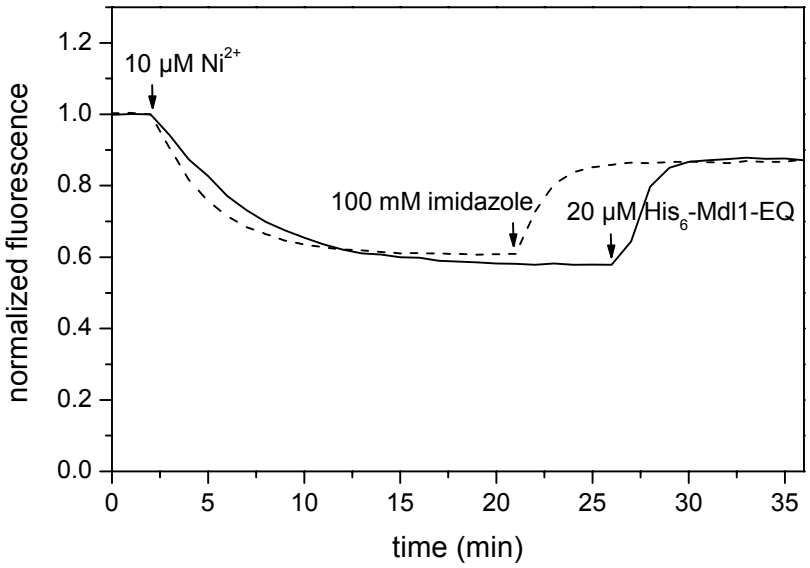


**Figure 40: Relief of nickel ion-mediated quenching of receptor peptide is comparable for His-tagged protein and imidazole.** Nickel ions (10 µM) trigger quenching of receptor peptide (50 nM), which is reversible to a similar extent by His-tagged Mdl-1 NBD (EQ mutant, bold line, 20 µM) or by imidazole (100 mM, dashed line).

If the fluorescence intensity of the components and complexes was determined after certain incubation times and not online, the response (metal-ion quenching and recovery by diverse His-tagged biomolecules) could be enhanced drastically (Table 14). This observation indicates that formation of the fluorescein-IDA-peptide/$Ni^{2+}$-complex and the ternary complex with the His-tagged biomolecule is kinetically controlled. Additionally, online-determination of the fluorescence underlies adverse effects like adsorption of metal ions or fluorescent molecules to the quartz glass of the cuvette. Experiments were also performed on non-His-tagged proteins and peptides. Proteins like casein and bovine serum albumin (BSA) and peptides like $(GS)_{10}$ and RRYQKSTEL are able to display electrostatic or hydrophobic interactions with the building block Ψ. But the fluorescence intensity of the metal-loaded fluorescein-IDA-peptide was not shifted in their presence, confirming that interaction was specific and based solely on coordinative binding.

| | Fluorescence intensity (%) |
|---|---|
| **IDA-peptide** | 100 |
| + $Ni^{2+}$ | 20 |
| + $Ca^{2+}$ | 100 |
| + $Mg^{2+}$ | 100 |
| **IDA-peptide + $Ni^{2+}$** | 20 |
| + His-tagged peptide, $(GS)_{10}H_6$ | 95 |
| + $(GS)_{10}$ | 20 |
| + RRYQKSTEL | 20 |
| **IDA-peptide + $Ni^{2+}$** | 20 |
| + His-tagged proteasome | 79 |
| + His-tagged Mdl-1 NBD | 88 |
| + casein | 20 |
| + BSA | 19 |

**Table 14: Specific binding of nickel ions and His-tagged biomolecules to the receptor peptide.** Summary of fluorescence intensity changes ($\lambda_{ex/em}$ = 470/535 nm of the IDA-peptide (RRYC(fluorescein)ΨSTEL, 50 nM) in the presence of different metal ions (1 µM), peptides (1 mM) or proteins (0.35 – 2 µM). All fluorescence intensities were normalized to the fluorescence intensity of the fluorescein-IDA-peptide in the absence of metal ions.

### 8.3.2 *Förster* transfer between fluorescence-donor-labeled IDA-peptide and fluorescence-acceptor-labeled His-tagged protein

Interaction of $Ni^{2+}$-coordinated donor-labeled IDA-peptide and fluorescence acceptor-labeled $His_6$-OpuAA can be demonstrated by the observation of FRET between the complex partners. After incubation of fluorescence donor (fluorescein-IDA-peptide) and fluorescence acceptor (Texas-Red-labeled $His_6$-OpuAA) with nickel ions the fluorescence emission of the donor is decreased (-5 %) compared to the $Ni^{2+}$-coordinated fluorescein-IDA-peptide in the presence of non-labeled $His_6$-OpuAA (Figure 41).

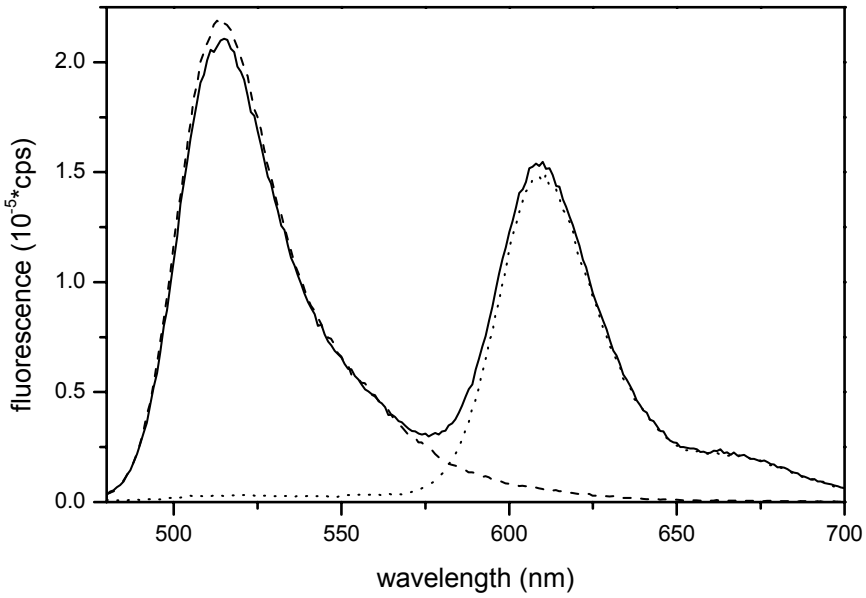


**Figure 41: FRET studies with fluorescein-IDA-peptide and Texas Red-labeled His-tagged protein demonstrate complex formation by nickel ions.** Fluorescence spectra ($\lambda_{ex/em}$ = 470 / 480 - 700 nm) were recorded after incubation (25 min, 25 °C) of RRYC(fluorescein)ΨSTEL (50 nM) and Texas Red-labeled $His_6$-OpuAA (2 µM) in the presence of $NiCl_2$ (10 µM) (solid line). As control, RRYC(fluorescein)ΨSTEL (50 nM) was incubated with unlabeled $His_6$-OpuAA (2 µM) in the presence of nickel ions (10 µM) and the fluorescence was monitored (dashed line). The fluorescence emission of Texas Red-labeled $His_6$-OpuAA (2 µM) after incubation with nickel ions (10 µM) is indicated as dotted line.

The fluorescence emission of Texas Red-labeled $His_6$-OpuAA/$Ni^{2+}$/fluorescein-IDA-peptide has a higher intensity than the fluorescence acceptor alone, but this is solely due to the fact that the fluorescence emission of the FRET donor contributes to the emission spectrum of the FRET acceptor. Thus the net effect is a small reduction in donor fluorescence, which indicates a weak FRET. The FRET could not be enhanced by substituting the IDA-peptide and a His-tagged peptide/protein vice versa with donor and acceptor fluorophores or by forming a complex via copper ions. The efficiency of energy transfer between fluorescence-donor and fluorescence acceptor is rather small, presumably because the metal ions induce the occupation of triplet states of the donor fluorophore as well as the acceptor fluorophore. This speculation is supported by preliminary results of an autocorrelation analysis of the system. Therefore, efficient fluorescence resonance energy transfer might be abolished due to a depletion of the excitable singulet state.

### 8.3.3 Complex formation between IDA-peptide and His-tagged peptide

To demonstrate formation of metal complexes with the building block Ψ the IDA-peptide was incubated with nickel or copper ions after modification of the cysteine residue with 2-iodoacetamide (Hutschenreiter et al., 2003). In the absence of metal ions the IDA-peptide eluted as a single peak in a reversed-phase HPLC at alkaline pH. Preincubation of the IDA-peptide with nickel or copper ions, but not with calcium or magnesium ions, altered the elution profile. A new product eluted later in the acetonitrile gradient, whereas the peak corresponding to uncomplexed IDA-peptide could no longer be detected. A second minor peak most likely arose from dimerization of the IDA-peptide via complex formation of two IDA-groups.

Additionally, reversed-phase HPLC studies at alkaline pH were performed with a 5xHis-tagged peptide and the thiol-blocked IDA-peptide in the presence of nickel and copper ions to demonstrate specific complex formation. Accordingly, the 5xHis-tagged peptide eluted in the presence of metal ions later in the acetonitrile gradient (third peak) than in the absence of metal ions (second peak). The collected metal-coordinated species was separated in a second reversed-phase HPLC at low pH and led to coelution of the 5xHis-tagged peptide (theoretical molecular mass: 1881.9 Da) and the modified IDA-peptide (theoretical molecular mass: 1328.7 Da), as indicated by MALDI-MS (Figure 42). Thus formation of a ternary His-tagged peptide/metal ion/IDA-peptide complex could be proven. By evaluating the relief of fluorescence quenching during the titration of a His-tagged peptide with nickel-loaded fluorescein-IDA-peptide the dissociation constant of the forming ternary complex could be determined to 96 ± 15 µM (Hutschenreiter et al., 2003).

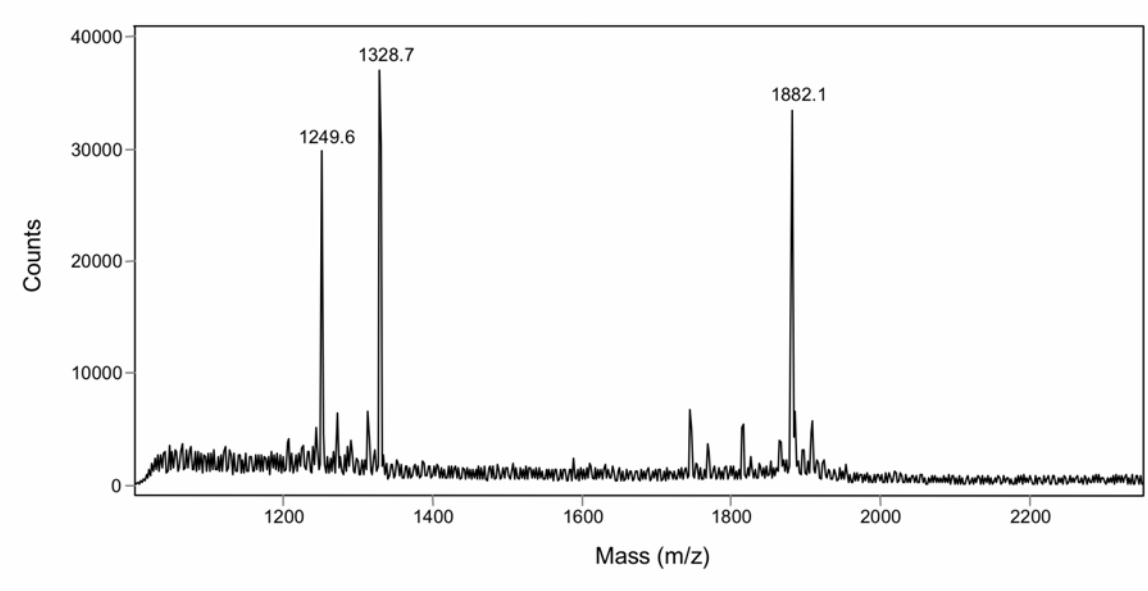


**Figure 42: MALDI spectrum of the IDA-peptide/His-tagged peptide complex.** The IDA-peptide (RRYC(carbamidomethyl)ΨSTEL) was incubated in 100 mM ammonium acetate, 300 mM NaCl, pH 8.0 (buffer $A_1$) with a His-tagged peptide (HHHHHGSGSAWRHPQGG) in the presence of copper ions and applied to a reversed-phase column, which was equilibrated in buffer $A_1$. The complex was eluted using a linear gradient of buffer $A_1$ to buffer $B_1$ (100 mM ammonium acetate, 300 mM NaCl, 50 % (v/v) acetonitrile, pH 8.0). Fractions containing the complex were concentrated and subsequently applied to a reversed-phase column equilibrated in 0.1 % (v/v) TFA in $H_2O$ (buffer A). The components of the complex were eluted by applying a linear gradient of buffer A to buffer B (0.1 % TFA (v/v) in acetonitrile) and analyzed by MALDI-MS. One peak corresponds to the IDA-peptide (1328.7 Da) and one peak corresponds to the His-tagged peptide (1882.1 Da).

## 8.4 Discussion

The data demonstrate that the chelating amino acid ψ binds $Ni^{2+}$ but not $Ca^{2+}$ or $Mg^{2+}$, with nanomolar affinity. The fact that neither $Ca^{2+}$ nor $Mg^{2+}$ interfere with the measurement is of high importance for studies of proteins where the function or stability depends on the presence of $Ca^{2+}$ or $Mg^{2+}$. Due to fluorescence as read-out for metal ion binding, a highly sensitive set-up was developed which needs only minimal sample concentration or volume. This approach is superior to introduction of 8-hydroxyquinoline (oxine) into peptides as sensor of metal binding, because the use is not limited by detection efficiency (Jotterand et al., 2001). In addition, the fluorescence recovery upon binding of His-tagged proteins might be a new and valuable tool in the detection of histidine fusion proteins, for instance, within whole-cell extracts. Control peptides or proteins without a His-tag did not bind to the IDA-peptide, thus indicating the high specificity and selectivity of the recognition process. But even more sophisticated applications can be envisioned. Combinatorial peptide libraries containing more than one metal-chelating amino acid ψ can be used for

selection of optimal, high affinity peptide partners extending the concept to multivalent binding. Thereby novel high-affinity peptide-peptide interaction pairs (biochemical tweezers) can be selected. Alternatively, placing the chelator amino acid at defined positions of a polypeptide chain by *in vitro* translation (Cornish et al., 1994; Mendel et al., 1992) or the intein strategy (Clarke, 1994; Cooper and Stevens, 1995; Muir, 2003) would generate protein-protein interfaces for switchable intra- and intermolecular interactions. Metal-chelating amino acids may further guide the design of proteins with novel properties.

# 9. Literature

Adams, G.M., Crotchett, B., Slaughter, C.A., DeMartino, G.N. and Gogol, E.P. (1998) Formation of proteasome-PA700 complexes directly correlates with activation of peptidase activity. *Biochemistry*, **37**, 12927-12932.

Adams, G.M., Falke, S., Goldberg, A.L., Slaughter, C.A., DeMartino, G.N. and Gogol, E.P. (1997) Structural and functional effects of PA700 and modulator protein on proteasomes. *J. Mol. Biol.*, **273**, 646-657.

Adams, J., Palombella, V.J., Sausville, E.A., Johnson, J., Destree, A., Lazarus, D.D., Maas, J., Pien, C.S., Prakash, S. and Elliott, P.J. (1999) Proteasome inhibitors: a novel class of potent and effective antitumor agents. *Cancer Res.*, **59**, 2615-2622.

Ahn, K., Erlander, M., Leturcq, D., Peterson, P.A., Früh, K. and Yang, Y. (1996) In-vivo characterization of the proteasome regulator PA28. *J. Biol. Chem.*, **271**, 18237-18242.

Aki, M., Shimbara, N., Takashina, M., Akiyama, K., Kagawa, S., Tamura, T., Tanahashi, N., Yoshimura, T., Tanaka, K. and Ichihara, A. (1994) Interferon-γ induces different subunit organizations and functional diversity of proteasomes. *J. Biochem. (Tokyo)*, **115**, 257-269.

Akopian, T.N., Kisselev, A.F. and Goldberg, A.L. (1997) Processive degradation of proteins and other catalytic properties of the proteasome from *Thermoplasma acidophilum*. *J. Biol. Chem.*, **272**, 1791-1798.

Altuvia, Y. and Margalit, H. (2000) Sequence signals for generation of antigenic peptides by the proteasome: implications for proteasomal cleavage mechanism. *J. Mol. Biol.*, **295**, 879-890.

Arendt, C.S. and Hochstrasser, M. (1997) Identification of the yeast 20S proteasome catalytic centers and subunit interactions required for active-site formation. *Proc. Natl. Acad. Sci. U. S. A.*, **94**, 7156-7161.

Arendt, C.S. and Hochstrasser, M. (1999) Eukaryotic 20S proteasome catalytic subunit propeptides prevent active site inactivation by N-terminal acetylation and promote particle assembly. *EMBO J.*, **18**, 3575-3585.

Baumeister, W., Walz, J., Zühl, F. and Seemüller, E. (1998) The proteasome - paradigm of a self-compartmentalizing protease. *Cell*, **92**, 367-380.

Benaroudj, N. and Goldberg, A.L. (2000) PAN, the proteasome-activating nucleotidase from archaebacteria, is a protein-unfolding molecular chaperone. *Nat. Cell Biol.*, **2**, 833-839.

Benaroudj, N., Zwickl, P., Seemüller, E., Baumeister, W. and Goldberg, A.L. (2003) ATP hydrolysis by the proteasome regulatory complex PAN serves multiple functions in protein degradation. *Mol. Cell*, **11**, 69-78.

Bence, N.F., Sampat, R.M. and Kopito, R.R. (2001) Impairment of the ubiquitin-proteasome system by protein aggregation. *Science*, **292**, 1552-1555.

Beninga, J., Rock, K.L. and Goldberg, A.L. (1998) Interferon γ can stimulate post-proteasomal trimming of the N-terminus of an antigenic peptide by inducing leucine aminopeptidase. *J. Biol. Chem.*, **273**, 18734-18742.

Bittner, M., Kupferer, P. and Morris, C.F. (1980) Electrophoretic transfer of proteins and nucleic acids from slab gels to diazobenzyloxymethyl cellulose or nitrocellulose sheets. *Anal. Biochem.*, **102**, 459-471.

Bochtler, M., Ditzel, L., Groll, M. and Huber, R. (1997) Crystal structure of heat shock locus V (HslV) from *Escherichia coli*. *Proc. Natl. Acad. Sci. U. S. A.*, **94**, 6070-6074.

Bochtler, M., Hartmann, C., Song, H.K., Bourenkov, G.P., Bartunik, H.D. and Huber, R. (2000) The structures of HsIU and the ATP-dependent protease HsIU-HsIV. *Nature*, **403**, 800-805.

Bogyo, M., Mcmaster, J.S., Gaczynska, M., Tortorella, D., Goldberg, A.L. and Ploegh, H. (1997) Covalent modification of the active-site threonine of proteasomal β-subunits and the *Escherichia coli* homolog HslV by a new class of inhibitors. *Proc. Natl. Acad. Sci. U. S. A.*, **94**, 6629-6634.

Braig, K., Otwinowski, Z., Hegde, R., Boisvert, D.C., Joachimiak, A., Horwich, A.L. and Sigler, P.B. (1994) The crystal structure of the bacterial chaperonin GroEL at 2.8 Å. *Nature*, **371**, 578-586.

Braun, B.C., Glickman, M., Kraft, R., Dahlmann, B., Kloetzel, P.M., Finley, D. and Schmidt, M. (1999) The base of the proteasome regulatory particle exhibits chaperone-like activity. *Nat. Cell Biol.*, **1**, 221-226.

Brinker, A., Pfeifer, G., Kerner, M.J., Naylor, D.J., Hartl, F.U. and Hayer-Hartl, M. (2001) Dual function of protein confinement in chaperonin-assisted protein folding. *Cell*, **107**, 223-233.

Brodbeck, U., Denton, W.L., Tanahashi, N. and Ebner, K.E. (1967) The isolation and identification of the B protein of lactose synthetase as α-lactalbumin. *J. Biol. Chem.*, **242**, 1391-1397.

Burri, L., Hockendorff, J., Boehm, U., Klamp, T., Dohmen, R.J. and Levy, F. (2000) Identification and characterization of a mammalian protein interacting with 20S proteasome precursors. *Proc. Natl. Acad. Sci. U. S. A.*, **97**, 10348-10353.

Cardozo, C., Michaud, C. and Orlowski, M. (1999) Components of the bovine pituitary multicatalytic proteinase complex (proteasome) cleaving bonds after hydrophobic residues. *Biochemistry*, **38**, 9768-9777.

Cascio, P., Call, M., Petre, B.M., Walz, T. and Goldberg, A.L. (2002) Properties of the hybrid form of the 26S proteasome containing both 19S and PA28 complexes. *EMBO J.*, **21**, 2636-2645.

Chaudhuri, T.K., Farr, G.W., Fenton, W.A., Rospert, S. and Horwich, A.L. (2001) GroEL/GroES-mediated folding of a protein too large to be encapsulated. *Cell*, **107**, 235-246.

Chen, P. and Hochstrasser, M. (1996) Autocatalytic subunit processing couples active-site formation in the 20S proteasome to completion of assembly. *Cell*, **86**, 961-972.

Chu-Ping, M., Vu, J.H., Proske, R.J., Slaughter, C.A. and DeMartino, G.N. (1994) Identification, purification, and characterization of a high molecular weight, ATP-dependent activator (PA700) of the 20 S proteasome. *J. Biol. Chem.*, **269**, 3539-3547.

Clarke, N.D. (1994) A proposed mechanism for the self-splicing of proteins. *Proc. Natl. Acad. Sci. U. S. A.*, **91**, 11084-11088.

Cooper, A.A. and Stevens, T.H. (1995) Protein splicing: self-splicing of genetically mobile elements at the protein level. *Trends Biochem. Sci.*, **20**, 351-356.

Cornish, V.W., Benson, D.R., Altenbach, C.A., Hideg, K., Hubbell, W.L. and Schultz, P.G. (1994) Site-specific incorporation of biophysical probes into proteins. *Proc. Natl. Acad. Sci. U. S. A.*, **91**, 2910-2915.

da Costa, C.A., Ancolio, K. and Checler, F. (1999) C-terminal maturation fragments of presenilin 1 and 2 control secretion of APP α and A β by human cells and are degraded by proteasome. *Mol. Med.*, **5**, 160-168.

Dahlmann, B., Kopp, F., Kuehn, L., Niedel, B., Pfeifer, G., Hegerl, R. and Baumeister, W. (1989) The multicatalytic proteinase (prosome) is ubiquitous from eukaryotes to archaebacteria. *FEBS Lett.*, **251**, 125-131.

Dahlmann, B., Kuehn, L., Grziwa, A., Zwickl, P. and Baumeister, W. (1992) Biochemical properties of the proteasome from *Thermoplasma acidophilum*. *Eur. J. Biochem.*, **208**, 789-797.

Dantuma, N.P., Lindsten, K., Glas, R., Jellne, M. and Masucci, M.G. (2000) Short-lived green fluorescent proteins for quantifying ubiquitin/proteasome-dependent proteolysis in living cells. *Nat. Biotechnol.*, **18**, 538-543.

Danziger, O., Rivenzon-Segal, D., Wolf, S.G. and Horovitz, A. (2003) Conversion of the allosteric transition of GroEL from concerted to sequential by the single mutation Asp-155 -> Ala. *Proc. Natl. Acad. Sci. U. S. A.*, **100**, 13797-13802.

DeMartino, G.N., Moomaw, C.R., Zagnitko, O.P., Proske, R.J., Chu, P.M., Afendis, S.J., Swaffield, J.C. and Slaughter, C.A. (1994) PA700, an ATP-dependent activator of the 20 S proteasome, is an ATPase containing multiple members of a nucleotide-binding protein family. *J. Biol. Chem.*, **269**, 20878-20884.

DeMartino, G.N., Proske, R.J., Moomaw, C.R., Strong, A.A., Song, X.L., Hisamatsu, H., Tanaka, K. and Slaughter, C.A. (1996) Identification, purification, and characterization of a PA700-dependent activator of the proteasome. *J. Biol. Chem.*, **271**, 3112-3118.

Dick, L.R., Cruikshank, A.A., Grenier, L., Melandri, F.D., Nunes, S.L. and Stein, R.L. (1996a) Mechanistic studies on the inactivation of the proteasome by lactacystin - a central role for clasto-lactacystin β-lactone. *J. Biol. Chem.*, **271**, 7273-7276.

Dick, T.P., Nussbaum, A.K., Deeg, M., Heinemeyer, W., Groll, M., Schirle, M., Keilholz, W., Stevanovic, S., Wolf, D.H., Huber, R., Rammensee, H.G. and Schild, H. (1998) Contribution of proteasomal β-subunits to the cleavage of peptide-substrates analyzed with yeast mutants. *J. Biol. Chem.*, **273**, 25637-25646.

Dick, T.P., Ruppert, T., Groettrup, M., Kloetzel, P.M., Kuehn, L., Koszinowski, U.H., Stevanovic, S., Schild, H. and Rammensee, H.G. (1996b) Coordinated dual

cleavages induced by the proteasome regulator PA28 lead to dominant MHC ligands. *Cell*, **86**, 253-262.

Dietrich, C., Boscheinen, O., Scharf, K.D., Schmitt, L. and Tampé, R. (1996) Functional immobilization of a DNA-binding protein at a membrane interface via histidine tag and synthetic chelator lipids. *Biochemistry*, **35**, 1100-1105.

Dietrich, C., Schmitt, L. and Tampé, R. (1995) Molecular organization of histidine-tagged biomolecules at self-assembled lipid interfaces using a novel class of chelator lipids. *Proc. Natl. Acad. Sci. U. S. A.*, **92**, 9014-9018.

Ding, Q., Lewis, J.J., Strum, K.M., Dimayuga, E., Bruce-Keller, A.J., Dunn, J.C. and Keller, J.N. (2002) Polyglutamine expansion, protein aggregation, proteasome activity, and neural survival. *J. Biol. Chem.*, **277**, 13935-13942.

Ditzel, L., Huber, R., Mann, K., Heinemeyer, W., Wolf, D.H. and Groll, M. (1998) Conformational constraints for protein self-cleavage in the proteasome. *J. Mol. Biol.*, **279**, 1187-1191.

Dorn, I.T., Eschrich, R., Seemüller, E., Guckenberger, R. and Tampé, R. (1999) High-resolution AFM-imaging and mechanistic analysis of the 20 S proteasome. *J. Mol. Biol.*, **288**, 1027-1036.

Dorn, I.T., Neumaier, K.R. and Tampé, R. (1998) Molecular recognition of histidine-tagged molecules by metal-chelating lipids monitored by fluorescence energy transfer and correlation spectroscopy. *J. Am. Chem. Soc.*, **121**, 2753-2763.

Driscoll, J., Brown, M.G., Finley, D. and Monaco, J.J. (1993) MHC-linked LMP gene products specifically alter peptidase activities of the proteasome. *Nature*, **365**, 262-264.

Dubiel, W., Pratt, G., Ferrell, K. and Rechsteiner, M. (1992) Purification of an 11 S regulator of the multicatalytic protease. *J. Biol. Chem.*, **267**, 22369-22377.

Eigen, M. and Rigler, R. (1994) Sorting single molecules: application to diagnostics and evolutionary biotechnology. *Proc. Natl. Acad. Sci. U. S. A.*, **91**, 5740-5747.

Ellis, R.J. (1996) Revisiting the Anfinsen cage. *Fold Des.*, **1**, R9-15.

Ellis, R.J. (2001) Molecular chaperones: Inside and outside the Anfinsen cage. *Curr. Biol.*, **11**, R1038-1040.

Elofsson, M., Splittgerber, U., Myung, J., Mohan, R. and Crews, C.M. (1999) Towards subunit-specific proteasome inhibitors: synthesis and evaluation of peptide α',β'-epoxyketones. *Chem. Biol.*, **6**, 811-822.

Emmerich, N.P., Nussbaum, A.K., Stevanovic, S., Priemer, M., Toes, R.E., Rammensee, H.G. and Schild, H. (2000) The human 26 S and 20 S proteasomes generate overlapping but different sets of peptide fragments from a model protein substrate. *J. Biol. Chem.*, **275**, 21140-21148.

Erbse, A., Dougan, D.A. and Bukau, B. (2003) A folding machine for many but a master of none. *Nat. Struct. Biol.*, **10**, 84-86.

Falke, S., Fisher, M.T. and Gogol, E.P. (2001) Structural changes in GroEL effected by binding a denatured protein substrate. *J. Mol. Biol.*, **308**, 569-577.

Farr, G.W., Fenton, W.A., Chaudhuri, T.K., Clare, D.K., Saibil, H.R. and Horwich, A.L. (2003) Folding with and without encapsulation by cis- and trans-only GroEL-GroES complexes. *EMBO J.*, **22**, 3220-3230.

Fenteany, G. and Schreiber, S.L. (1998) Lactacystin, proteasome function, and cell fate. *J. Biol. Chem.*, **273**, 8545-8548.

Fenteany, G., Standaert, R.F., Lane, W.S., Choi, S., Corey, E.J. and Schreiber, S.L. (1995) Inhibition of proteasome activities and subunit-specific amino-terminal threonine modification by lactacystin *Science* **268**, 726-731.

Ferdous, A., Gonzalez, F., Sun, L., Kodadek, T. and Johnston, S.A. (2001) The 19S regulatory particle of the proteasome is required for efficient transcription elongation by RNA polymerase II. *Mol. Cell*, **7**, 981-991.

Förster, A., Whitby, F.G. and Hill, C.P. (2003) The pore of activated 20S proteasomes has an ordered 7-fold symmetric conformation. *EMBO J.*, **22**, 4356-4364.

Förster, T. (1948) Intermolecular energy migration and fluorescence. *Ann. Phys.*, **2**, 55-75.

Foss, G.S., Larsen, F., Solheim, J. and Prydz, H. (1998) Constitutive and interferon-γ-induced expression of the human proteasome subunit multicatalytic endopeptidase complex-like 1. *Biochim. Biophys. Acta*, **1402**, 17-28.

Gaczynska, M., Osmulski, P.A., Gao, Y., Post, M.J. and Simons, M. (2003) Proline- and arginine-rich peptides constitute a novel class of allosteric inhibitors of proteasome activity. *Biochemistry*, **42**, 8663-8670.

Gaczynska, M., Rock, K.L. and Goldberg, A.L. (1993) γ-interferon and expression of MHC genes regulate peptide hydrolysis by proteasomes. *Nature*, **365**, 264-267.

Gardner, R.C., Assinder, S.J., Christie, G., Mason, G.G., Markwell, R., Wadsworth, H., McLaughlin, M., King, R., Chabot-Fletcher, M.C., Breton, J.J., Allsop, D. and Rivett, A.J. (2000) Characterization of peptidyl boronic acid inhibitors of mammalian 20 S and 26 S proteasomes and their inhibition of proteasomes in cultured cells. *Biochem. J.*, **346 Pt 2**, 447-454.

Geier, E., Pfeifer, G., Wilm, M., Lucchiari-Hartz, M., Baumeister, W., Eichmann, K. and Niedermann, G. (1999) A giant protease with potential to substitute for some functions of the proteasome. *Science*, **283**, 978-981.

Glas, R., Bogyo, M., Mcmaster, J.S., Gaczynska, M. and Ploegh, H.L. (1998) A proteolytic system that compensates for loss of proteasome function. *Nature*, **392**, 618-622.

Glickman, M.H., Rubin, D.M., Coux, O., Wefes, I., Pfeifer, G., Cjeka, Z., Baumeister, W., Fried, V.A. and Finley, D. (1998) A subcomplex of the proteasome regulatory particle required for ubiquitin-conjugate degradation and related to the COP9-signalosome and eIF3. *Cell*, **94**, 615-623.

Goldberg, A.L. (2003) Protein degradation and protection against misfolded or damaged proteins. *Nature*, **426**, 895-899.

Gregori, L., Fuchs, C., Figueiredo-Pereira, M.E., Van Nostrand, W.E. and Goldgaber, D. (1995) Amyloid β-protein inhibits ubiquitin-dependent protein degradation in vitro. *J. Biol. Chem.*, **270**, 19702-19708.

Griffin, T.A., Nandi, D., Cruz, M., Fehling, H.J., Vankaer, L., Monaco, J.J. and Colbert, R.A. (1998) Immunoproteasome assembly - cooperative incorporation of interferon-γ (IFN-γ)-inducible subunits. *J. Exp. Med.*, **187**, 97-104.

Grimaud, R., Kessel, M., Beuron, F., Steven, A.C. and Maurizi, M.R. (1998) Enzymatic and structural similarities between the *Escherichia coli* ATP-dependent proteases, ClpXP and ClpAP. *J. Biol. Chem.*, **273**, 12476-12481.

Groettrup, M., Standera, S., Stohwasser, R. and Kloetzel, P.M. (1997) The subunits MECL-1 and LMP2 are mutually required for incorporation into the 20S proteasome. *Proc. Natl. Acad. Sci. U. S. A.*, **94**, 8970-8975.

Groll, M., Bajorek, M., Köhler, A., Moroder, L., Rubin, D.M., Huber, R., Glickman, M.H. and Finley, D. (2000) A gated channel into the proteasome core particle. *Nat. Struct. Biol.*, **7**, 1062-1067.

Groll, M., Brandstetter, H., Bartunik, H., Bourenkow, G. and Huber, R. (2003) Investigations on the maturation and regulation of archaebacterial proteasomes. *J. Mol. Biol.*, **327**, 75-83.

Groll, M., Ditzel, L., Löwe, J., Stock, D., Bochtler, M., Bartunik, H.D. and Huber, R. (1997) Structure of 20S proteasome from yeast at 2.4 Å resolution. *Nature*, **386**, 463-471.

Groll, M., Heinemeyer, W., Jager, S., Ullrich, T., Bochtler, M., Wolf, D.H. and Huber, R. (1999) The catalytic sites of 20S proteasomes and their role in subunit maturation: a mutational and crystallographic study. *Proc. Natl. Acad. Sci. U. S. A.*, **96**, 10976-10983.

Groll, M., Koguchi, Y., Huber, R. and Kohno, J. (2001) Crystal structure of the 20 S proteasome: TMC-95A complex: a non-covalent proteasome inhibitor. *J. Mol. Biol.*, **311**, 543-548.

Grziwa, A., Maack, S., Puhler, G., Wiegand, G., Baumeister, W. and Jaenicke, R. (1994) Dissociation and reconstitution of the *Thermoplasma* proteasome. *Eur. J. Biochem.*, **223**, 1061-1067.

Harris, C.A., Hunte, B., Krauss, M.R., Taylor, A. and Epstein, L.B. (1992) Induction of leucine aminopeptidase by interferon γ. Identification by protein microsequencing after purification by preparative two-dimensional gel electrophoresis. *J. Biol. Chem.*, **267**, 6865-6869.

Hartmann-Petersen, R., Tanaka, K. and Hendil, K.B. (2001) Quaternary structure of the ATPase complex of human 26S proteasomes determined by chemical cross-linking. *Arch. Biochem. Biophys.*, **386**, 89-94.

Heinemeyer, W., Fischer, M., Krimmer, T., Stachon, U. and Wolf, D.H. (1997) The active sites of the eukaryotic 20 S proteasome and their involvement in subunit precursor processing. *J. Biol. Chem.*, **272**, 25200-25209.

Hendil, K.B., Hartmann-Petersen, R. and Tanaka, K. (2002) 26 S proteasomes function as stable entities. *J. Mol. Biol.*, **315**, 627-636.

Hochuli, E. (1990) Purification of recombinant proteins with metal chelate adsorbent. *Genet. Eng. (NY)*, **12**, 87-98.

Hochuli, E., Bannwarth, W., Döbeli, H., Gentz, R. and Stüber, D. (1988) Genetic approach to factilitate purification of recombinant proteins with a novel metal chelate adsorbent. *Bio/Technology*, **6**, 1321-1325.

Holzhütter, H.G., Frommel, C. and Kloetzel, P.M. (1999) A theoretical approach towards the identification of cleavage-determining amino acid motifs of the 20 S proteasome. *J. Mol. Biol.*, **286**, 1251-1265.

Horwich, A.L., Weber-Ban, E.U. and Finley, D. (1999) Chaperone rings in protein folding and degradation. *Proc. Natl. Acad. Sci. U. S. A.*, **96**, 11033-11040.

Hoskins, J.R., Pak, M., Maurizi, M.R. and Wickner, S. (1998) The role of the ClpA chaperone in proteolysis by ClpAP. *Proc. Natl. Acad. Sci. U. S. A.*, **95**, 12135-12140.

Hoskins, J.R., Singh, S.K., Maurizi, M.R. and Wickner, S. (2000) Protein binding and unfolding by the chaperone ClpA and degradation by the protease ClpAP. *Proc. Natl. Acad. Sci. U. S. A.*, **97**, 8892-8897.

Hoskins, J.R., Yanagihara, K., Mizuuchi, K. and Wickner, S. (2002) ClpAP and ClpXP degrade proteins with tags located in the interior of the primary sequence. *Proc. Natl. Acad. Sci. U. S. A.*, **99**, 11037-11042.

Huang, H.C. and Goldberg, A.L. (1997) Proteolytic activity of the ATP-dependent protease HslVU can be uncoupled from ATP hydrolysis. *J. Biol. Chem.*, **272**, 21364-21372.

Hutschenreiter, S., Neumann, L., Rädler, U., Schmitt, L. and Tampé, R. (2003) Metal-chelating amino acids as building blocks for synthetic receptors sensing metal ions and histidine-tagged proteins. *ChemBiochem*, **4**, 1340-1344.

Hutschenreiter, S., Tinazli, A., Model, K. and Tampé, R. (2004) Two-substrate association with the 20 S proteasome at single-molecule level. *EMBO J.*, **in press**.

Ishikawa, T., Beuron, F., Kessel, M., Wickner, S., Maurizi, M.R. and Steven, A.C. (2001) Translocation pathway of protein substrates in ClpAP protease. *Proc. Natl. Acad. Sci. U. S. A.*, **98**, 4328-4333.

Jackson, G.S., Staniforth, R.A., Halsall, D.J., Atkinson, T., Holbrook, J.J., Clarke, A.R. and Burston, S.G. (1993) Binding and hydrolysis of nucleotides in the chaperonin

catalytic cycle: implications for the mechanism of assisted protein folding. *Biochemistry*, **32**, 2554-2563.

Jäger, S., Groll, M., Huber, R., Wolf, D.H. and Heinemeyer, W. (1999) Proteasome β-type subunits: Unequal roles of propeptides in core particle maturation and a hierarchy of active site function. *J. Mol. Biol.*, **291**, 997-1013.

Jotterand, N., Pearce, D.A. and Imperiali, B. (2001) Asymmetric synthesis of a new 8-hydroxyquinoline-derived alpha-amino acid and its incorporation in a peptidylsensor for divalent zinc. *J. Org. Chem.*, **66**, 3224-3228.

Junn, E., Lee, S.S., Suhr, U.T. and Mouradian, M.M. (2002) Parkin accumulation in aggresomes due to proteasome impairment. *J. Biol. Chem.*, **277**, 47870-47877.

Kapanidis, A.N., Ebright, Y.W. and Ebright, R.H. (2001) Site-specific incorporation of fluorescent probes into protein: hexahistidine-tag-mediated fluorescent labeling with ($Ni^{2+}$:nitrilotriacetic acid $)_n$-fluorochrome conjugates. *J. Am. Chem. Soc.*, **123**, 12123-12125.

Kapelari, B., Bech-Otschir, D., Hegerl, R., Schade, R., Dumdey, R. and Dubiel, W. (2000) Electron microscopy and subunit-subunit interaction studies reveal a first architecture of COP9 signalosome. *J. Mol. Biol.*, **300**, 1169-1178.

Keiler, K.C., Waller, P.R. and Sauer, R.T. (1996) Role of a peptide tagging system in degradation of proteins synthesized from damaged messenger RNA. *Science*, **271**, 990-993.

Kessel, M., Maurizi, M.R., Kim, B., Kocsis, E., Trus, B.L., Singh, S.K. and Steven, A.C. (1995) Homology in structural organization between *Escherichia coli* ClpAP protease and the eukaryotic 26S proteasome. *J. Mol. Biol.*, **250**, 587-594.

Kessel, M., Wu, W.F., Gottesman, S., Kocsis, E., Steven, A.C. and Maurizi, M.R. (1996) 6-fold rotational symmetry of ClpQ, the *Escherichia coli* homolog of the 20S proteasome, and its ATP-dependent activator, ClpY. *FEBS Lett.*, **398**, 274-278.

Kettling, U., Koltermann, A., Schwille, P. and Eigen, M. (1998) Real-time enzyme kinetics monitored by dual-color fluorescence cross-correlation spectroscopy. *Proc. Natl. Acad. Sci. U. S. A.*, **95**, 1416-1420.

Kim, T.W., Pettingell, W.H., Hallmark, O.G., Moir, R.D., Wasco, W. and Tanzi, R.E. (1997) Endoproteolytic cleavage and proteasomal degradation of presenilin 2 in transfected cells. *J. Biol. Chem.*, **272**, 11006-11010.

Kim, Y.I., Burton, R.E., Burton, B.M., Sauer, R.T. and Baker, T.A. (2000) Dynamics of substrate denaturation and translocation by the ClpXP degradation machine. *Mol. Cell*, **5**, 639-648.

Kimura, Y., Takaoka, M., Tanaka, S., Sassa, H., Tanaka, K., Polevoda, B., Sherman, F. and Hirano, H. (2000) $N^{\alpha}$-acetylation and proteolytic activity of the yeast 20 S proteasome. *J. Biol. Chem.*, **275**, 4635-4639.

Kisselev, A.F., Akopian, T.N., Castillo, V. and Goldberg, A.L. (1999a) Proteasome active sites allosterically regulate each other, suggesting a cyclical bite-chew mechanism for protein breakdown. *Mol. Cell*, **4**, 395-402.

Kisselev, A.F., Akopian, T.N. and Goldberg, A.L. (1998) Range of sizes of peptide products generated during degradation of different proteins by archaeal proteasomes. *J. Biol. Chem.*, **273**, 1982-1989.

Kisselev, A.F., Akopian, T.N., Woo, K.M. and Goldberg, A.L. (1999b) The sizes of peptides generated from protein by mammalian 26 and 20 S proteasomes - Implications for understanding the degradative mechanism and antigen presentation. *J. Biol. Chem.*, **274**, 3363-3371.

Kisselev, A.F., Garcia-Calvo, M., Overkleeft, H.S., Peterson, E., Pennington, M.W., Ploegh, H.L., Thornberry, N.A. and Goldberg, A.L. (2003) The caspase-like sites of proteasomes: substrate specificity, new inhibitors and substrates, and allosteric interactions with the trypsin-like sites. *J. Biol. Chem.*

Kisselev, A.F., Kaganovich, D. and Goldberg, A.L. (2002) Binding of hydrophobic peptides to several non-catalytic sites promotes peptide hydrolysis by all active sites of 20 S proteasomes. Evidence for peptide-induced channel opening in the α-rings. *J. Biol. Chem.*, **277**, 22260-22270.

Kisselev, A.F., Songyang, Z. and Goldberg, A.L. (2000) Why does threonine, and not serine, function as the active site nucleophile in proteasomes? *J. Biol. Chem.*, **275**, 14831-14837.

Knowlton, J.R., Johnston, S.C., Whitby, F.G., Realini, C., Zhang, Z.G., Rechsteiner, M. and Hill, C.P. (1997) Structure of the proteasome activator REGα (PA28α). *Nature*, **390**, 639-643.

Kohl, T., Heinze, K.G., Kuhlemann, R., Koltermann, A. and Schwille, P. (2002) A protease assay for two-photon crosscorrelation and FRET analysis based solely on fluorescent proteins. *Proc. Natl. Acad. Sci. U. S. A.*, **99**, 12161-12166.

Köhler, A., Cascio, P., Leggett, D.S., Woo, K.M., Goldberg, A.L. and Finley, D. (2001) The axial channel of the proteasome core particle is gated by the Rpt2 ATPase and controls both substrate entry and product release. *Mol. Cell*, **7**, 1143-1152.

Koltermann, A., Kettling, U., Bieschke, J., Winkler, T. and Eigen, M. (1998) Rapid assay processing by integration of dual-color fluorescence cross-correlation spectroscopy: high throughput screening for enzyme activity. *Proc. Natl. Acad. Sci. U. S. A.*, **95**, 1421-1426.

Kubalek, E.W., Le Grice, S.F. and Brown, P.O. (1994) Two-dimensional crystallization of histidine-tagged, HIV-1 reverse transcriptase promoted by a novel nickel-chelating lipid. *J. Struct. Biol.*, **113**, 117-123.

Kuttler, C., Nussbaum, A.K., Dick, T.P., Rammensee, H.G., Schild, H. and Hadeler, K.P. (2000) An algorithm for the prediction of proteasomal cleavages. *J. Mol. Biol.*, **298**, 417-429.

Kuwajima, K., Hiraoka, Y., Ikeguchi, M. and Sugai, S. (1985) Comparison of the transient folding intermediates in lysozyme and α-lactalbumin. *Biochemistry*, **24**, 874-881.

Lämmli, U.K. and Quittner, S.F. (1974) Maturation of the head of bacteriophage T4. IV. The proteins of the core of the tubular polyheads and in vitro cleavage of the head proteins. *Virology*, **62**, 483-499.

Lee, C., Prakash, S. and Matouschek, A. (2002) Concurrent translocation of multiple polypeptide chains through the proteasomal degradation channel. *J. Biol. Chem.*, **277**, 34760-34765.

Lee, C., Schwartz, M.P., Prakash, S., Iwakura, M. and Matouschek, A. (2001) ATP-dependent proteases degrade their substrates by processively unraveling them from the degradation signal. *Mol. Cell*, **7**, 627-637.

Liu, C.W., Corboy, M.J., DeMartino, G.N. and Thomas, P.J. (2003) Endoproteolytic activity of the proteasome. *Science*, **299**, 408-411.

Löwe, J., Stock, D., Jap, R., Zwickl, P., Baumeister, W. and Huber, R. (1995) Crystal-structure of the 20S proteasome from the archaeon T. acidophilum at 3.4 Å resolution. *Science*, **268**, 533-539.

Lunkes, A., Lindenberg, K.S., Ben-Haiem, L., Weber, C., Devys, D., Landwehrmeyer, G.B., Mandel, J.L. and Trottier, Y. (2002) Proteases acting on mutant huntingtin generate cleaved products that differentially build up cytoplasmic and nuclear inclusions. *Mol. Cell*, **10**, 259-269.

Ma, C.P., Slaughter, C.A. and DeMartino, G.N. (1992) Identification, purification, and characterization of a protein activator (PA28) of the 20 S proteasome (macropain). *J. Biol. Chem.*, **267**, 10515-10523.

Ma, J. and Lindquist, S. (1999) De novo generation of a $PrP^{Sc}$-like conformation in living cells. *Nat. Cell Biol.*, **1**, 358-361.

Ma, J. and Lindquist, S. (2001) Wild-type PrP and a mutant associated with prion disease are subject to retrograde transport and proteasome degradation. *Proc. Natl. Acad. Sci. U. S. A.*, **98**, 14955-14960.

Ma, J. and Lindquist, S. (2002) Conversion of PrP to a self-perpetuating $PrP^{Sc}$-like conformation in the cytosol. *Science*, **298**, 1785-1788.

Ma, J., Wollmann, R. and Lindquist, S. (2002) Neurotoxicity and neurodegeneration when PrP accumulates in the cytosol. *Science*, **298**, 1781-1785.

Marambaud, P., Ancolio, K., Lopez-Perez, E. and Checler, F. (1998) Proteasome inhibitors prevent the degradation of familial Alzheimer's disease-linked presenilin 1 and potentiate A β 42 recovery from human cells. *Mol. Med.*, **4**, 147-157.

Maurizi, M.R., Clark, W.P., Katayama, Y., Rudikoff, S., Pumphrey, J., Bowers, B. and Gottesman, S. (1990) Sequence and structure of Clp P, the proteolytic component of the ATP-dependent Clp protease of *Escherichia coli*. *J. Biol. Chem.*, **265**, 12536-12545.

Maurizi, M.R., Thompson, M.W., Singh, S.K. and Kim, S.H. (1994) Endopeptidase Clp - ATP-dependent Clp protease from *Escherichia coli*. *Methods Enzymol.*, **244**, 314-331.

McCutchen-Maloney, S.L., Matsuda, K., Shimbara, N., Binns, D.D., Tanaka, K., Slaughter, C.A. and DeMartino, G.N. (2000) cDNA cloning, expression, and functional characterization of PI31, a proline-rich inhibitor of the proteasome. *J. Biol. Chem.*, **275**, 18557-18565.

McGuire, M.J., McCullough, M.L., Croall, D.E. and DeMartino, G.N. (1989) The high molecular weight multicatalytic proteinase, macropain exist in a latent form in human erythrocytes. *Biochim. Biophys. Acta*, **995**, 181, 186.

Mendel, D., Ellman, J.A., Chang, Z., Veenstra, D.L., Kollman, P.A. and Schultz, P.G. (1992) Probing protein stability with unnatural amino acids. *Science*, **256**, 1798-1802.

Miller, D.W., Ahmad, R., Hague, S., Baptista, M.J., Canet-Aviles, R., McLendon, C., Carter, D.M., Zhu, P.P., Stadler, J., Chandran, J., Klinefelter, G.R., Blackstone, C. and Cookson, M.R. (2003) L166P mutant DJ-1, causative for recessive Parkinson's disease, is degraded through the ubiquitin-proteasome system. *J. Biol. Chem.*, **278**, 36588-36595.

Muir, T.W. (2003) Semisynthesis of proteins by expressed protein ligation. *Annu. Rev. Biochem.*, **72**, 249-289.

Mykles, D.L. (1989) Purification and characterization of a multicatalytic proteinase from crustacean muscle: comparison of latent and heat-activated forms. *Arch. Biochem. Biophys.*, **274**, 216-228.

Myung, J., Kim, K.B., Lindsten, K., Dantuma, N.P. and Crews, C.M. (2001) Lack of proteasome active site allostery as revealed by subunit-specific inhibitors. *Mol. Cell*, **7**, 411-420.

Navon, A. and Goldberg, A.L. (2001) Proteins are unfolded on the surface of the ATPase ring before transport into the proteasome. *Mol. Cell*, **8**, 1339-1349.

Nussbaum, A.K., Dick, T.P., Keilholz, W., Schirle, M., Stevanovic, S., Dietz, K., Heinemeyer, W., Groll, M., Wolf, D.H., Huber, R., Rammensee, H.G. and Schild, H. (1998) Cleavage motifs of the yeast 20S proteasome β subunits deduced from digests of enolase 1. *Proc. Natl. Acad. Sci. U. S. A.*, **95**, 12504-12509.

Ortega, J., Lee, H.S., Maurizi, M.R. and Steven, A.C. (2002) Alternating translocation of protein substrates from both ends of ClpXP protease. *EMBO J.*, **21**, 4938-4949.

Osmulski, P.A. and Gaczynska, M. (2000) Atomic force microscopy reveals two conformations of the 20 S proteasome from fission yeast. *J. Biol. Chem.*, **275**, 13171-13174.

Osmulski, P.A. and Gaczynska, M. (2002) Nanoenzymology of the 20S proteasome: proteasomal actions are controlled by the allosteric transition. *Biochemistry*, **41**, 7047-7053.

Petrucelli, L., O'Farrell, C., Lockhart, P.J., Baptista, M., Kehoe, K., Vink, L., Choi, P., Wolozin, B., Farrer, M., Hardy, J. and Cookson, M.R. (2002) Parkin protects against the toxicity associated with mutant α-synuclein: proteasome dysfunction selectively affects catecholaminergic neurons. *Neuron*, **36**, 1007-1019.

Piccinini, M., Tazartes, O., Mostert, M., Musso, A., DeMarchi, M. and Rinaudo, M.T. (2000) Structural and functional characterization of 20S and 26S proteasomes from bovine brain. *Mol. Brain Res.*, **76**, 103-114.

Porath, J., Carlsson, J., Olsson, I. and Belfrage, G. (1975) Metal chelate affinity chromatography, a new approach to protein fractionation. *Nature*, **258**, 598-599.

Rädler, U., Mack, J., Persike, N., Jung, G. and Tampé, R. (2000) Design of supported membranes tethered via metal-affinity ligand-receptor pairs. *Biophys. J.*, **79**, 3144-3152.

Ramos, P.C., Hockendorff, J., Johnson, E.S., Varshavsky, A. and Dohmen, R.J. (1998) Ump1p is required for proper maturation of the 20S proteasome and becomes its substrate upon completion of the assembly. *Cell*, **92**, 489-499.

Ranson, N.A., Farr, G.W., Roseman, A.M., Gowen, B., Fenton, W.A., Horwich, A.L. and Saibil, H.R. (2001) ATP-bound states of GroEL captured by cryo-electron microscopy. *Cell*, **107**, 869-879.

Reid, B.G., Fenton, W.A., Horwich, A.L. and Weber-Ban, E.U. (2001) ClpA mediates directional translocation of substrate proteins into the ClpP protease. *Proc. Natl. Acad. Sci. U. S. A.*, **98**, 3768-3772.

Renart, J., Reiser, J. and Stark, G.R. (1979) Transfer of proteins from gels to diazobenzyloxymethyl-paper and detection with antisera: a method for studying antibody specificity and antigen structure. *Proc. Natl. Acad. Sci. U. S. A.*, **76**, 3116-3120.

Rohrwild, M., Coux, O., Huang, H.C., Moerschell, R.P., Yoo, S.J., Seol, J.H., Chung, C.H. and Goldberg, A.L. (1996) HslV-HslU: A novel ATP-dependent protease complex in *Escherichia coli* related to the eukaryotic proteasome. *Proc. Natl. Acad. Sci. U. S. A.*, **93**, 5808-5813.

Rohrwild, M., Pfeifer, G., Santarius, U., Muller, S.A., Huang, H.C., Engel, A., Baumeister, W. and Goldberg, A.L. (1997) The ATP-dependent HslVU protease from *Escherichia coli* is a 4-ring structure resembling the proteasome. *Nat. Struct. Biol.*, **4**, 133-139.

Ruiz, de, Mena, I, Mahillo, E., Arribas, J. and Castano, J.G. (1993) Kinetic mechanism of activation by cardiolipin (diphosphatidylglycerol) of the rat liver multicatalytic proteinase. *Biochem. J.*, 93-97.

Rye, H.S., Roseman, A.M., Chen, S., Furtak, K., Fenton, W.A., Saibil, H.R. and Horwich, A.L. (1999) GroEL-GroES cycling: ATP and nonnative polypeptide direct alternation of folding-active rings. *Cell*, **97**, 325-338.

Satoh, K., Sasajima, H., Nyoumura, K.I., Yokosawa, H. and Sawada, H. (2001) Assembly of the 26S proteasome is regulated by phosphorylation of the p45/Rpt6 ATPase subunit. *Biochemistry*, **40**, 314-319.

Savory, P.J. and Rivett, A.J. (1993) Leupeptin-binding site(s) in the mammalian multicatalytic proteinase complex. *Biochem. J.*, 45-48.

Saxova, P., Buus, S., Brunak, S. and Kesmir, C. (2003) Predicting proteasomal cleavage sites: a comparison of available methods. *Int. Immunol.*, **15**, 781-787.

Schägger, H. and von Jagow, G. (1987) Tricine-sodium dodecyl sulfate-polyacrylamide gel electrophoresis for the separation of proteins in the range from 1 to 100 kDa. *Anal. Biochem.*, **166**, 368-379.

Schmidtke, G., Emch, S., Groettrup, M. and Holzhutter, H.G. (2000) Evidence for the existence of a non-catalytic modifier site of peptide hydrolysis by the 20 S proteasome. *J. Biol. Chem.*, **275**, 22056-22063.

Schmidtke, G., Kraft, R., Kostka, S., Henklein, P., Frommel, C., Löwe, J., Huber, R., Kloetzel, P.M. and Schmidt, M. (1996) Analysis of mammalian 20S proteasome biogenesis: the maturation of beta-subunits is an ordered two-step mechanism involving autocatalysis. *EMBO J.*, **15**, 6887-6898.

Schmitt, L., Bohanen, T.M., Denziger, S., Ringsdorf, H. and Tampé, R. (1996) Specific protein docking to chelator lipid monolayers monitored by FT-IR spectroscopy at the air-water interface. *Angew. Chem. Int. Ed. Engl.*, **35**, 317-320.

Schmitt, L., Dietrich, C. and Tampé, R. (1994) Synthesis and characterization of chelator lipids for reversible immobilization of engineered proteins at self-assembled lipid interfaces. *J. Am. Chem. Soc.*, **116**, 8485-8491.

Schmitt, L., Ludwig, M., Gaub, H.E. and Tampé, R. (2000) A metal-chelating microscopy tip as a new toolbox for single-molecule experiments by atomic force microscopy. *Biophys. J.*, **78**, 3275-3285.

Seemüller, E., Lupas, A. and Baumeister, W. (1996) Autocatalytic processing of the 20S proteasome. *Nature*, **382**, 468-470.

Seemüller, E., Lupas, A., Stock, D., Löwe, J., Huber, R. and Baumeister, W. (1995a) Proteasome from *Thermoplasma acidophilum* - a threonine protease. *Science*, **268**, 579-582.

Seemüller, E., Lupas, A., Zühl, F., Zwickl, P. and Baumeister, W. (1995b) The proteasome from *Thermoplasma acidophilum* is neither a cysteine nor a serine protease. *FEBS Lett.*, **359**, 173-178.

Seol, J.H., Yoo, S.J., Shin, D.H., Shim, Y.K., Kang, M.S., Goldberg, A.L. and Chung, C.H. (1997) The heat-shock-protein HslVU from *Escherichia coli* is a protein-activated ATPase as well as an ATP-dependent proteinase. *Eur. J. Biochem.*, **247**, 1143-1150.

Shimbara, N., Ogawa, K., Hidaka, Y., Nakajima, H., Yamasaki, N., Niwa, S., Tanahashi, N. and Tanaka, K. (1998) Contribution of proline residue for efficient production of MHC class-I ligands by proteasomes. *J. Biol. Chem.*, **273**, 23062-23071.

Shnek, D.R., Pack, D.W., Sasaki, D.Y. and Arnold, F.H. (1994) Specific protein attachment to artificial membranes via coordination to lipid-bound copper (II). *Langmuir*, **10**, 2382-2388.

Sigal, G.B., Bamdad, C., Barberis, A., Strominger, J. and Whitesides, G.M. (1996) A self-assembled monolayer for the binding and study of histidine-tagged proteins by surface plasmon resonance. *Anal. Chem.*, **68**, 490-497.

Singh, S.K., Grimaud, R., Hoskins, J.R., Wickner, S. and Maurizi, M.R. (2000) Unfolding and internalization of proteins by the ATP-dependent proteases ClpXP and ClpAP. *Proc. Natl. Acad. Sci. U. S. A.*, **97**, 8898-8903.

Skovronsky, D.M., Pijak, D.S., Doms, R.W. and Lee, V.M. (2000) A distinct ER/IC γ-secretase competes with the proteasome for cleavage of APP. *Biochemistry*, **39**, 810-817.

Snyder, H., Mensah, K., Theisler, C., Lee, J., Matouschek, A. and Wolozin, B. (2003) Aggregated and monomeric α-synuclein bind to the S6' proteasomal protein and inhibit proteasomal function. *J. Biol. Chem.*, **278**, 11753-11759.

Song, X., Molt, J.D., Vonkampen, J., Pramanik, B., Tanaka, K., Slaughter, C.A. and DeMartino, G.N. (1996) A model for the quaternary structure of the proteasome activator, PA28. *Mol. Biol. Cell*, **7**, 1067-1067.

Sousa, M.C., Trame, C.B., Tsuruta, H., Wilbanks, S.M., Reddy, V.S. and McKay, D.B. (2000) Crystal and solution structures of an HslUV protease-chaperone complex. *Cell*, **103**, 633-643.

Stein, R.L., Melandri, F. and Dick, L. (1996) Kinetic characterization of the chymotryptic activity of the 20S proteasome. *Biochemistry*, **35**, 3899-3908.

Stenberg, E., Persson, B., Roos, H. and Urbaniczky, C. (1991) Quantitative determination of surface concentration of protein with surface plasmon resonance by using radiolabeled proteins. *L. Colloid Interface Sci.*, **143**, 513-526.

Stothart, P.H. (1984) Determination of partial specific volume and absolute concentration by densimetry. *Biochem. J.*, **219**, 1049-1052.

Strickland, E., Hakala, K., Thomas, P.J. and DeMartino, G.N. (2000) Recognition of misfolding proteins by PA700, the regulatory subcomplex of the 26 S proteasome. *J. Biol. Chem.*, **275**, 5565-5572.

Studier, F.W. (1973) Analysis of bacteriophage T7 early RNAs and proteins on slab gels. *J. Mol. Biol.*, **79**, 237-248.

Tanaka, K., Ii, K., Ichihara, A., Waxman, L. and Goldberg, A.L. (1986) A high molecular weight protease in the cytosol of rat liver. I. Purification, enzymological properties, and tissue distribution. *J. Biol. Chem.*, **261**, 15197-15203.

Teicher, B.A., Ara, G., Herbst, R., Palombella, V.J. and Adams, J. (1999) The proteasome inhibitor PS-341 in cancer therapy. *Clin. Cancer Res.*, **5**, 2638-2645.

Tenzer, S., Stoltze, L., Schonfisch, B., Dengjel, J., Müller, M., Stevanovic, S., Rammensee, H.G. and Schild, H. (2004) Quantitative analysis of prion-protein

degradation by constitutive and immuno-20S proteasomes indicates differences correlated with disease susceptibility. *J. Immunol.*, **172**, 1083-1091.

Thess, A., Hutschenreiter, S., Hofmann, M., Tampé, R., Baumeister, W. and Guckenberger, R. (2002) Specific orientation and two-dimensional crystallization of the proteasome at metal-chelating lipid interfaces. *J. Biol. Chem.*, **277**, 36321-36328.

Thompson, M.W., Singh, S.K. and Maurizi, M.R. (1994) Processive degradation of proteins by the ATP-dependent Clp protease from Escherichia coli - requirement for the multiple array of active sites in ClpP but not ATP hydrolysis. *J. Biol. Chem.*, **269**, 18209-18215.

Todd, M.J., Viitanen, P.V. and Lorimer, G.H. (1994) Dynamics of the chaperonin ATPase cycle: implications for facilitated protein folding. *Science*, **265**, 659-666.

Towbin, H., Staehelin, T. and Gordon, J. (1979) Electrophoretic transfer of proteins from polyacrylamide gels to nitrocellulose sheets: procedure and some applications. *Proc. Natl. Acad. Sci. U. S. A.*, **76**, 4350-4354.

Turner, G.C. and Varshavsky, A. (2000) Detecting and measuring cotranslational protein degradation in vivo. *Science*, **289**, 2117-2120.

Uebel, S. and Tampé, R. (1999) Specificity of the proteasome and the TAP transporter. *Curr. Opin. Immunol.*, **11**, 203-208.

Venien-Bryan, C., Balavoine, F., Toussaint, B., Mioskowski, C., Hewat, E.A., Helme, B. and Vignais, P.M. (1997) Structural study of the response regulator HupR from *Rhodobacter capsulatus*. Electron microscopy of two-dimensional crystals on a nickel-chelating lipid. *J. Mol. Biol.*, **274**, 687-692.

Verma, R., Aravind, L., Oania, R., McDonald, W.H., Yates, J.R., 3rd, Koonin, E.V. and Deshaies, R.J. (2002) Role of Rpn11 metalloprotease in deubiquitination and degradation by the 26S proteasome. *Science*, **298**, 611-615.

Voges, D., Zwickl, P. and Baumeister, W. (1999) The 26S proteasome: a molecular machine designed for controlled proteolysis. *Annu. Rev. Biochem.*, **68**, 1015-1068.

Wang, E.W., Kessler, B.M., Borodovsky, A., Cravatt, B.F., Bogyo, M., Ploegh, H.L. and Glas, R. (2000) Integration of the ubiquitin-proteasome pathway with a cytosolic oligopeptidase activity. *Proc. Natl. Acad. Sci. U. S. A.*, **97**, 9990-9995.

Wang, J., Hartling, J.A. and Flanagan, J.M. (1997) The structure of ClpP at 2.3 Å resolution suggests a model for ATP-dependent proteolysis. *Cell*, **91**, 447-456.

Wang, J.D., Herman, C., Tipton, K.A., Gross, C.A. and Weissman, J.S. (2002) Directed evolution of substrate-optimized GroEL/S chaperonins. *Cell*, **111**, 1027-1039.

Wang, R., Chait, B.T., Wolf, I., Kohanski, R.A. and Cardozo, C. (1999a) Lysozyme degradation by the bovine multicatalytic proteinase complex (proteasome): evidence for a nonprocessive mode of degradation. *Biochemistry*, **38**, 14573-14581.

Wang, Z., Feng, H., Landry, S.J., Maxwell, J. and Gierasch, L.M. (1999b) Basis of substrate binding by the chaperonin GroEL. *Biochemistry*, **38**, 12537-12546.

Weissman, J.S. (2001) The ins and outs of GroEL-mediated protein folding. *Mol. Cell*, **8**, 730-732.

Wenzel, T., Eckerskorn, C., Lottspeich, F. and Baumeister, W. (1994) Existence of a molecular ruler in proteasomes suggested by analysis of degradation products. *FEBS Lett.*, **349**, 205-209.

Whitby, F.G., Masters, E.I., Kramer, L., Knowlton, J.R., Yao, Y., Wang, C.C. and Hill, C.P. (2000) Structural basis for the activation of 20S proteasomes by 11S regulators. *Nature*, **408**, 115-120.

Wickner, S., Maurizi, M.R. and Gottesman, S. (1999) Posttranslational quality control: folding, refolding, and degrading proteins. *Science*, **286**, 1888-1893.

Wilson, H.L., Ou, M.S., Aldrich, H.C. and Maupin-Furlow, J. (2000) Biochemical and physical properties of the *Methanococcus jannaschii* 20S proteasome and PAN, a homolog of the ATPase (Rpt) subunits of the eucaryal 26S proteasome. *J. Bacteriol.*, **182**, 1680-1692.

Witt, E., Zantopf, D., Schmidt, M., Kraft, R., Kloetzel, P.M. and Krüger, E. (2000) Characterisation of the newly identified human Ump1 homologue POMP and analysis of LMP7(β5i) incorporation into 20 S proteasomes. *J. Mol. Biol.*, **301**, 1-9.

Wojtyra, U.A., Thibault, G., Tuite, A. and Houry, W.A. (2003) The N-terminal zinc binding domain of ClpX is a dimerization domain that modulates the chaperone function. *J. Biol. Chem.*, **278**, 48981-48990.

Woo, K.M., Chung, W.J., Ha, D.B., Goldberg, A.L. and Chung, C.H. (1989) Protease Ti from *Escherichia coli* requires ATP hydrolysis for protein breakdown but not for hydrolysis of small peptides. *J. Biol. Chem.*, **264**, 2088-2091.

Xu, Z., Horwich, A.L. and Sigler, P.B. (1997) The crystal structure of the asymmetric GroEL-GroES-$(ADP)_7$ chaperonin complex. *Nature*, **388**, 741-750.

Yang, Y., Früh, K., Ahn, K. and Peterson, P.A. (1995) In vivo assembly of the proteasomal complexes, implications for antigen processing. *J. Biol. Chem.*, **270**, 27687-27694.

Yano, M., Mori, S. and Kido, H. (1999) Intrinsic nucleoside diphosphate kinase-like activity is a novel function of the 20 S proteasome. *J. Biol. Chem.*, **274**, 34375-34382.

Yao, T. and Cohen, R.E. (2002) A cryptic protease couples deubiquitination and degradation by the proteasome. *Nature*, **419**, 403-407.

Yedidia, Y., Horonchik, L., Tzaban, S., Yanai, A. and Taraboulos, A. (2001) Proteasomes and ubiquitin are involved in the turnover of the wild-type prion protein. *EMBO J.*, **20**, 5383-5391.

Zühl, F., Seemüller, E., Golbik, R. and Baumeister, W. (1997) Dissecting the assembly pathway of the 20 S proteasome. *FEBS Lett.*, **418**, 189-194.

Zwickl, P. and Baumeister, W. (1999) AAA-ATPases at the crossroads of protein life and death. *Nat. Cell Biol.*, **1**, E97-98.

Zwickl, P., Grziwa, A., Pühler, G., Dahlmann, B., Lottspeich, F. and Baumeister, W. (1992) Primary structure of the *Thermoplasma* proteasome and its implications for the structure, function, and evolution of the multicatalytic proteinase. *Biochemistry*, **31**, 964-972.

Zwickl, P., Kleinz, J. and Baumeister, W. (1994) Critical elements in proteasome assembly. *Nat. Struct. Biol.*, **1**, 765-770.

Zwickl, P., Lottspeich, F., Dahlmann, B. and Baumeister, W. (1991) Cloning and sequencing of the gene encoding the large (alpha-) subunit of the proteasome from *Thermoplasma acidophilum*. *FEBS Lett.*, **278**, 217-221.

Zwickl, P., Ng, D., Woo, K.M., Klenk, H.P. and Goldberg, A.L. (1999) An archaebacterial ATPase, homologous to ATPases in the eukaryotic 26 S proteasome, activates protein breakdown by 20 S proteasomes. *J. Biol. Chem.*, **274**, 26008-26014.

# Lebenslauf

**Persönliche Daten:**

| | |
|---|---|
| Name: | Silke Hutschenreiter |
| Geburtsdatum/-ort: | 16.02.1969, Kassel |
| Staatsangehörigkeit: | deutsch |
| Konfession: | evangelisch |

| | | |
|---|---|---|
| **Schulbildung:** | 1975-1979 | Grundschule am Heideweg, Kassel |
| | 1979-1988 | Wilhelmsgymnasium, Kassel |
| | 06/1988 | Allgemeine Hochschulreife |
| **Studium:** | 10/1988-10/1992 | Studium der Pharmazie, Universität Marburg |
| | 11/1992-11/1993 | Pharmaziepraktikum in öffentlicher Apotheke bzw. Krankenhausapotheke |
| | 02/1994 | Approbation als Apothekerin |
| | 04/1994-10/1994 | Studium der Chemie, Universität Freiburg |
| | 10/1994-10/1995 | Vorlesungen und Praktika des Ergänzungsstudienganges Humanbiologie (Biochemie, Physiologie, Histologie, Molekularbiologie, Immunologie), Universität Marburg |
| | 10/1995-12/1997 | Studium der Chemie, Universität Marburg |
| | 01/1998-06/1998 | Diplomarbeit in Neurochemie, wegen zu starker medizinischer Orientierung vorzeitig beendet |
| | 07/1998-06/1999 | Diplomarbeit unter Betreuung von Prof. Dr. B. Kadenbach, Thema: „Einfluss von Effektoren auf Struktur und Funktion der Cytochrom c Oxidase“ |
| | 06/1999 | Diplom in Chemie |
| | 08/1999-06/2004 | Promotion an der Universität Marburg bzw. Frankfurt unter der Betreuung von Prof. Dr. R. Tampé, Thema: „Charakterisierung des Prozessierungsmechanismus des 20 S Proteasomkomplexes“ |